CO_2 Flooding in Chalk Reservoirs

Experiments with X-Ray Computed Tomography and Reactive Transport Modelling

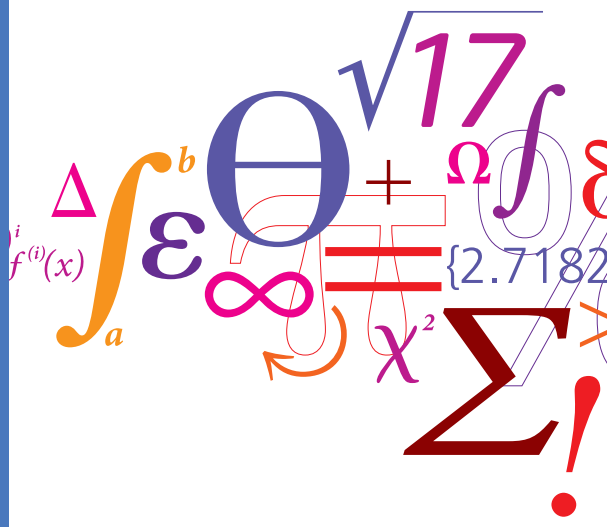

Ben Niu

Ph.D. Thesis

August 2010

DTU Chemical Engineering

Department of Chemical and Biochemical Engineering

CO_2 Flooding in Chalk Reservoirs

Experiments with X-Ray Computed Tomography and Reactive Transport Modelling

PhD Thesis

Ben Niu

August 2010

Center for Energy Resources Engineering
Department of Chemical and Biochemical Engineering
Technical University of Denmark

Address: Center for Energy Resources Engineering
Department of Chemical and
Biochemical Engineering
Technical University of Denmark
Søltofts Plads, Building 229
DK-2800 Kgs. Lyngby
Denmark
Phone: +45 4525 2800
Fax: +45 4525 4588
Web: www.cere.dtu.dk

Print: J&R Frydenberg A/S
København
januar 2011

ISBN: 978-87-92481-28-3

CO_2 Flooding i Kalk Reservoirs

Eksperimenter med X-Ray Computer Tomografi
og Modellering af Reaktiv Transport

Preface

The work presented in this thesis is the partial fulfilment of the requirements for the degree of Doctor of Philosophy at the Technical University of Denmark (DTU). The work was carried out at Center for Energy Resource Engineering (CERE), from September 2006 to August 2010 under the supervision of Professor Erling H. Stenby, Associate Professor Wei Yan, and Associate Professor Alexnader A. Shapiro, to all of whom I wish to express my gratitude.

I am grateful to DTU, Danish National Advanced Technology Foundation and DONG Energy for co-financing the project.

I wish to thank Technicians Thoung Dang, Duc Thuong Vu, Zacarias Tecle and Poul Valdemar Andersen for assisting me in the laboratory.

Furthermore, the CERE is a very international, dynamic and inspiring environment where I have enjoyed working. I wish to thank my fellow Ph.D. students Leila Faramarzi, Rasmus Risum Boesen, Sidsel Marie Nielsen, Xuan Zhang and Sara Bülow Sandersen, with whom I shared office and get through the whole period of my study.

Finally, I wish to thank my colleagues at CERE for an enjoyable time.

Copenhagen, August 2010

Ben Niu

Summary

This thesis addresses the issues regarding CO_2 injection in chalk reservoirs by performing experimental work and modelling study. The experimental work focuses on improving the current methods for determination of in situ phase saturation during CO_2 flooding in low permeable chalk at reservoir conditions. A number of trial flooding experiments and two successful tertiary CO_2 flooding experiments have been completed. The modelling study focuses on coupling geochemical reactions with multiphase flow in CO_2 enhanced oil recovery (EOR) process. The thesis consists of five chapters. The content of each chapter is summarized below:

Chapter 1 introduces the background of CO_2 EOR process and its importance in CO_2 sequestration. It contains motivation and the objective of the Ph.D. project.

Chapter 2 presents the principles of X-ray CT scanning, important factors that influence the image quality and its recent applications in core analysis. The history and the generations of CT scanners and the principles of X-ray imaging are introduced first. Then, determination of quantitative information, such as porosity, saturation and density, from CT scanning is addressed in terms of mathematical formulations. After that, the factors influencing the image quality and principles of using dopants are summarized. Finally, a thorough literature review about the applications of CT scanning in core analysis is given, where many earlier studies and some of the most recent researches are grouped into several application categories, such as core description, fundamental mechanisms, improved oil recovery, formation damage, dual energy scanning and geochemical reactions.

Chapter 3 presents the experimental work on carbon dioxide flooding with the application of CT scanning. The focus of the study is to determine in situ phase saturation during CO_2 flooding in low permeable chalk at the reservoir conditions. Firstly, the chapter describes a newly established core flooding rig for X-ray CT scanning and the X-ray CT scanner used in the study. Since there is no open literature available on reporting in situ phase saturation in CO_2 flooding in low permeable chalk, trial experiments have been performed first to examine the feasibility of the current available methods and the necessarily of applying dopants to enhance the contrast between various fluids. In the trial experiments, the adsorption of dopants and the upper limit of CT scanner have been found to have negative effects on image quality while applying dual energy scanning. The results from the trial experiments also suggest that the dual energy scanning is not suitable for low permeable chalk sample under experimental conditions in this study, even with application of K_{edge} dopants.

Based on the experience from the trial experiments, a new experimental method was proposed and applied in the experiments of tertiary CO_2 flooding on low permeable chalk at reservoir conditions to determine in situ saturations, especially gas saturations at three-phase conditions, by use of X-ray CT. The detailed data analysis has confirmed that CO_2 flooding is a highly effective approach to enhance oil recovery on our selected samples and the saturations obtained from CT images agree well with those from mass balance, indicating that our proposed method is successful in saturation determination. Finally, the factors which may result in the deviations between gas saturations obtained from CT scanning and those from mass balance are discussed.

Chapter 4 first presents a literature study on geochemical transport in porous media for CO_2 injection into aquifers and CO_2 EOR process, and mathematical modelling on coupling miscible flow and geochemistry for CO_2 EOR process. The literature study shows the importance of evaluating geochemical impacts during CO_2 storage in aquifers and oil reservoir. A classification of geochemical and solute transport models has been given. In particular, the necessity of introducing geochemical reaction into modelling on CO_2 EOR process is discussed and illustrated by evidences from the existing literatures.

The numerical modelling is based on the finite element simulation software, COMSOL Multiphysics. To investigate whether COMSOL is suitable to model miscible flow and transport-reactive flow, two cases with known analytical solutions, gas flooding and polymer flooding, have been used to validate the results from COMSOL. Then, the model, aiming at the integration of geochemical reactions into multiphase flow during CO_2 EOR process, has been proposed. The system of general equations for three-phase flow and geochemical reaction between dissolved CO_2, water and calcite are formulated. A series of assumptions to simplify the general equations to a particular model used in the study are discussed. The solution method, sequential iterative approach, is used in our model to solve those coupled equations. Further, the developed model has been validated by comparison to the results from a one dimension simulator written in FORTRAN code in simulating CO_2 flooding without geochemical reactions. Finally, the results of one-dimension simulations on CO_2 flooding with geochemical reactions has been discussed on two different spatial scales, reservoir scale flooding and lab scale flooding, indicating that the CO_2 solubility in water could retard the movement of gas front on both scales, while the geochemical reaction could slow the process in reservoir scale with changing porosity and permeability. The importance of reactive surfaces has been addressed, which could significantly affect the molar concentration of calcium during the flow transport at the lab

scale. The reaction of carbonate dissolution could be treated as equilibrium reaction in the flooding at reservoir scale, while it is still under kinetic control at the lab scale.

Chapter 5 presents the conclusions from the thesis and the suggestions for further developing the experimental and modelling work.

Resumé

Denne afhandling varetager og omhandler problemstillinger angående CO_2 injektion i kalk reservoirs. Der er udført eksperimentelt arbejde, samt modellering. De innovative eksperimentelle metoder til bestemmelse af in situ fase mætning for CO_2 flooding i lav permeabelt kalk ved reservoir betingelser er præsenteret og et modelleringsstudie, af de sammenhængende geokemiske reaktioner i multifase flow i CO_2-forbedret olieudvindingsprocesser, (EOR), er også udført. Afhandlingen er inddelt i 5 kapitler. Det overordnede indhold af hvert kapitel er introduceret i det følgende.

Kapitel 1 Introducerer baggrunden for CO_2-EOR-processen og dens betydning i CO_2-sekvestrering. Indeholder endvidere motivation og formålet med dette Ph.D.-projekt.

Kapitel 2 Præsenterer overordnet X-ray CT scanning, vigtige faktorer, der påvirker billedkvaliteten og de seneste anvendelsesmuligheder i core-analyse. Anvendelsen af CT scanneren og principperne om X-ray billeder blev indført i etaper. De kvantitative informationer, såsom porøsitet, mætning, densitet, heterogenitet osv., opnået fra anvendelsen af CT scanning i core-analyse er blevet behandlet sammen med egnede matematiske formuleringer. I følge af dette blev faktorerne, der påvirker billedkvaliteten og principper for at brug dopants opsummerede. Endelig er der et grundigt litteraturstudie om anvendelse af CT-scanner i core-analyse. Dette indbefatter flere tidligere studier, samt det seneste forskning indenfor reservoir kategorien. Herunder core-beskrivelse, grundlæggende mekanismer, forbedret olieudvinding, skader der forekommer ved dannelse, energiscanning og geokemiske reaktioner mv.

Kapitel 3 Præsenterer det essentielle eksperimentelle arbejde med CO_2-flooding, hvor CT scanning er anvendt. Omfanget af dette studie er at bestemme in situ fasemætningen i CO_2-flooding på lav permeabelt kalk ved reservoirbetingelser. Først blev, core-flooding udstyret med X-ray scanner, designet og bygget af forfatteren, diskuteret og sammeholdt med den X-ray CT scanner der er anvendt i dette studium. Dette setup inkluderer state-of-the art udstyr, som carbonfiber-indpakket core-indehaver, som kan simulere højt tryk og temperatur, svarende til de betingelser der optræder i et reservoir. Der er givet et overblik over flooding eksperimenterne med diskussion om de fysiske egenskaber for cores, væsker og eksperimentelle betingelser. Da der ikke eksisterer noget tilgængeligt litteratur om indberetning af in situ fasemætning for CO_2-flooding på lav permeabelt kalk, er der udført eksperimenter for at udforske mulighederne for de nuværende tilgængelige metoder, samt den behovet for at tilføre dopants for at forstærke kontrasten mellem forskellige væsker. I de udførte eksperimenter er adsorption af dopants blevet observeret, hvor dens

indflydelse på billedkvaliteten, samt den beregnede mætning er diskuteret. Samtidig blev fundet, at den øvre grænse for CT scanneren har en negativ indvirkning på billedkvalitet under anvendelsen dual energy scanning og derfor en korrektionsmetode baseret på den ikke-lineære Huber estimering blevet foreslået. Ud fra resultaterne fra disse eksperimenter er den nuværende eksperimentelle metode ikke egnet for lav permeable kalk-prøver ved de eksperimentelle betingelser der har været gældende i dette studie. Dette er endda på trods af at K_{edge} dopant har været anvendt.

Det unikke ved dette arbejde er ikke grundet det anvendte core materiale, men snarere de innovative eksperimentelle metoder. Baseret på erfaringerne fra eksperimenterne er nye eksperimentelle metoder blevet foreslået og anvendt på Nordsø kalk, hvor der er anvendt levende olie.De generelle procedurer og egenskaber for væsker og nye fremgangsmåder til at tilpasse dopantkoncentrationen i forskellige væsker blev behandlet først. Derefter er eksperimenterne med tertiære CO_2-flooding på lav permeabelt kalk ved reservoirbetingelser, til at bestemme in situ mætninger, især gas mætninger, med anvendelse af X-ray CT, diskuteret for at validere vores nye metoder og evaluere effektiviteten og udbyttet af CO_2 EOR. Den detaljerede dataanalyse bekræftede, at CO_2-flooding er en betydeligt effektiv tilgang til at øge olieindvindingen på vores udvalgte prøver og mætningerne fra CT billederne stemmer overens med massebalancen, hvilket indikerer at den nye fremgangsmåde er vellykket gennemført. Endelig blev de faktorer og de nødvendige præferentielle parametre for en vellykket gennemførelse af den foreslåede metode, med at bruge X-ray CT til multifase strømme i kalksten også drøftet.

Kapitel 4 Indeholder litteraturstudie af geokemiske transport i porøse medier for CO_2-injektion i grundvandsmagasiner og CO_2 EOR processer, samt matematisk modellering af koblingen af blandbar flow og geokemi for CO_2 EOR proces. I litteraturstudiet blev betydningen af at evaluere geokemiske konsekvenser i løbet af CO_2-lagring i grundvandsmagasiner og olie reservoir først behandlet ved at introducere de vigtigste mekanismer i CO_2-bindinger og fremhæver påvirkningen af de geokemiske reaktioner. Derefter er klassificeringen af geokemiske og opløsligheds stoftransport modeller introduceret i rækkefølge, herunder reaktionrække model, hydrodynamisk model og reaktiv transport model. Endelig blev anvendelse af ovennævnte modeller diskuteret i detaljer, som kan opdeles i fem områder; eksperiment, integritet, nær god injectivitet, kortsigtet CO_2-lagring og langsigtet CO_2-lagring. Især nødvendigheden af at introducere geokemiske reaktioner i modelleringen af CO_2 EOR processer blev drøftet og illustreret af beviser fra eksisterende litteratur.

I modelleringsdelen bliver de analytiske og numeriske metoder til modellering gennemgået. Den numeriske test af det endelige element-simulerings-software, COMSOL Multiphysics, blev gennemført først til at evaluere sin tilpasningsegnethed til modellering af blandbar flow og transport-reaktivt flow, med to tilfælde; gas flooding og polymer flooding. Resultaterne blev sammenlignet med analytiske løsninger fra litteraturen. Derefter blev system af ligninger for trefase flow og geokemiske reaktioner mellem opløst CO_2, vand og kalciumkarbonat formuleret. De var sammensat af transport ligninger og Darcy's love for tre faser, ligninger for kinetisk kontrolleret reaktioner og ligninger for porøsitet og permeabilitet, som kunne ændres ved geokemiske reaktioner i løbet af CO_2 flooding. En række antagelser for at forenkle de generelle ligninger til en særlig model, der anvendes i studiet og løsningsmetoden, sekventiel iterative tilgang, blev drøftet i detaljer. Den udviklede model blev valideret ved sammenligning med resultaterne fra en dimension simulator skrevet i FORTRAN kode til simulering af CO_2 flooding uden geokemiske reaktioner. Endelig blev resultaterne af en dimension simuleringer af CO_2 flooding med geokemiske reaktioner drøftet i to forskellige rumlige skalaer, reservoir skalering flooding og lab skala flooding. I begge tilfælde er mætningsprofilen og ion koncentrationen genereret. Virkningerne af geokemiske reaktioner og faseligevægtsammensætning ved mætning blev undersøgt. Især i laboratorie skala var indflydelsen af reaktive specifikke områder for porøsitet af core-prøven rettet mod.

Kapitel 5 Præsenterer konklusionerne fra Ph.D.-afhandlingen og forslag til fremtidig udvikling for både det eksperimentelle arbejde og det numeriske studie.

Table of Contents

List of Figures

List of Tables

Nomencluture

a	Air
a_i	Activity of aqueous component i
$\mathrm{A_m}$	Reactive surface area, m^2/m^3
$\mathrm{c_{CO_2,w}}$	Volumetric gas water ratio
CT	CT number
D	Artificial diffusion coefficient, m^2/s
f_i	Frational flow of component i
F_i	Overall fractional volumetric flow of component i
g	Gas
G_i	Overall molar concentration of component i, mol/m^3
H_i	Overall molar flow of component i, mol/m^3
$\mathrm{k_m}$	Chemical reaction rate, $mol/(m^2 s)$
$\mathrm{k_{sp}}$	Solubility product
K	Permeability, *md*
$m_{i,j}$	Molar concemtration of component i in phase j, mol/m^3
M	Viscosity ration between oil and gas
N_i	Overall volume fraction of component i
o	Oil
P	Pressure, *bar*
r	Rock
S	Saturation
$x_{i,j}$	Molar fraction of component i in the phase j
μ	Viscosity, cp
ρ	Molar density, mol/m^3
w	Water
ϕ	Porosity

Chapter 1. Introduction

1.1 Background and motivation

A range of techniques have been developed and applied to improve oil recovery to meet the increasing demands on energy resources. According to a survey of the EOR projects in the United States [1], thermal methods, gas injection and chemical methods are the most widely used methods. Application of chemical methods has declined significantly from the mid 90s. However, thermal methods and gas injection remain the most common techniques, as shown in Figure 1. Figure 1 also shows that CO_2 is the most common injectant among different gases in more than 60% of the total gas injection projects, compared with other injectant such as hydrocarbon and nitrogen. One of the most famous and successful CO_2 injection projects is the huge CO_2 project in Permian basin, West Texas. CO_2 flooding has been used effectively in mature and in water flooded reservoir in Permian basin, thanks to the availability of natural CO_2 source close to the oilfields.

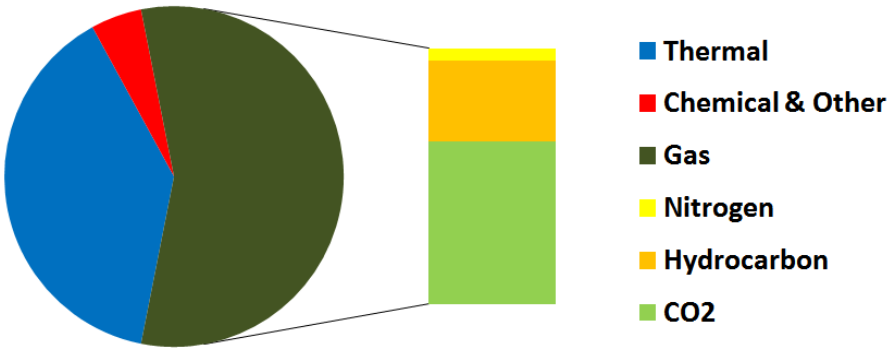

Figure 1 Trends in enhanced oil recovery in US [2]

At the same time, in the North Sea area, based on the maturity and EOR potential of different techniques and an evaluation of the importance and complexity of the technology, OG21 (Oil and Gas in the 21st century) identified nine technology target areas aiming at obtaining the average recovery factors of 50% for oil and 75% for gas on the Norwegian Continental Shelf [3]. These nine techniques have been divided into three groups based on their priorities in practice, and CO_2 flooding is viewed as one of the methods in the 1st group, which will be focused by the future research.

The new dawn of CO_2 flooding is coming and it is expected to continue to expand in the near future, which can be attributed to two reasons: (1) the increasing energy costs for thermal projects and the

increasing natural gas prices for hydrocarbon gas injection improved the migration towards CO_2 flooding; (2) climate change requires the reduction of CO_2 concentration in the atmosphere.

As one of the anthropogenic greenhouse gases, CO_2 is considered a major contributor to global warming. To decrease its rising concentration in atmosphere, CO_2 capture and possible large-scale storage of CO_2 in the geological formation, such as aquifers, coal bed and oil reservoirs, are identified as efficient approaches. Oil reservoirs are one of the prospective geological structures for CO_2 storage. CO_2 storage in oil reservoirs has several clear advantages, especially for quick implementation. Besides the economic benefit from CO_2 EOR, the mature technology of CO_2 flooding has been developed for more than thirty years, and the abundant data concerning geological information of reservoir has been accumulated, which are essential for the safety of long-term CO_2 storage. In the past, although CO_2 has advantages as, lower minimum miscibility pressure (MMP) compared with hydrocarbon gas injection and low energy cost compared with thermal projects, its application has been limited by the location of CO_2 source and the network of CO_2 transporting pipelines. However, The CO_2 captured from large power plants serves as an alternative source for possible large-scale application of CO_2 flooding, instead of traditional natural CO_2 sources.

The mechanisms of CO_2 injection to enhance oil recovery are similar to those of other gas injection. The development of miscibility between CO_2 and oil during the displacement processes is essential to the efficiency of CO_2 flooding. When the reservoir pressure is near or above the MMP, CO_2 could displace oil with high efficiency. The MMP strongly depends on the reservoir temperature and the composition of oil in reservoir. Therefore, the fluid characterization and accurate MMP correlation have important status in the CO_2 EOR study and have been investigated widely [4].

Most of the studies regarding CO_2 flooding concentrated on the multiphase flow and the thermodynamic properties of CO_2 and oil with experimental work and modelling study, which is a relatively mature field of research. Nowadays, the compositional simulator used in the oil industry could be adequate for describing complex processes as CO_2 flooding. However, there are still some basic questions that have not been answered yet. One of them is to get insight into the flow inside the porous media to investigate how different phases flow and how the miscibility develops. Visualization of CO_2 flow in core samples under reservoir conditions is one way to answer the question. Visualization of the flow also provides data that can be used in history matching of numerical simulations. In this work, X-ray CT scanning is used as an attempt to determine the saturation change during CO_2 flooding and qualitatively visualize fluid flow.

Furthermore, combination of CO_2 flooding in oil reservoir with long-term CO_2 storage has brought new topics into the research areas. Those topics are related to improvement of the efficiency of CO_2 sequestration during flooding processes and understanding of the influence of geochemical reactions on well injectivity, well integrity and the sealing performance of cap rock. This thesis has focused on a challenge in simulation due to the combination of miscible flooding simulation and geochemical reactions.

From a practical viewpoint, more efforts are required to investigate the above questions and topics. This is also the basic motivation for the work presented in this thesis.

1.2 Scope and objectives

The objectives of this study are:

- To determine phase saturations during the tertiary CO_2 flooding in the low permeable chalk from the North Sea under reservoir conditions.
- To develop a mathematical model, which describes the multiphase flow together with geochemical reaction during CO_2 flooding.

The issues regarding CO_2 flooding in porous media can be divided into various topics, and most of them are related to the thermodynamic properties of CO_2 and oil mixture and the multiphase flow behaviour during the injection process. Flooding experiments aiming at providing direct evidence to validate models have been conducted. However, the information concerning in situ saturation of different phases, which are valuable for understanding the basic mechanisms of multiphase flow in porous media and further validating and tuning the mathematical model, was seldom determined especially for low permeable chalk in the experiment. Meanwhile, the geochemical reactions, which are neglected in previous mathematical modelling describing CO_2 flooding in porous media, has gained more attentions, since oil reservoirs can also serve as CO_2 storage places.

The present work is devoted to develop experimental methods used to obtain in situ phase saturations for CO_2 flooding in low permeable chalk under reservoir conditions, and attempt to bridge the gap between mathematical models on short-term CO_2 flooding and those on long-term CO_2 storage.

Experimental works are presented in Chapters 2 and 3. Chapter 2 introduces the principles of X-ray CT scanning and its importance as an assisting tool in core analysis. The factors, which could influence quality of CT images, and further the accuracy of the quantitative information obtained from them, are discussed. A comprehensive literature research on the applications of X-ray CT to different areas in reservoir engineering is also made. Chapter 3 describes the experimental work on the low permeable chalk. The limits of previous experimental methods are discussed by analyzing data from trial experiments, which has been seldom addressed previously. Following this, the new experimental methods have been proposed and applied on the North Sea chalk with using live oil, and further the detailed data analysis indicated the successful application of our proposed method.

Chapter 4 is dedicated to the development of numerical models with the implication of multiphase flow and geochemical reactions for CO_2 flooding in oil reservoir. A detailed literature study about the numerical models used in CO_2 injection into aquifers and oil reservoir and the domains of their applications, has been conducted. The necessity of considering geochemical reactions while modelling CO_2 flooding process is discussed. A one dimension model has been developed to simulate the process. The novelty of the model is the introduction of geochemical reaction into multiphase flow models. The simulation results are discussed based on various spatial scale, reservoir scale and lab scale, where the geochemical reactions affect the multiphase flow in different ways. Furthermore, the influence of various parameters, such as the solubility of CO_2 in water phase and reactive surface area, on the multiphase flow, is addressed.

Chapter 5 presents the conclusions from the thesis and the suggestions for the future work.

References

[1] E. Manrique, V. Muci, and M. Gurfinkel, “EOR Field Experiences in Carbonate Reservoirs in the United States,” *SPE Reservoir Evaluation & Engineering*, vol. 10, no. 6, pp. 667–686, December 2006.

[2] A. Espie. (2005, 21-23 November) A New Dawn for CO_2 EOR. Paper SPE 10935 presented at the International Petroleum Technology Conference, Doha, Qatar.

[3] A. Awan, R. Teigland, and J. Kleppe. (2006, 22-26 April) EOR Survey in the North Sea. Paper SPE 99546 presented at the SPE/DOE Symposium on Improved Oil Recovery, Tulsa, Oklahoma, USA.

[4] K. Jessen and E. Stenby, “Fluid Characterization for Miscible EOR Projects and CO_2 Sequestration,” *SPE Reservoir Evaluation & Engineering*, vol. 10, no. 5, pp. pp. 482–488, October 2007.

Chapter 2 X-Ray CT Scanning and Its Application in Core Analysis

Oil production from a petroleum reservoir is often achieved by injecting a certain fluid to displace the oil in the porous media, such as water, gas and steam. A core flooding experiment is commonly performed to investigate the efficiency of such process. In the experiment, the porous media is saturated with water and oil to simulate the original condition of oil reservoir, and the oil is then displaced by water, gas, steam or chemicals based on different EOR methods. The core flooding experiment provides information about the total amount of fluids injected and produced, and oil recovery curve is the final results obtained. The oil recovery curve is not only important in evaluating the performance of EOR methods in the field-scale flood, but also significant in calibrating the numerical model for the simulation of such process. However, the recovery curve alone cannot identify multiphase fluids flow and their distributions in the porous media. Therefore, the observation of the in situ displacement process during the flooding is needed.

The rapid developments of imaging technology over the last decades bring various solutions to the detailed visualization of displacement in the core flooding. Many methods have been adopted to determine the in situ saturations during the core flooding experiments, e.g. transparent porous media made of finely powdered glass [1], resistivity [2], magnetic susceptibility [3], NMR [4], X-ray and gamma-ray attenuation [5][6][7], and microwave adsorption [8]. Most of the above mentioned methods can only provide areal average value of saturations.

X-ray computed tomography (CT) has been utilized by the petroleum industry to perform both qualitative and quantitative investigations on cores and become an important tool for core analysis. The method can produce images with fine resolution and high accuracy by detecting the radiation that passes through a cross section of the core. The image data can be further processed to obtain information about the physical properties of the core (density [9], porosity [10], mineralogy and heterogeneities [11]) and the fluid within the core (saturations [12] and diffusion coefficient [13]). The first CT system was designed in 1972 by Godfrey Hounsfield of EMI Laboratories, England and by the South African-born physicist Allan Cormack of Tufts University, Massachusetts. Later, Hounsfield and Cormack were awarded the Nobel Prize for their contributions to medicine and science. The first clinical CT was installed in 1972 in the Atkinson Morley Hospital in London.

Compared with the methods mentioned earlier for in situ saturation determination, CT can generate dynamic 3-D images of multiphase fluid flow in porous media at reservoir temperatures and pressures. As an excellent technique to visualize flow phenomena in porous media, CT scanning has

been widely used in the petroleum engineering studies, such as multiphase relative permeability, dispersion, gravity segregation, viscous finger, wettability, lithologic characterization, and evaluation of damage in unconsolidated cores.

This chapter presents the principles of X-ray CT scanning, important factors that influence the image quality and the recent applications in the core analysis.

2.1 Principles of CT scanners

2.1.1 History and generations of CT scanners

Tomography, known as a method to represent a single slice of the body on the radiographic film, was originally proposed by the Italian radiologist Alessandro in the early 1900s [14]. In Greek, the word ‘‘tomos’’ means ‘‘slice” or ‘‘section’’, and the word ‘‘graphia’’ means ‘‘describing’’. The first CT system was invented in 1972 by Godfrey Hounsfield of EMI Laboratories, which was installed in Atkinson Morley Hospital in Wimbledon, England, and the images produced from this scanner had relatively low resolution, with 80×80 pixels [15]. In the U.S., the first installation was at the Mayo clinic. During its 27-year history, tremendous researches and developments have been made to provide better image quality at the lowest possible X-ray dose. Therefore, CT has great improvements in speed and resolution, as shown in the Figure 2.

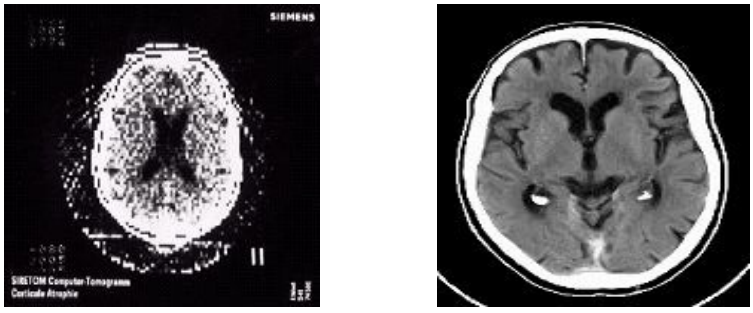

(1) Original axial CT image obtained at 1975 128×128 matrix image

(2) Axial CT image obtained nowadays 512×512 matrix image

Figure 2 Developments on the image quality [16]

There are four generations of CT scanners, classified by the arrangement of components and the mechanical motion required to collect the data. The generation number is given in the chronological

order of their invention. One should not assume that a higher generation number necessarily means a higher performance system. Nowadays, the third generation CT scanner can have better performance than the fourth generation ones.

The first generation of CT scanners is mainly composed of a single X-ray source and a single X-ray detector cell for collecting the data for a single slice. The coupled source and detector measures the attenuation of radioactive beam, which translating across the patient at one angle, and this process is repeated for each projection angle to obtain the projection measurement [17], as shown in the Figure 3[18], in which the grey part represents the source and the green part is the detector. The whole process is called as the translation and rotation process, which is very slow and takes almost 120 seconds for each scan.

The efficiency of measuring projections of the second generation is improved significantly by using multiple detectors, because the X-ray source emits a narrow fan beam of radioactive ray, which can be received by multiple detectors at each translation step [17], as shown in Figure 3[18]. Because of the translation and rotation process, the first and second generations of CT scanner are referred to as a translate/rotate scanner.

In the third generation, a detector array with enough high spatial resolution cells is designed to allow the simultaneous measurement of a fan-beam projection of the entire patient cross-section [17], as shown in Figure 3[18]. Therefore, no translation step is required, which enables the imaging process significantly faster than the first or the second generation systems. To distinguish it from the previous two generations, the third generation is often referred to as rotate/rotate scanner. , if any one of the detectors is out of order in the third generation, it will result in a circular artefact by giving consistent errors regarding at each angular position [19]. Therefore, very high performance detectors are needed.

To avoid the sensitivity of the third generation to ring artefacts, the fourth generation of CT scanner is developed by using a stationary detector ring and a rotating X-ray tube [17], as shown in Figure 3. Therefore, to achieve the same spatial resolution as a third generation system, more detectors are needed in the fourth generation, which represents a potentially higher cost [17].

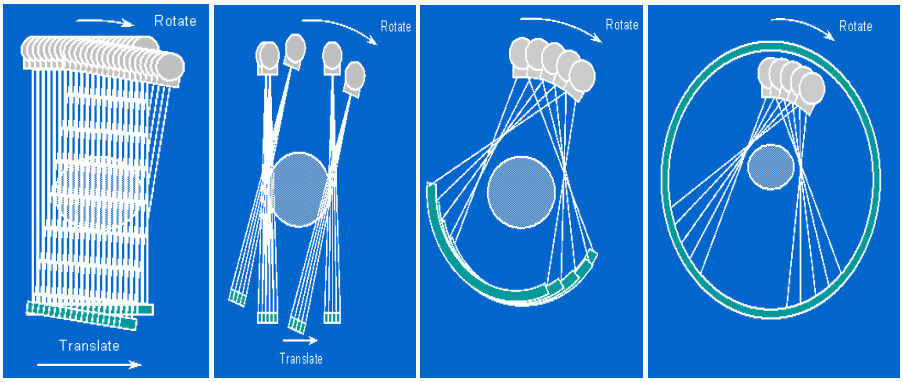

(1) First generation (2) Second generation (3) Third generation (4) Fourth generation

Figure 3 the geometry of X-ray source (tube) and detectors in various generations of X-ray CT scanners [18]

2.1.2 Principles of X-ray CT imaging

The principles of X-ray CT imaging have been discussed extensively in many articles [20] [21] and CT user's guide [22][23], which can be used as reference for readers who want to go deep into this topic. In this section, only basic mechanisms and concepts concerning the X-ray adsorption are addressed. When an X-ray beam passes through an object, its intensity is reduced as the X-ray photons is either absorbed (photoelectric absorption) or scattered (Compton scattering and Rayleigh scattering). Since the Rayleigh scattering plays a minor role in CT scanning, it will not be discussed in details.

2.1.2.1 Photoelectric absorption

When the incident X-ray photon collides with orbital electrons of an atom, if the energy of colliding photon exceeds the binding energy of collided electron, the photon can be completely disappear and the electron is released with the energy transferred from the photon. This process is called as photoelectric adsorption, which is mainly influenced by the atomic number of the object and the energy of the X-ray beam [22].

Since the bending energy varies at different atomic shells, the larger the atomic number, the larger the energy required to displace an electron. The kinetic energy of the released electron, the difference between the incoming energy of the photon and the binding energy of the electron in the atomic shell, can be expressed as,

$$E_{kin} = hf - E_{binding} \tag{1}$$

where h is Planck's constant and f is the frequency of the wave.

2.1.2.2 Compton scattering

When the incident X-ray photon collides with orbital electrons of an atom, the colliding photon can be deflected from its original path while the collided electron ejected from its orbital position. This process is called as Compton scattering, which does not depends on the atomic number, but primarily affected by the bulk density of the object.

2.1.2.3 Attenuation coefficients

Attenuation coefficient, also called liner attenuation coefficient, is a quantity that characterizes how easily a material or medium can be penetrated by a beam of X-ray. It can be expressed as a function of the X-ray beam photon energy, the atomic number, and the electron density of the substance. The mass attenuation coefficient is a function with the contributions from three different photon interactions mode [22]:

$$\frac{\mu}{\rho} = \frac{\mu_R}{\rho} + \frac{\mu_\tau}{\rho} + \frac{\mu_C}{\rho} \tag{2}$$

where, ρ is the mass density, R, τ and C represents Rayleigh scattering, photoelectric adsorption, and Compton scattering respectively. Each part of the equation can be expressed by the total photon interaction cross-section per atom, σ_{tot}:

$$\frac{\mu}{\rho} = \frac{N_A Z \sigma_{tot}}{A} \tag{3}$$

where N_A is Avogadro's number, Z is the number of electrons per atom and A is the atomic mass of the absorber.

The final relation for the linear attenuation coefficient can be expressed as [24],

$$\mu = \rho N_g \left[\sigma_C + C_1 \left(\frac{\overline{Z}_R^k}{E^l} \right) + C_2 \left(\frac{\overline{Z}_\tau^m}{E^n} \right) \right] \tag{4}$$

where, $\overline{Z}_R$ and $\overline{Z}_\tau$ are the effective atomic number for Raleigh scattering and photoelectric adsorption respectively, E is the photon energy, the superscripts (k, l, m and n) and coefficients (C_1

and C_2) are constants, σ_C is the cross-section per atom from Compton scattering, N_g is the mass electron density, which is,

$$N_g = \frac{N_A Z}{A}$$

If the Raleigh scattering is neglected, then the attenuation coefficient can be expressed approximately as the sum of Compton and photoelectric contributions [25]:

$$\mu = \rho N_g \left(\sigma_C(E) + \frac{bZ^{3.8}}{E^{3.2}} \right) \tag{5}$$

where $\sigma_C(E)$ is the Klein-Nishima function, which is the relativistic form of the Compton scattering, Z is the effective atomic number, E is the photon energy in keV and b is a constant [24]. Eq. (5) indicates that the heavier elements with larger Z have greater photoelectric cross section and the contribution from photoelectric absorption decreases rapidly as the X-ray energy increases. Therefore, by use of a high-energy X-ray source, the contribution from photoelectric absorption can be negligible and the attenuation coefficient becomes proportional to the bulk density of the object, as the Compton scattering dominated.

To measure the intensity of X-ray after it penetrates the material, Lambert-Beer's law is given [22]:

$$I = I_0 exp(-\mu\lambda) \tag{6}$$

where, λ is the thickness of the penetrated material, I_0 and I are the intensity of the incident x-ray and the transmitted x-ray respectively. Although Lambert-Beer's law is used to describe the X-ray beam with monochromatic spectrum penetrating the material with uniform density, it reveals that for the X-ray beam with polychromatic spectrum, the photons with lower energy is absorbed first and the remains are those with higher energy, therefore the beam becomes harder. This leads the overall attenuation to change with distance and produce an artefact known as the beam hardening. This phenomenon has significant influence on the image quality and will be discussed in section 2.4.1.

In CT images, CT number is often used as a normalized value of attenuation coefficient from a single pixel. When a heterogeneous object, for example, a core saturated with oil and water, is imaged, the

CT number could change with locations. The process of determining the spatial attenuation coefficients, $\mu(x, y)$ on the CT image is considered as 'Image reconstruction', which id fundamental and important to the image techniques.

2.2 Quantitative information from CT scanning

The measured attenuation coefficients transformed using the value for pure water as reference, are presented as CT numbers in Hounsfield units,

$$CT = 1000\frac{\mu - \mu_{water}}{\mu_{water}} \tag{7}$$

where, μ and μ_{water} are the linear attenuation coefficients for the tested material and pure water. Therefore, the CT number of pure water is zero. Since the overall CT number is an additive function of all the materials present in the scan slice [22], the CT number of various fluids saturated core is given by

$$CT_{ir} = (1 - \Phi)CT_r + \Phi CT_i \tag{8}$$

where, subscript r and i refer to the rock and fluid respectively. When the core is saturated with two fluids i and j, the overall CT number becomes

$$CT_{ijr} = (1 - \Phi)CT_r + \Phi S_i CT_i + \Phi S_j CT_j \tag{9}$$

where S_i and S_j are the saturation for each fluid respectively.

2.2.1 Porosity

Porosity is determined by scanning the dry core and then scanning it fully saturated with a certain fluid, for instance, pure water. Using eq. (8) for air and water, we obtain

$$CT_{ar} = (1 - \Phi)CT_r + \Phi CT_a \tag{10}$$

$$CT_{wr} = (1 - \Phi)CT_r + \Phi CT_w \tag{11}$$

Substituting eq. (11) into eq. (10) , one can obtain the equation for the porosity

$$\Phi = \frac{CT_{wr} - CT_{ar}}{CT_w - CT_a} \tag{12}$$

Eq. (12) shows that the CT numbers of pure fluids are needed to calculate the porosity. Normally in the room temperature and atmosphere pressure condition, the pure fluids can be carried by plastic bottle and then be scanned to obtain its CT number. If the CT number of pure fluids needs to be measured in the high pressure and temperature condition, e.g. reservoir condition, the pure fluids should be placed inside the core holder instead of the core, which is hard to be done in practice. The CT numbers of air and pure water are approximately -1000 and 0, respectively.

2.2.2 Two-phase saturations

In water flooding experiments, the single energy scanning, where the core is scanned at single energy level, is normally used to calculate the saturation of water and oil. The assumption that X-ray attenuation for pure component is constant over the complete scan area is commonly used in most of such studies [23]. Apply of eq. (9) and (11) for oil-water system gives

$$CT_{owr} = (1-\Phi)CT_r + \Phi S_w CT_w + \Phi S_o CT_o \tag{13}$$

$$CT_{or} = (1-\Phi)CT_r + \Phi CT_o \tag{14}$$

$$S_w + S_o = 1 \tag{15}$$

By substituting eqs. (11), (14) and (15) into eq. (13), one obtains

$$S_o = \frac{CT_{owr} - CT_{wr}}{CT_{or} - CT_{wr}} \tag{16}$$

The error analysis based on the oil saturation is achieved by differentiating eq. (16) with respect to each of CT number, then,

$$\frac{\partial S_o}{\partial CT_{owr}} = \frac{1}{(CT_{or} - CT_{wr})} \tag{17}$$

$$\frac{\partial S_o}{\partial CT_{wr}} = \frac{CT_{owr} - CT_{or}}{(CT_{or} - CT_{wr})^2} \tag{18}$$

$$\frac{\partial S_o}{\partial CT_{or}} = \frac{CT_{wr} - CT_{owr}}{(CT_{or} - CT_{wr})^2} \tag{19}$$

By using the rules for the propagation of errors, the total error in S_o becomes,

$$dS_o^2 = \left[\frac{\partial S_o}{\partial CT_{owr}} \cdot dCT_{owr}\right]^2 + \left[\frac{\partial S_o}{\partial CT_{wr}} \cdot dCT_{wr}\right]^2 + \left[\frac{\partial S_o}{\partial CT_{or}} \cdot dCT_{or}\right]^2 \quad (20)$$

2.2.3 Three-phase saturations

In a general oil production process or any core flooding experiment simulating that process, there are always three coexisting fluid phases, gas, water and oil. Therefore, simultaneous determination of three-phase saturations is therefore necessary. In principle, their saturations can be determined by a dual energy scanning where the core is scanned at two different energy levels. For each of the two energy levels, the total CT number is given by

$$CT_{wr1}S_w + CT_{or1}S_o + CT_{gr1}S_g = CT_1 \quad (21)$$

$$CT_{wr2}S_w + CT_{or2}S_o + CT_{gr2}S_g = CT_2 \quad (22)$$

$$S_w + S_o + S_g = 1 \quad (23)$$

By solving eq. (21) - (23) for saturations, one obtains,

$$S_o = \frac{(CT_1 - CT_{wr1})(CT_{gr2} - CT_{wr2}) - (CT_2 - CT_{wr2})(CT_{gr1} - CT_{wr1})}{(CT_{or1} - CT_{wr1})(CT_{gr2} - CT_{wr2}) - (CT_{or2} - CT_{wr2})(CT_{gr1} - CT_{wr1})} \quad (24)$$

$$S_g = \frac{(CT_1 - CT_{wr1})(CT_{or2} - CT_{wr2}) - (CT_2 - CT_{wr2})(CT_{or1} - CT_{wr1})}{(CT_{or2} - CT_{wr2})(CT_{gr1} - CT_{wr1}) - (CT_{or1} - CT_{wr1})(CT_{gr2} - CT_{wr2})} \quad (25)$$

$$S_w = 1 - S_o - S_g \quad (26)$$

where,

$$\begin{aligned} CT_1 &= CT_{g,o,w,r,level1} & \qquad CT_2 &= CT_{g,o,w,level2} \\ CT_{gr1} &= CT_{g,r,level1} & \qquad CT_{gr2} &= CT_{g,r,level2} \\ CT_{wr1} &= CT_{w,r,level1} & \qquad CT_{wr2} &= CT_{w,r,level2} \\ CT_{or1} &= CT_{o,r,level1} & \qquad CT_{or2} &= CT_{o,r,level2} \end{aligned}$$

If the water saturation is known beforehand, for instance, in a core with irreducible water saturation S_{wi}, the water is assumed to be immobile in the next three-phase gas flooding [22]. Therefore, the application of dual energy technique can be avoided, only single energy method is needed, and the expressions for the oil and gas saturations can be reduced to

$$S_o = \frac{CT_1 - CT_{gr}}{\Phi(CT_{or} - CT_{gr})} - S_{wi}\frac{CT_w - CT_g}{\Phi(CT_o - CT_g)} \tag{27}$$

$$S_g = \frac{CT_1 - CT_{or}}{\Phi(CT_{or} - CT_{gr})} - S_{wi}\frac{CT_w - CT_o}{\Phi(CT_o - CT_g)} \tag{28}$$

The oil phase saturation could also be expressed without knowing any of the pure fluid CT numbers. By application of eqs. (10), (11), (13), (14) and (21)-(23), S_o becomes

$$S_o = \frac{CT_1 - CT_{owr}}{CT_{or} - CT_{gr}} - \frac{CT_{owr} - CT_{wr}}{CT_{wr} - CT_{or}} \tag{29}$$

Similar to the error analysis based on the oil saturation in the two-phase saturation, they can be achieved by differentiating eq. (24) with respect to each CT number (CT_{o1} as example),

$$\frac{\partial S_o}{\partial CT_{or1}} = \frac{\left[(CT_1 - CT_{wr1})\cdot(CT_{gr2} - CT_{wr2}) - (CT_2 - CT_{wr2})\cdot(CT_{gr1} - CT_{wr1})\right](CT_{wr2} - CT_{gr2})}{\left[(CT_{or1} - CT_{wr1})\cdot(CT_{gr2} - CT_{wr2}) - (CT_{or2} - CT_{wr2})\cdot(CT_{gr1} - CT_{wr1})\right]^2} \tag{30}$$

The sensitivity of calculated saturations to measured CT numbers can also be evaluated through the coefficient matrix A in eq. (31),

$$\mathbf{A}\overrightarrow{x} = \mathbf{B} \tag{31}$$

where

$$\mathbf{A} = \begin{bmatrix} 1 & \dfrac{CT_{or1} - CT_{wr1}}{CT_{gr1} - CT_{wr1}} \\ 1 & \dfrac{CT_{or2} - CT_{wr2}}{CT_{gr2} - CT_{wr2}} \end{bmatrix}, \overrightarrow{x} = \begin{bmatrix} S_g \\ S_o \end{bmatrix}, \mathbf{B} = \begin{bmatrix} \dfrac{CT_1 - CT_{wr1}}{CT_{gr1} - CT_{wr1}} \\ \dfrac{CT_2 - CT_{wr2}}{CT_{gr2} - CT_{wr2}} \end{bmatrix}$$

Eq. (31) is obtained by substituting eq. (23) into eqs. (21) and (22). The determinant or the conditional number of coefficient matrix A indicates whether eq. (31) is ill-conditioned.

2.3 Dopants and K-edge

2.3.1 Dopants

As indicated in the eq. (17)-(20), the CT numbers of the water and oil saturated core should differ as much as possible to reduce errors. However, in the core flooding experiments, the difference in attenuation coefficients (CT numbers) between different fluids could be small, e.g. water and dead

oil at the room temperature and atmospheric pressure condition, gas and live oil at reservoir conditions. Therefore, dopants are normally needed to increase the CT number of fluids. Most dopants used in the liquid phase contain a halide, which has a high atomic number, thus causing more attenuation of x ray. Normally, sodium bromide or sodium iodide is used as the water dopant [26] with bromo-dodecane and iodo-dodecane [25] as oil dopant. Radioactive inert gas, Xenon and Krypton, can be used as a contrast with air [27].

The usage of dopants should be very careful since they will change the composition of fluids, and further affect the thermodynamic properties of water and oil phase, e.g. viscosity, bubble point and minimum miscibility pressures. At the same time, the adsorption of dopants in the core could happen during the experiment [28]. Details regarding to the above topics will be discussed in Chapter 3.

2.3.2 K-edge

K-edge, also called K-absorption edge, describes a sudden increase in the attenuation coefficient of photons, when the photoelectric adsorption happens to the K shell electron of the atoms [29]. Since each element has a unique distribution of atomic electrons, and the K shell has the highest binding energy, K-edge is normally used to identify various heavy metal contaminants and radioactive metals, e.g. thorium and uranium, in facilities of the deactivated and decommissioned weapons lab [30]. In the dual-energy CT scanning, in addition to the difference between the Compton and photoelectric cross section as shown in eq. (5), the K-edges of the heavy elements in the photoelectric region can also be utilized to increase the difference of CT numbers of various fluids under two energy levels. As shown in Figure 4, the change of the mass attenuation coefficient of pure soltrol®130 (a commercial mixture of C10−C13 isoalkanes produced by Chevron Philips Chemical Company [31]) around the K-edge energy (33.2keV) is much smaller than that of iododododecane/Soltrol®130 mixtures [25].

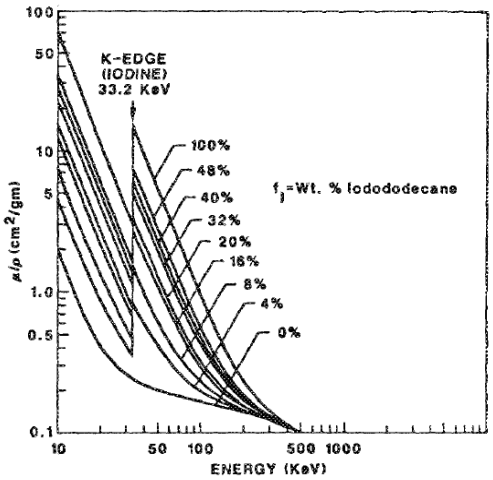

Figure 4 Mass attenuation coefficent vs energy for iodododecane/Soltrol mixtures [25]

Vinegar et al. [25] listed the K-edge energies for commonly used dopants in the core flooding experiments (see Table 1). Both Figure 4 and Table 1 indicate that the application of K edge could be quite limited in core flooding experiment, since the dual energy levels must be close enough to K-edge value to obtain the sudden increase in the CT numbers, which is difficult for medical CT scanner with fixed energy level choice. For example, the fourth generation Siemens SOMATOM scanner with three energy levels, 80kV, 120kV and 137kV. At the same time, K-edge values of most dopants are quite low. Therefore, when incident X ray with such low energy passes through the core material, only small amount of them could be transmitted, which has significant influence the image quality. The details on the above topics will be discussed in section 2.4.1.

Table 1 Dopants for brine, oil and gas phases [25]

	Dopants	K-edge (keV)
Brine phase	NaBr	13.2
	Na_2MoO_4	20.0
	NaI	33.2
	Na_2WO_4	69.5
	TlF	85.5
	Tl-EDTA	85.5
	$Pb(NO_3)_2$	88
	Pb-EDTA	88
	Bi-EDTA	90.5
Oil phase	Bromated oils	13.2
	Iodated oils	33.2
	$(C_2H_5)_4Pb$	88
	$(CH_3)_4Pb$	88
Gas phase	Krypton	14.3
	Xenon	34.6

2.4 Factors influencing the image quality

The most important aspect in CT scanning is to ensure good image quality, the following sub-sections will discuss artefacts which affect image quality and provide a few guidelines about the design of experiment and the selection of machine parameters.

2.4.1 Artefacts

Image artefacts are features, not present in the original object but in the CT image, which produced by the imaging process. It is one of the most important factors in downgrading the CT image quality. For a X-ray CT, the term 'Artefact' is defined as the difference between the CT number in CT image and the true attenuation coefficient of the objects.

In the area of medicine, artefacts are usually classified into four categories [19], physical-based artefacts, patient-based artefacts, scanner-based artefacts and helical and multi-section artefacts. In the application of CT scanner in the core analysis, the most noticeable and damaging one is the physical based artefact induced by the beam hardening.

Beam hardening exists because the X-ray beams from medical CT scanner are polychromatic with a moderately broad energy spectrum, as shown in the Figure 5 [32]. These polychromatic beams are hardened when they are transmitted through the material. Because the low-energy photons are more readily attenuated than the high-energy photons, beam hardening is the process of removing low-energy X-rays from the beam, which becomes harder and more penetrating.

The amount of beam hardening depends on the initial X-ray spectrum and the composition of the material traversed [33]. Images affected by the beam hardening are typically characterized with high attenuation coefficients around the periphery of the object and low attenuation coefficients in the center of the object. This artefact is also called 'Cupping artefacts '. In practice, a filter can be used to reduce the influence of beam hardening on the image.

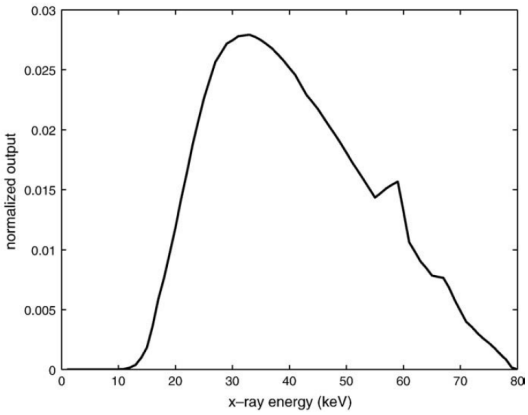

Figure 5 X-ray spectrum for tube voltage 80kV [32]

Besides beam hardening, photon starvation, which causes streak artefacts, has also significant influence on the image quality. The Photon starvation artefact arises because noise appears in some parts of individual projection due to the insufficient photons passing through the widest part of the materials [32]. This artefacts normally happens when the core or core holder are scanned vertically.

2.4.2 Design considerations

The most important in the design is to use the core holder made of aluminium or carbon fiber. Aluminium core holder can be used in the low pressure condition, and carbon fiber wrapped aluminium core holder is suitable for high pressure condition, because with increasing thickness of aluminium, more photons are absorbed by core holder before they enter the core plug.

Furthermore, to avoid the photon starvation artefacts, all measured objects should be round because the geometry of the scanner is circular. Since every object in the scan plane absorbs X-rays, the table should be made of wood and the diameter of the surrounding lines should be as small as possible, which could reduce the loss of photons as low as possible. Whenever the object is removed and later returned to the scanner, care must be taken to guarantee the object staying at its original position [22], which is especially important to the scanning on the highly heterogeneous cores.

2.4.3 Machine Parameters

2.4.3.1 The potential difference across the tube

The greater the potential difference across the tube (with unit kV), the faster the electrons move and the higher the energy of the X-ray photons. The average CT number of an object decreases with the increasing kV setting, and the quality of image is enhanced.

2.4.3.2 The output of the tube

The output of the tube is the product of mA (milliamps) and s (second). The higher the mA·s is, the greater the intensities of beam are, and correspondingly, the less noise is in the center of the object. The image quality therefore is enhanced with increasing output. On the other hand, the tube life is reduced.

2.4.3.3 Filtration

Filtration is an important tool to reduce the influence of beam hardening effects. It is normally a flat piece of attenuating metallic material used to sharpen the beam by filtering out the low energy components. In the core flooding experiment, the aluminium core holder itself, could serve as an additional filter to further harden the edges of the beam before it pass through the core material.

2.5 Applications of X-ray CT scanning in core analysis

X-ray CT has been applied in core analysis in the oil industry over thirty years [34]. Apart from medical application, the oil industry is probably the area which is most involved in CT. In the early time, researchers focused on the principle of X-ray CT scan and applied it in convenient areas, like visualization of two-phase flow in the porous media and core description, in the oil industry. Vinegar and Wellington at Shell Bellaire Research Center in the 1980s has made comprehensive study on the methodology and application of CT scanner in core flooding experiment, including the principle of x-ray CT scan [35], petrophysical application [36], and the methods for the determination of three-phase saturations with dual energy [37]. Later, Withjack et al. applied CT scanning in the determination of rock properties [38], the study of miscible displacement in the laboratory cores [38], and 3D physical models of a 5-Spot well pattern [39]. At the same time, Kantzas et al. also discussed the important issue of image reconstruction and demonstrated CT scanning for gas injection in porous media [40] and the local changes in the porosity of dry sand packs as a function of the imposed overburden [41]. Hunt et al. [42] and Withjack [43] published their literature study on the role of X-ray computed tomography in core analysis as the development of technology in oil industry. Nowadays, CT scanning has become a widely used core analysis tool and also been applied in newly developed areas, as gas hydrates and CO_2 sequestration in the coal mines.

The main objective of this section is to group many earlier studies and most recent researches on the application of CT scanning in the core analysis into several application catalogaries for convenient reference.

2.5.1 Core description

One of the applications of the core scanning is to provide quantitative information for mineral distribution and mud invasion, which can be used for the correlation with well log [44]. Gupta et al. [45] discussed the use of CT scanners as analytical tools in the recovery and stated that the spatial resolution of an industrial CT scanner designed for high-resolution application is adequate to resolve mineral distribution within a core. Honarpour et al. [46] applied the CT scanner in core characterization studies and presented the X-ray attenuation characterization of crystalline solids, randomly oriented mineral grains and preferentially oriented mineral solids, North Sea Danish chalk, and Wyoming Phosphoria formation core to study the reservoir heterogeneity. By using CT core structure visualization on the unconsolidated cores from the Alaskan North Slope, MacGregor et al. [47] developed a method to estimate the retrieval rates to minimize the core damage.

Another application is to study the fracture system by taking CT scan across a section of the fractured core. Bergosh et al. [48] demonstrated the use of CT scanning for fracture analysis on the full diameter whole core samples from Monterey Formation. Later, they also found that fracture porosity can be easily determined by the use of CT scanning [49]. Moss [50] proposed a method of dual-scan CT for measuring the constituent porosity in a dual porosity matrix. The paper illustrated the successful application of the method on the core samples from Monterey and Bakken shale, which was validated by the results from helium porosimetry.

The application of CT scanning in the analysis of vuggy carbonates was reported by Sprunt et al. [51] as early as 1980s. He discussed procedures and concerns regarding core analysis of heterogeneous rock, and found that due to the local vug-matrix heterogeneity and connectivity of vuggs, assumptions used in the core analysis to other types of rock could fail. Recently, Vik et al. [11] presented the vuggy carbonate rock characterization based on the Nuclear Magnetic Resonance (NMR), Micro Computed Tomography (μCT) and Computed Tomography (CT) measurement. The paper evaluates the different roles of three methods in the measurements of various petrophysical properties about the vuggy carbonates.

The contributions on standardizing CT techniques for quantitative analysis was made by Kantzas et al. [52] and Coles et al. [53][54]. Kantzas et al. [52] discussed the CT calibrations required to obtain bulk density, and the reliability of such determinations compared to conventional core analysis [43]. In the SCA (Society of Core Analysts) workshop on CT scanning (1994), Coles et al. [53] [54] discussed the accuracy and reliability of CT data from different labs and suggestions on the reference materials and calibration methods for CT laboratory.

2.5.2 Fundamental mechanisms

One advantage of using CT for core flooding experiment is to visualize the fluid movement, which could monitor the unsteady state displacement and improve further understanding of oil recovery mechanisms. In the early time, Cromwell et al. [55] used the first generation of CT scanner to analyze the fluid flow movement in the Danish chalk and Berea sandstones. Wang et al. [56] discussed the reconstruction of oil saturation distribution histories during immiscible liquid and liquid displacement by the use of CT scanners. Miscible displacements in heterogeneous core were addressed by Sorbie et al. [57]. Ekwere et al. [58] demonstrated the application of CT scanning on the investigation of the patterns of viscous fingering in core floods. The paper discussed the effect of flow rate on the viscous fingering and its random nature. The gravity-assisted inert gas injection in the long Berea core with using CT scanning was conducted by Chatzis et al. [59]. Oshita et al. [60] investigated the early water breakthrough in the oil-wet core with X-ray CT visualization. Displacement in the heterogeneous carbonate cores were reported by Oseto et al. [61] recently, and included visualization of the non-uniform flow field using 3D sectional views.

Foam flow in porous media has been investigated by Nguyen et al. [62] under the conditions that are relevant for acid diversion induced by foam. The experiments were conducted using Bentheim and Berea sandstone cores and nitrogen foam and the fluid partitioning was determined by CT scanning. Later, they [63] continued the experiment in isolated and capillary-communicating double layer cores to investigate the effect of crossflow on Foam-induced diversion in layered formations. At the same time, Zitha et al. [64] and Du et al. [65] also conducted the experiments on the influence of flow velocity and core heterogeneity on foam flow media and carbon dioxide foam rheology in the Bentheim and Berea sandstone cores.

2.5.3 Improved oil recovery

In the early time, Hove et al. [66] demonstrated the application of CT scanning for enhanced oil recovery by Xanthan polymer flooding. This work illustrated the injection of polymers can improve the areal sweep efficiency of water flooding and studied the behavior of biopolymer flood in heterogeneous Rosbra sandstone. The influence of minimum miscible pressure on the behavior of foaming agent (alpha olefin sulfonate, AOS) in the CO_2 injection is reported by Farajzadeh et al. [67]. This work demonstrated the monitoring of foam movement and its contact with oil in Bentheimer sandstone. Gupta et al. [68] conducted CT monitored experiment to evaluate the performance of a biodegradable surfactant (Glucopon-425N) in recovering a residually trapped dense non-aqueous phase liquid from sand packs. Gabitto et al. [69] reported on the use of CT scanning on demonstrating the effect of mobility control and oil production through a core flooded by surfactant-polymer mixture. In the report several surfactant solution were tested in the flooding experiment to find out the inexpensive one with efficient tertiary oil recovery.

2.5.4 Formation damage

The formation of scale caused by mineral precipitation is considered as one of the most commonly occurring formation damage mechanisms in reservoir rock pores [43]. Aliaga et al. [70] performed early CT studies to monitor the formation and migration of barium sulfate in the sand pack and investigate the permeability reduction mechanisms caused by the mineral precipitates. Krilov et al. [71] used CT to measure the invasion depths of barite solids penetration and study the permeability reduction due to filter cake formation. The shell swelling due to the interaction between drilling mud and shale was investigated by Cook et al. [72]. Three kinds of mud were used to react with Pierre1 shale and CT scanning was employed to visualize the swollen zone. Later, they [73] studied the influence of bedding plane orientation on shell swelling, using CT to monitor the damage in a model wellbore geometry.

2.5.5 Dual energy scanning

Visualization of flow experiments involves three mobile phases by dual-energy scanning was first presented by Vinegar and Wellington [25]. They developed the relevant equations, proposed the application of K-edge in selecting dopants and provided the candidate of dopants used in the different phases. They concluded that, for photon energies above 100keV, X-ray interact with matter was dominated by Compton scattering, which is dependent on electron density. For X-ray energy

below 100keV, on the other hand, photo electric adsorption becomes important. This type is strongly dependent on atomic number. In the paper, they demonstrated the use of sodium tungstate and iododododecane in the CO_2 flooding under two different energies (90kV and 140kV). Later, Chatzis et al. [40] used the CT scanner to study the physical properties of porous media and saturation profiles during two- and three-phase flow systems. For three-phase flow, however, the visualization was only qualitatively. Sahni et al. [74] used dual energy scanning to measure the three-phase relative permeability during the gravity drainage. In this work, only brine was doped with 10% sodium bromide, due to the low pressure condition of experiments. Later, Akervoll et al. [75] was successful on performing history matching on water-alternated-gas (WAG) experiment with in situ saturation measurements by dual energy scanning at reservoir conditions. In this work, sodium tungstate and iododododecane was used to dope water and oil respectively. The detailed discussion is available in the Chapter 3.

2.5.6 Geochemical reaction

In the reservoir, acid solution is typically used for scale removal and dissolving the formation matrix to stimulate the reservoir. The application of CT on the quantitative analysis of porosity change due to the acid treatment was first reported by Bartko et al. [76]. Bazin et al. [77] analyzed the factors that affect the growth of wormholes in the matrix during the carbonate acidizing by using CT scanning, and their work confirmed industry accepted relationship between applied pressure differential and acid wormhole growth [43]. Recently, Al-Ghamdi [78] investigated the questions regarding how diversion occurs as surfactant-acid mixed solution flow inside the carbonate reservoir and what are the parameters controlling the diverting process, using CT scanning to generate 3-D images to describe the shape of wormhole. To deal with global warming, CO_2 sequestration into reservoir becomes attractive and the chemical reaction between dissolved CO_2 and the rock formation is important for the storage of CO_2. Izgec et al. [79] demonstrated the use of CT to monitor the change of porosity due to the geochemical reactions. This work investigated various factors, including temperature, salinity and injection rate, effect of heterogeneity and pH, on the dissolve of carbonate rocks.

2.5.7 Viscous oil

Heavy oil is regarded as unconventional resource because of the difficulties and cost involved in its production. However, due to the increasing oil price, it becomes popular again. History matching of steam floods with CT monitored in situ saturations was carried out by Cuthiell et al. [80] to derive capillary pressure models. Kewen et al. [81] used CT to study the mathematical model of steam-

water capillary pressure. Tang et al. [82] demonstrated the application of CT scan in the heavy oil solution gas drive to monitor the in situ gas saturation. In this work, the effect of heavy oils with different compositions and various injection pressures on gas saturation distribution in the sand pack were evaluated. A novel method to estimate relative permeability and capillary pressure from in situ aqueous-phase saturation profiles obtained from CT scanning during high-temperature imbibitions experiments was proposed by Schembre et al. [83]. To understand the foamy-oil properties during pressure depletes in the live heavy-oil, Goodarzi et al. [84] suggested a novel technique by use of CT scanning and low field nuclear magnetic resonance (NMR) techniques. Luo et al. [85] [13] reported a method to measure the mutual diffusion coefficient of heavy oil and Hydrocarbon system solvent system in the room temperature and pressure. They initially focused on the effect of volume change due to the mixing on diffusion coefficient of the system without considering porous media, and extend the experiments to heavy oil saturated sand.

2.5.8 Gas hydrate

Natural gas hydrates can hold significant amount of methane, which accounts for an immense resource conservatively estimated to be twice the amount of energy stored in other fossil fuels [43]. Tomutsa et al. [86] reported the use of CT scanning to resolve the reduction in density of the hydrate/sand aggregate due to the dissociation of methane hydrate spatially, with validation from gas flow and temperature measurements.

2.5.9 CO_2 sequestration in coal bed

Sequestrating CO_2 in coal beds, as an attractive option for geological sequestration of CO_2, could enhance methane production and trap CO_2 for long periods of time. Therefore, measurements of sorption isotherms and transport properties of CO_2 in coal cores are important. Jikich et al. [87] recently demonstrated the use of CT on calculating density variations and CO_2 concentrations, sorption, and transport rate in the coal cores at reservoir confining pressure. This work illustrates the application of dual energy CT scanning to calculate average slice density increased during the CO_2 intake periods.

Reference

[1] P. V. Meurs, “The Use of Transport Three-Dimensional Models for Studying the Mechanism of Flow Processes in Oil Reservoirs,” *Petroleum Transactions, AIME*, vol. 210, pp. 295–301, 1957.

[2] M. C. Leverett, “Flow of Oil-Water Mixtures through Unconsolidated Sands,” *Petroleum Transactions, AIME*, vol. 132, pp. 149–171, 1939.

[3] J. Whalen, “A Magnetic Susceptibility Method for the Determination of Liquid Saturation in Porous Materials,” *Journal of Petroleum Technology*, vol. 6, no. 9, pp. 111–116, September 1954.

[4] D. Saraf and I. Fatt, “Three-Phase Relative Permeability Measurement Using a Nuclear Magnetic Resonance Technique for Estimating Fluid Saturation,” *SPE Journal*, vol. 7, no. 3, pp. 235–242, September 1967.

[5] R. L. Boyer, F. Morgan, and M. Muskat, “A New Method for Measurement of Oil Saturation in Cores,” *Petroleum Transactions, AIME*, vol. 170, pp. 15–33, 1947.

[6] A. D. K. Laird and J. A. Putnam, “Fluid Saturation in Porous Media by X-Ray Technique,” *Petroleum Transactions, AIME*, vol. 192, pp. 275–284, 1951.

[7] R. L. Slobod and B. H. Caudle, “X-Ray Shadowgraph Studies of Areal Sweepout Efficiencies,” *Petroleum Transactions, AIME*, vol. 195, pp. 265–270, 1952.

[8] R. W. Parsons, “Microwave Attenuation - A New Tool for Monitoring Saturations in Laboratory Flooding Experiments,” *SPE Journal*, vol. 15, no. 4, pp. 302–310, August 1975.

[9] S. Siddiqui and A. A. Khamees. (2004, 26-29 September) Dual-Engergy CT-Scanning Applications in Rock Characterization. Paper SPE 90520 presented at the SPE Annual Technical Conference and Exhibition, Houston, Texas.

[10] P. J. Hicks, “X-Ray Computer-Assisted Tomography for Laboratory Core Studies,” *Journal of Petroleum Technology*, vol. 48, no. 12, pp. 1120–1122, December 1996.

[11] B. Vik, K. Djurhuus, K. Spildo, and A. Skauge. (2007, 28-31 October) Characterisation of Vuggy Carbonates. Paper SPE 111434 presented at the SPE/EAGE Reservoir Characterization and Simulation Conference, Abu Dhabi, UAE.

[12] A. Sahni, F. Gadelle, M. Kumur, A. Kovscek, and L. Tomusta. (2001, 30 September-3 October 2001) Experiments and Analysis of Heavy Oil Solution Gas Drive. Paper SPE 71498 presented at the SPE Annual Technical Conference and Exhibition, New Orleans, Louisiana.

[13] H. Luo and A. Kantzas. (2008, 20-23 April) Investigation of Diffusion Coefficients of Heavy Oil and Hydrocarbon Solvent Systems in Porous Media. Paper SPE 113995 presented at the SPE/DOE Symposium on Improved Oil Recovery, Tulsa, Oklahoma, USA.

[14] http://en.wikipedia.org/wiki/X-ray_computed_tomography.

[15] A. G. Filler. (2009, July) The History, Development and Impact of Computed Imaging in Neurological Diagnosis and Neurosurgery: CT, MRI, and DTI.
http://precedings.nature.com/documents/3267/version/5.

[16] http://www.imaginis.com/ct scan/history.asp.

[17] http://www.medcyclopaedia.com/library/topics/volume_i/c/ct_generation.aspx.

[18] http://www.impactscan.org/slides/xrayct/.

[19] J. F. Barrett and N. Keat, “Artefacts in CT: Recognition and Avoidance,” *RadioGraphics*, vol. 24, pp. 1679–1691, November 2004.

[20] G. N. Hounsfield, “Computerized Transverse Axial Scanning (Tomography): Part 1. Description of System,” *British Journal of Radiology*, vol. 46, pp. 1016–102, 1973.

[21] R. S. Ledley, G. D. Chiro, A. J. Luessenhop, and H. L. Twigg, “Computerized Transaxial X-Ray Tomography of the Human Body,” *Science*, vol. 186, no. 4160, pp. 207–212, October 1974.

[22] K. Mogensen, *CT User’s Guide: How to Use X-ray Computed Tomography in Core Analysis of Tight North Sea Chalk*, Engineering Research Center (IVC-SEP), Department of Chemical Engineering, Technical University of Denmark, August 1997.

[23] J. Burger, *CT Development Guide*, Department of Petroleum Engineering, Stanford University, January 1996.

[24] E. McCullough, "Photon Attenuation in Computed Tomography," *Medical Physics*, vol. 2, pp. 307–320, 1975.

[25] H. J. Vinegar and S. L. Wellington, "Tomographic Imaging of Three-Phase Flow Experiment," *Rev.Sci.Instrum.*, vol. 58, pp. 96–107, January 1987.

[26] S. YU, I. Akervo, O. Torsaeter, J. Stensen, J. Kleppe, and S. Micftlyng. (1998, 2-6 November) History Matching Gas Injection Processes with In Situ Saturation Measurements and Process Hysteresis. Paper SPE 488421 presented at the SPE International Oil and Gas Conference and Exhibition in China, Beijing, China.

[27] T. V. Nguyen and C. E. Stevens. (1988, 23-25 March) The Use of Inert Gas Radioactive Tracers for Steam Injection Profiling. Paper SPE 17419 presented at the SPE California Regional Meeting, Long Beach, California.

[28] B. Niu, W. Yan, A. A. Shapiro, and E. H. Stenby. (2009, 27-30 September) Phase Identification and Saturation Determination in Carbon Dioxide Flooding of Water Flooded Chalk using X-Ray Computed Tomography. Paper SCA2009-19 presented at the the International Symposium of the Society of Core Analysts held in Noordwijk, The Netherlands.

[29] http://www.medcyclopaedia.com/library/topics/volume_i/k/k_edge.aspx.

[30] T. Jensen, T. Aljundi, and J. N. Gray. (1998, 13-18 September) Application of X-Ray K-Edge Densitometry in D&D Operation. Presented at the International Conference on Decommissioning and Decontamination (Spectrum '98), Denver, Colorado.

[31] http://www.cpchem.com/enu/specialty_chemicals_p_hydrocarbons.asp.

[32] F. Meng, N. Zhang, and W. Wang, "Virtual Experimentation of Beam Hardening Effect in X-Ray CT Measurement of Multiphase Flow," *Powder Technology*, vol. 194, pp. 153–157, 2009.

[33] M. Yazdi and L. Beaulieu, “Artefacts in Spiral X-Ray CT Scanners: Problems and Solutions,” *International Journal of Biological and Medical Sciences*, vol. 4, no. 3, pp. 135–139, 2009.

[34] A. Kantzas, “Investigation of Physical Properties of Porous Rocks and Fluid Flow Phenomena in Porous Media Using Computer Assisted Tomography,” *In Situ*, vol. 14, no. 1, pp. 77–132, 1990.

[35] S. L. Wellington and H. J. Vinegar, “X-Ray Computerized Tomography,” *Journal of Petroleum Technology*, vol. 39, no. 8, pp. 885–898, August 1987.

[36] H. Vinegar, “X-Ray CT and NMR Imaging of Rocks,” *Journal of Petroleum Technology*, vol. 38, no. 3, pp. 257–259, March 1986.

[37] S. L. Wellington and H. J. Vinegar. (1985, 22-26 September) CT Studies of Surfactant-Induced CO_2 Mobility Control. Paper SPE 14393 presented at the SPE Annual Technical Conference and Exhibition, Las Vegas, Nevada.

[38] E. M. Withjack, “Computed Tomography for Rock-Property Determination and Fluid-Flow Visualization,” *SPE Formation Evaluation*, vol. 3, no. 4, pp. 696–704, December 1988.

[39] E. M. Withjack and I. Akervoll. (1988, 2-5 October) Computed Tomography Studies of 3-D Miscible Displacement Behavior in a Laboratory Five-Spot Model. Paper SPE 18906 presented at the SPE Annual Technical Conference and Exhibition, Houston, Texas.

[40] I. Chatzis, A. Kantzas, and F. A. L. Dullien. (1988, 2-5 October) On the Investigation of Gravity-Assisted Inert Gas Injection Using Micromodels, Long Berea Sandstone Cores, and Computer-Assisted Tomography. Paper SPE 18284 presented at the SPE Annual Technical Conference and Exhibition, Houston, Texas.

[41] A. Kantzas, L. Rothenburg, and S. V. L. Barrett. (1992, 26-27 February) Determination of Stress-Strain Characteristics of Sand Packs under Uniform Loads by the Use of Computer-Assisted Tomography and Finite Element Modelling. Paper SPE 23791 presented at the SPE Formation Damage Control Symposium, Lafayette, Louisiana.

[42] P. K. Hunt, P. Engler, and C. Bajsarowicz, “Computed Tomography as a Core Analysis Tool: Applications, Instrument Evaluation, and Image Improvement Techniques,” *Journal of Petroleum Technology*, vol. 40, no. 8, pp. 1203–1210, September 1988.

[43] E. Withjack, C. Devier, and G. Michael. (2003, 19-24 May) The Role of X-Ray Computed Tomography in Core Analysis. Paper SPE 83467 presented at the SPE Western Regional/AAPG Pacific Section Joint Meeting, Long Beach, California.

[44] P. K. Hunt, P. Engler, and C. Bajsarowicz, “Computed Tomography as A Core Analysis Tool: Applications, Instrument Evaluation, and Image Improvement Techniques,” *Journal of Petroleum Technology*, vol. 40, no. 9, pp. 1203–1210, September 1988.

[45] N. K. Gupta. (1986, 29 September - 3 October) Computerd Tomography as an Analytiacl Tool in Oil Recovery. Presented at the 1986 Fall Conference of the American society for Non-Destructive Testing, New Orleans, Louisiana.

[46] M. M. Honarpour, V. Cromwell, D. Hatton, and R. Satchwell. (1995, 22-26 September) Reservoir Rock Descriptions Using Computed Tomography (ct). Paper SPE 14272 presented at the SPE Annual Technical Conference and Exhibition, Las Vegas, Nevada.

[47] K. W. MacGregor, E. I. Park, K. J. Sincock, and E. J. Piekenbrock. (1991, 29-31 May) Effective Unconsolidated Core Preservation in the Arctic Environment: An Aid to Accurate Reservoir Evaluation. Paper SPE 22128 presented at the International Arctic Technology Conference, Anchorage, Alaska.

[48] J. L. Bergosh, T. R. Marks, and A. F. Mitkus. (1985, 27-29 March) New Core Analysis Techniques for Naturally Fractured Reservoirs. Paper SPE 13653 presented at the SPE California Regional Meeting, Bakersfield, California.

[49] J. L. Bergosh and G. D. Lord. (1987, 27-30 September) New Developments in the Analysis of Cores from Naturally Fractured Reservoirs. Paper SPE 16805 presented at the SPE Annual Technical Conference and Exhibition, Dallas, Texas.

[50] R. M. Moss, G. P. Pepin, and L. A. Davis. (1990, 15-16 August) Direct Measurement of the Constituent Porosities in a Dual Porosity Matrix. Paper 9003 presented at the Fourth Annual Technical Conference of the Society of core analysts, Dallas.

[51] E. S. Sprunt, "Arun Core Analysis: Special Procedures for Vuggy Carbonates," *The Log Analyst*, vol. 30, no. 5, pp. 353–362, September - October 1989.

[52] A. Kantzas, D. F. Marentette, and K. N. Jha, "Computer-Assisted Tomograhy: from Qualitative Visualization to Quantitative Core Analysis," *JCPT*, vol. 31, no. 9, pp. 48–56, November 1992.

[53] M. E. Coles, P. Spanne, E. L. Muegge, and K. W. Jones. (1994, 12-14 September) Computed Microtomography of Reservoir Core Samples. Paper 9401 presented at the CT Workshop, Society of Core Analysts.

[54] M. E. Coles, E. L. Muegge, F. M. Auzeraia, P. Phrulla, and A. Kantas. (1995, 12-14 September) Use of Attenuation Standards for CT Scanning. Paper 9513 presented at the Society of Core Analysts Conference.

[55] V. Cromwell, D. J. Kortum, and D. J. Bradle. (1984, 16-19 September) The use of a Medical Computer Tomography (CT) System to Observe Multiphase Flow in Porous Media. Paper SPE 13098 presented at the SPE Annual Technical Conference and Exhibition, Houston, Texas.

[56] S. Y. Wang, A. Seyda, and C. C. Gryte, "Computer-Assisted Tomography for the Observation of Oil Displacement in Porous Media," *SPE Journal*, vol. 24, no. 1, pp. 53–55, February 1984.

[57] K. Sorbie, R. M. S. Wat, A. O.Hove, V. Nilsen, and J. Leknes. (1989, 8-10 February) Miscible Displacements in Heterogeneous Core Systems: Tomographic Confirmation of Flow Mechanisms. Paper SPE 18493 presented at the SPE International Symposium on Oilfield Chemistry, Houston, Texas.

[58] P. Ekwere, J. A. Broman and H. William, "Computer Image Processing: A New Tool for Studying Viscous Fingering in Corefloods," *SPE Reservoir Engineering*, vol. 2, no. 4, pp. 720–728, November 1987.

[59] I. Chatzis, A. Kantzas, and F. A. L. Dullien. (1988, 2-5 October) On the Investigation of Gravity-Assisted Inert Gas Injection Using Micromodels, Long Lerea Sandstone Cores, and Computer-Assisted Tomography. Paper SPE 18284 presented at the SPE Annual Technical Conference and Exhibition, Houston, Texas.

[60] T. Oshita, H. Okabe, and T. Namba. (2000, 25-26 April) Early Water Breakthrough: X-Ray CT Visualizes How It Happens in Oil-Wet Cores. Paper SPE 59426 presented at the SPE Asia Pacific Conference on Integrated Modelling for Asset Management, Yokohama, Japan.

[61] K. Oseto, A. Al-Amoudi, and M. Suzuki. (2006, 5-8 November) Comprehensive Approach of Core Analysis to Predict Waterflooding Performance in a Heterogeneous Carbonate Reservoir, Offshore Abu Dhabi. Paper SPE 101287 presented at the Abu Dhabi International Petroleum Exhibition and Conference, Abu Dhabi, UAE.

[62] Q. P. Nguyen, P. K. Currie, and P. L. Zitha. (2003, 5-7 February) Determination of Foam Induced Fluid Partitioning in Porous Media Using X-Ray Computed Tomography. Paper SPE 80245 presented at the International Symposium on Oilfield Chemistry, Houston, Texas.

[63] Q. P. Nguyen, P. K. Currie, and P. L. Zitha, "Effect of Crossflow on Foam-Induced Diversion in Layered Formations," *SPE Journal*, vol. 10, no. 1, pp. 54–65, March 2005.

[64] P. L. Zitha, Q. P. Nguyen, and P. K. Currie. (2003, 9-11 September) Effect of Flow Velocity and Rock Layering on Foam Flow: An X-Ray Computed Tomography Study. Paper SPE 80530 presented at the SPE Asia Pacific Oil and Gas Conference and Exhibition, Jakarta, Indonesia.

[65] D. Du, P. L. Zitha, and M. G. Uijttenhout, "Carbon Dioxide Foam Rheology in Porous Media: A CT Scan Study," *SPE Journal*, vol. 12, no. 2, pp. 245–252, June 2007.

[66] A. O. Hove, V. Nilsen, and J. Leknes, "Visualization of Xanthan Flood Behavior in Core Samples by Means of X-Ray Tomography," *SPE Reservoir Engineering*, vol. 5, no. 4, pp. 475–480, November 1990.

[67] R. Farajzadeh, A. Andrianov, and P. L. J. Zitha, "Investigation of Immiscible and Miscible Foam for Enhancing Oil Recovery," *Industrial & Engineering Chemistry Research*, 2009.

[68] D. K. Gupta and K. K. Mohanty, "A Laboratory Study of Surfactant Flushing of DNAPL in the Presence of Macroemulsion," *Environ. Sci. Technol.*, vol. 35, no. 13, pp. 2836–2843, May 2001.

[69] J. Gabitto and K. K. Mohanty, "Surfactant-Polymer Interaction for Improved Oil Recovery," National Petroleum Technology Office, Tulsa, OK (US), Technical Report FG22-96PC96223, 07 January 2002.

[70] D. A. Aliaga, G. Wu, M. M. Sharma, and L. W. Lake, "Barium and Calcium Sulfate Precipitation and Migration Inside Sandpacks," *SPE Formation Evaluation*, vol. 7, no. 1, pp. 79–86, March 1992.

[71] Z. Krilov, I. Steiner, B. Goricnik, A. J. Wojtanowicz, and S. Cabrajac. (1991, 3-6 September) Quantitative Determination of Solids Invasion and Formation Damage Using CAT Scan and Barite Suspensions. Paper SPE 23102 presented at the offshore Europe Aberdeen, United Kingdom.

[72] J. M. Cook, G. Goldsmith, T. Geehan, A. M. Audibert, and J. Lecourtier. (1993, 22-25 February) Mud/Shale Interaction: Model Wellbore Studies Using X-Ray Tomography. Paper SPE 25729 presented at the SPE/IADC Drilling Conference, Amsterdam, Netherlands.

[73] J. M. Cook, G. Goldsmith, L. Bailey, A. M. Audibert, and M. Bieber. (1994, 29-31 August) X-Ray Tomographic Study of the Influence of Bedding Plane Orientation on Shale Swelling. Paper SPE 28061 presented at the Rock Mechanics in Petroleum Engineering, Delft, Netherlands.

[74] J. B. Akshay Sahni and M. Blunt. (1998, 19-22 April) Measurement of Three Phase Relative Permeability during Gravity Drainage Using CT Scanning. Paper SPE 39655 presented at the SPE/DOE Improved Oil Recovery Symposium, Tulsa, Oklahoma.

[75] I. Akervoll, M. Talukdar, S. Midtlyng, J. Stensen, and O. Torsaeter. (2000, 3-5 April) WAG Injection Experiments with In Situ Saturation Measurements at Reservoir Conditions and Simulations. Paper SPE 59323 presented at the SPE/DOE Improved Oil Recovery Symposium, Tulsa, Oklahoma.

[76] K. M. Bartko, D. P. Newhouse, C. A. Andersen, and R. J. Treinen. (1995, 22-25 October) The Use of CT Scanning in the Investigation of Acid Damage to Sandstone Core. Paper 2000-061 presented at the Canadian International Petroleum Conference, Calgary, Alberta.

[77] B. Bazin, M. Bieber, C. Roque, and M. Bouteca. (1996, 14-15 February) Improvement in the Characterization of Acid Wormholing by In Situ X-Ray CT Visualizations. Paper SPE 31073 presented at the SPE Formation Damage Control Symposium, Lafayette, Louisiana.

[78] A. H. Al-Ghamdi, M. A. Mahmoud, A. D. Hill, and H. A. Nasr-El-Din. (2009, 20-22 April) Diversion and Propagation of Viscoelastic Surfactant Based Acid in Carbonate Cores. Paper SPE 121713 presented at the SPE International Symposium on Oilfield Chemistry, The Woodlands, Texas.

[79] O. Izgec, B. Demiral, H. Bertin, and S. Akin. (2005, 30 March-01 April) CO_2 Injection in Carbonates. Paper SPE 93773 presented at the SPE Western Regional Meeting, Irvine, California.

[80] D. Cuthiell, G. Sedgwick, G. Kissel, and J. Woolley, "Steam Corefloods with Concurrent X-Ray CT Imaging," *JCPT*, vol. 32, no. 3, pp. 37–45, 1993.

[81] K. Li and R. N. Horne. (2000, 1-4 October) Steam-Water Capillary Pressure. Paper SPE 63224 presented at the SPE Annual Technical Conference and Exhibition, Dallas, Texas.

[82] G. Tang, T. Leung, L. Castanier, A. Sahni, F. Gadelle, M. Kunar, and A. Kovscek, "An Investigation of the Effect of Oil Composition on Heavy Oil Solution-Gas Drive," *SPE Journal*, vol. 11, no. 1, pp. 58–70, March 2006.

[83] J. Schembre, G. Q. Tang, and A. Kovscek, "Interrelationship of Temperature and Wettability on the Relative Permeability of Heavy Oil in Diatomaceous Rocks," *SPE Reservoir Evaluation & Engineering*, vol. 9, no. 3, pp. 239–250, June 2006.

[84] N. Goodarzi, J. Bryan, A. Mai, and A. Kantzas, "Novel Techniques for Measuring Heavy-Oil Fluid Properties," *SPE Journal*, vol. 12, no. 3, pp. 305–315, September 2007.

[85] H. Luo, D. Salama, S. Kryuchkov, and A. Kantzas. (2007, 11-14 November) The Effect of Volume Changes due to Mixing on Diffusion Coefficient Determination in Heavy Oil and Hydrocarbon Solvent System. Paper SPE 110522 presented at the SPE Annual Technical Conference and Exhibition, Anaheim, California, U.S.A.

[86] L. Tomutsa, B. Freifeld, T. J. Kneafsey, and L. A. Stern. (2002, 30 April-2 May) X-Ray Computed Tomography Observation of Methane Hydrate Dissociation. Paper SPE 75533 presented at the SPE Gas Technology Symposium, Calgary, Alberta, Canada.

[87] S. A. Jikich, R. McLendon, K. Seshadri, G. Irdi, and D. H. Smith, "Carbon Dioxide Transport and Sorption Behaviour in Confined Coal Cores for Enhanced Coalbed Methane and CO_2 Sequestration," *SPE Reservoir Evaluation & Engineering*, vol. 12, no. 1, pp. 124–136, February 2009.

Chapter 3. Experiments on Carbon Dioxide Flooding with the Application of CT Scanning

3.1 Introduction

Carbon dioxide injection into petroleum reservoirs has been considered for enhanced oil recovery (EOR) since early 1950's [1] and regarded as one of the most important EOR processes in U.S. carbonate reservoirs since the early 1980's [1]. Interest in this process has grown recently also due to other reasons, including (1) to reduce the emission of CO_2 to the atmosphere to mitigate the global warming and (2) to release hydrocarbon gas used in gas injection for sales to meet the growing demand in the world market [2]. This process is characterized by complex phase behavior and interaction between different phases: oil, water and CO_2. The mechanisms of multiphase flow and thermodynamic properties of various phases have been extensively discussed by many researchers, both theoretically [4] and experimentally [5].

In realistic conditions, the displacement efficiency of CO_2 flooding is mainly affected by the development of miscibility between the injected CO_2 and reservoir oil. During the flooding process, a continuous mass transfer takes place between the injected CO_2 and the initial reservoir oil, and a miscible zone is formed in between and displaced through the reservoir. Factors that affect the achievement of miscibility and displacement efficiency have been experimentally investigated extensively. Shyeh-Yung [6] evaluated the effects of pressures below and above the minimum miscibility pressure (MMP) on miscible and near-miscible displacements of oil by CO_2 flooding in Berea sandstone and suggested that both displacement and extraction of oil by CO_2 increase with increasing pressure. Holm et al. [7] studied the effect of oil composition on the displacement process and concluded that MMP increases with the decrease in oil API, the asphaltene content and the extractable hydrocarbons (C_5-C_{30}) in reservoir oil. The role of phase behavior and fluid properties are reported by Metcalfe et al. [8] and Rosman [9] respectively. The former conducted experiments at immiscible, multicontact miscible and first contact miscible conditions to demonstrate the relationship between phase behavior and oil recovery in CO_2 flooding. The latter showed that the decrease in interfacial tension (IFT) between CO_2 and oil phase results in increase of oil recovery. For a thorough literature review, paper from Shawket [10] is recommended, who cites over 80 references on global laboratory experience of CO_2-EOR flooding.

CT scanning, as an effective core analysis tool, has also been applied extensively in different experiments on CO_2 flooding. Wellington et al. [35] conducted six tertiary CO_2 core flooding by use of

X-ray CT to study the difference between immiscible and miscible displacements and the effects of gravity, viscous, and capillary forces on oil recovery. CT studies of surfactant-induced CO_2 mobility control was also reported by Wellington et al. [37]. CT images in this paper show that surfactants in the brine prevent the gravity and viscous instability, and enable CO_2 to displace oil from cores in a piston-like manner. Yamamoto et al. [13] conducted core flood tests to investigate the influence of layered reservoir with different permeabilities on CO_2 WAG process with the aids of CT scanner. CT monitored experiments on carbonate rock, designed to model fast near wellbore flow and slow reservoir flows, were conducted by Izgec et al. [79]. It was observed that the decrease of porosity and permeability induced by salt was less pronounced for low injection rate cases. Zitha et al. [64] and Du et al. [65] also conducted the experiments on the influence of flow velocity and core heterogeneity on foam flow media and carbon dioxide foam rheology in the Bentheim and Berea sandstone cores. However, in situ visualization of flooding process is still rare. The in situ identification of different phases and determination of their distributions in core flooding experiments by the application of X-ray computed tomography (CT) are needed since they can provide useful information for understanding the process of CO_2 flooding and future simulation.

The existing application of CT on in situ phase identification and saturation determination mainly focused on two-phase systems, e.g., oil and water [60], oil and gas [18], and gas and water [79]. The limited studies on phase identification in three-phase flooding either do not illustrate in situ saturation measurements or conduct the experiments at low pressure condition to keep gas at low density, which does not represent reservoir conditions. Vinegar et al. [25] discussed the mechanisms of X-ray CT scanner, properties of the dopants, and three-phase flow study, but without detailed analysis of the three-phase in situ saturations. Kantzas [34] and Chatzis et al. [40] applied X-ray CT to study the physical properties of porous media and saturation profiles during two- and three-phase flow in gravity-assisted displacement processes, with qualitatively visualizations of three-phase fluid distributions. Lackner et al. [22] investigated X-ray energy levels for three-phase saturation measurements and conducted three-phase experiments under low pressure, without analysis of phase saturations. Sahni et al. [23] measured three-phase relative permeability during the gravity drainage by using X-ray CT. In their study, three-phase in situ saturations were measured and only brine was doped with sodium bromide (NaBr), due to the low pressure condition of experiments. At the same time, there is almost no open discussion on the three-phase measurements in the chalk core, especially on the low permeable chalks at reservoir conditions.

This chapter consists of three major sections, in addition to the introduction and the conclusion. In section 3.2, two experimental set-ups for flooding experiments both at low and middle pressure, and at high pressure, will be described. Both flooding set-ups are designed for flooding with CT scanning. In section 3.3 some trial experiments on in situ phase identification and saturation determination will be introduced and discussed. In section 3.4, we present a method to quantitatively calculate the in situ saturation of gas phase in the carbon dioxide flooding of the water flooded low permeable chalk under deep reservoir conditions by using the X-ray CT and the applications of this method on North Sea chalk with live oil are discussed.

3.2 Experimental equipments

3.2.1 The general overview of experimental setup

The whole experimental setup was designed and built by the author, aiming at the quantitative measurement of in situ phase saturation with use of CT scanner and accurately recording the produced fluids and differential pressure across the core dynamically. As shown in Figure 6, the whole setup for high pressure experiments includes three-phase separator, differential pressure transducer, back pressure regulator (BPR), gas meter and recording system. The carbon fiber wrapped core holder, especially designed for high pressure and temperature experiments, is wrapped by insulating foam to reduce the heat loss so that a high temperature can be easily kept. The differential pressure transducer is VEGABAR® 17 pressure transmitter, which has maximum range as 22 bar and maximum working pressure 860 bar at room temperature. The BPR can work from room condition to harsh reservoir conditions (200 ^{o}C and 1000 bar). All equipments used for measuring pressure have been calibrated by a standard pressure gauge, METTLE 26000 M, before the start of experiments. The injection rate, injection pressure and differential pressure across the core can be recorded by a PC. The amounts of produced gas and oil are manually recorded. Frequent manual recording of the oil and gas production is necessary since the produced volumes are relatively small.

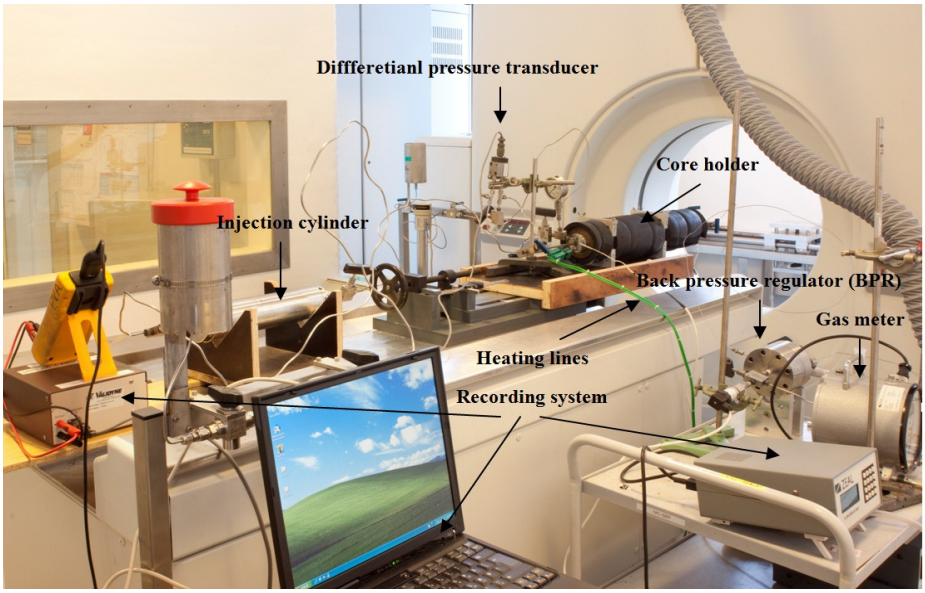

Figure 6 Core flooding setup with X-ray scanning

The experimental setup for high pressure experiments is shown schematically in Figure 7. The inlet of the core holder is connected to an injection cylinder driven by an ISCO-pump. The outlet of the core holder is connected to a three-phase separator through a BPR .The BPR is used toy keep the core flooding at reservoir pressure and the separation of the produced fluids happens in the separator at atmospheric pressure. The pump is used to inject various fluids at constant rate. To protect the core at the reservoir conditions, aluminium or copper filters were used at both ends of the core.

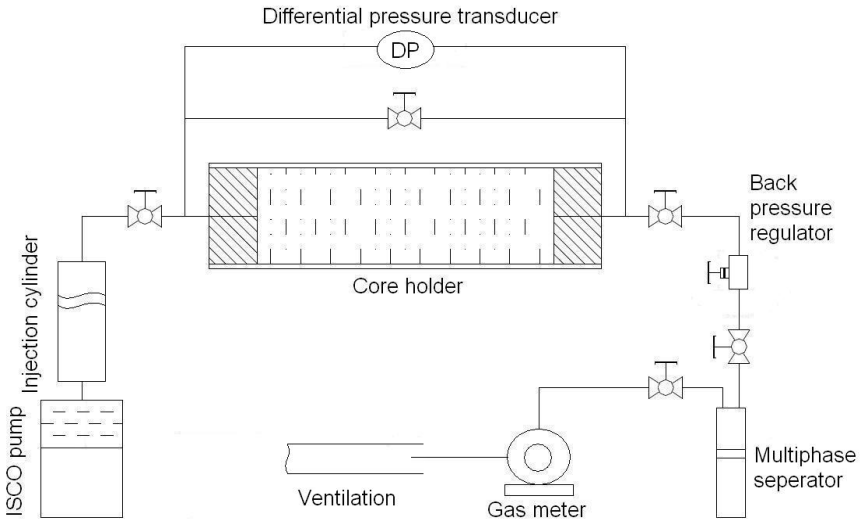

Figure 7 Schematic of the experimental setup

The main difference between the experimental setup at low and middle pressure, and at high pressure is that for experiments at low and middle pressure, the core aluminium core holder was used instead of carbon fiber wrapped core holder. An aluminium core holder with a maximum operation pressure of 100 bar can only work at the room temperature (Figure 8). The carbon fiber wrapped core holder, with a maximum operation pressure of 1000 bar can work up to maximum temperature of 150 ^{o}C (Figure 9 [24]). The core holder with aluminium body, which is wrapped with carbon fiber composite, can sustain higher pressure and absorb less X-ray than an all aluminium core holder. This kind of core holder is usually used for the experiments at high pressure and temperature.

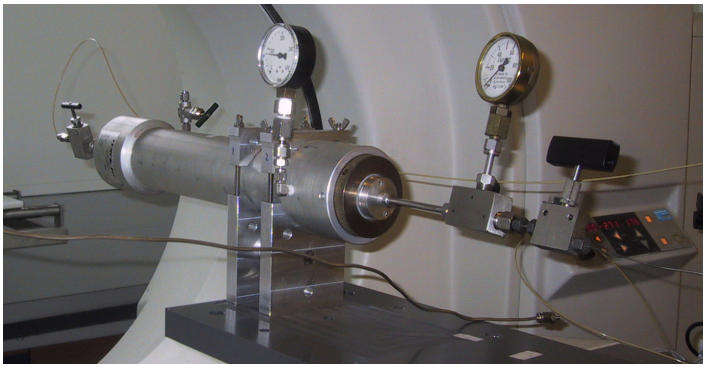

Figure 8 Aluminium core holder

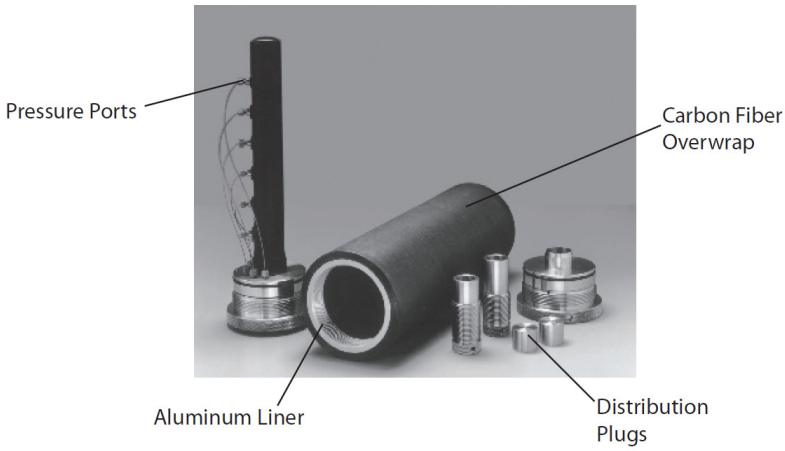

Figure 9 Carbon fiber wrapped core holder

3.2.2 The fourth generation Siemens SOMATOM scanner

The CT scanner used in our study is a fourth generation Siemens SOMATOM scanner (Figure 10) with 1200 stationary detectors. The X-ray tube rotates around the object in a 360° circular path. As the beam passes through the object, the lower energy photons are preferentially absorbed. The attenuation coefficient is usually scaled and reported as a CT number. CT numbers are generally presented in terms of an internationally standardized number scale subdivided into Hounsfield units (HU). The scale is linear, with CT numbers for air and water defined as –1000 and 0 respectively. The CT scanner has three different energy levels: 80 kV, 120 kV, and 137 kV, and a higher energy level provides better resolution. The maximum CT number is 3071 at all energy levels. An individual CT scan produces a digital 2-D image map of the X-ray attenuation in a tomographic slice through the object, and the image information is stored in a 512 by 512 matrix. The lighter color on the image indicates higher CT numbers. A series of 2-D images can be used to construct a 3-D image. All images are analyzed by special graphical software FPImage® (http://www.fpimage.com), ImageJ® (http://rsbweb.nih.gov/ij/) and in-house code developed by the author, using MATLAB®.

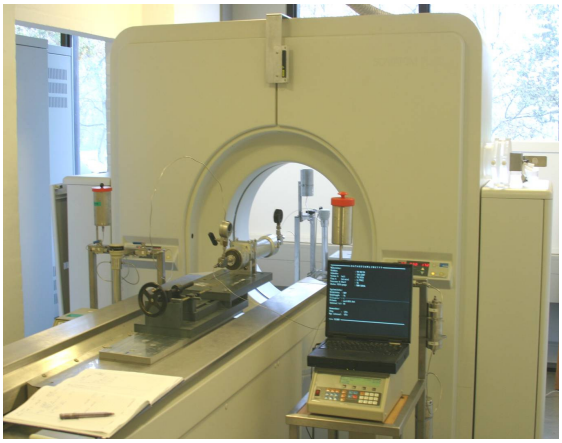

Figure 10 Fourth generation of Siemens SOMATOM scanner

To identify the in situ saturations, dual energy levels, 80 kV and 120 kV, were chosen, with composite factors (mA·s), 250 mA·s and 330 mA·s respectively. These two composite factors are the largest values which can be chosen in each energy level to reduce the beam hardening effects. For single energy scanning, energy level 120 kV, was chosen, with composite factors 330 mA·s. At 137 kV, the CT scanner cannot perform continuous scanning for more than 20 images due to the high temperature of the tube, although the image quality can be improved a little compared with that at 120 kV. Our choice of the energy levels was based on the image quality as well as the tube life of X-ray CT scanner.

3.3 Overview of flooding experiments

The overview of all experiments is provided in Table 2. There are nine low permeable chalk samples, with permeability range 0.1~1.06 md, were chosen as candidates for tests. In section 3.4, four similar core flooding experiments with core #1-5 at room temperature and different pressures are discussed to investigate if different phases could be identified simultaneously in the low permeable chalk by using dual energy scanning. The experimental pressures were set to be over the vapor pressure (50.87 bar) of CO_2 at 15 ^{o}C [25], so that CO_2 was kept at liquid state during experiments. A new method, to quantitatively calculate the in situ saturation of gas phase in the CO_2 flooding of the water flooded low permeable chalk, is also proposed.

Table 2 Overview of flooding experiments

Exp. Number	Plug sample properties					T,P cond.		Fluids	Remark
	Name	Length (mm)	Diameter (mm)	Porosity (%)	k_{water} (md)	P (bar)	T (^oC)		
Exp. #1	Core #1	44.00	25.70	35.50	0.32	65	15	Isopar-L Distilled water, CO_2	CO_2 flooding by using dual energy scanning
Exp. #2	Core #2	77.00	25.70	40.00	0.13	65	15	Isopar-L Distilled water, CO_2	Test performance of dopants
Exp. #3	Core #3	37.90	25.80	25.74	0.16	65	15	Isopar-L Distilled water, CO_2	CO_2 flooding with single energy scanning
Exp. #4	Core #4	74.00	38.00	24.40	—	100	15	n-decane Distilled water, CO_2	CO_2 flooding by using dual energy scanning
	Core #5	74.80	37.00	26.74	0.23	100	15		
Exp. #5	Core #6	31.60	38.00	32.98	1.31	385	115	Live oil Distilled water, CO_2	CO_2 flooding by using single energy scanning
	Core #7	120.20	37.00	29.87	0.49	385	115		
Exp. #6	Core #8	74.40	37.50	26.16	1.06	385	115	Live oil Distilled water, CO_2	CO_2 flooding by using single energy scanning
Exp. #7	Core #9	149.70	37.30	33.35	0.73	385	115	Live oil Distilled water, CO_2	CO_2 flooding by using single energy scanning

Then, in section 3.5, applications of the proposed method on North Sea chalk (core #6-9) with live oil are discussed. The general procedures for various experiments and the physical fluids are discussed in different chapters individually.

3.4 Trial experiments on in situ determination of phase saturations during flooding experiments

3.4.1 Experimental procedure

The core holder was installed horizontally on the CT platform. In order to guarantee accurate image positioning, the CT core holder was fixed during the flooding and only moved for scanning between

different flooding. The injection rates for water flooding and CO_2 flooding were both 6 ml/h. The CT images were taken every two millimeters along a core. Each scan takes 2.7 sec. All four experiments share a similar general procedure:

1. Scan dry core, CO_2 saturated core, doped oil saturated core, and doped water saturated core with dual energy. If necessary, clean the core with toluene and ethanol before changing the saturating fluid;
2. Flood the core with doped oil until S_{wi} is reached;
3. Flood the core with doped water until S_{or} is reached;
4. Flood the core with CO_2 until no fluid is produced;
5. Clean and dry the core.

A dual energy scanning was taken at the end of each step. Comparison between the scanning data of the dry core before and after the experiment is important for error estimation. During the flooding, produced oil, water and gas were separated at atmospheric condition and their volumes were recorded.

3.4.2 Fluids

The properties of fluids used in experiments without dopants are shown in Table 2 [25]. A light mineral oil, Isopar-L and n-decane were used as oil phase respectively in the different experiments. CO_2 is liquid at 65 bar and 100 bar. The density of CO_2 approaches to that of n-decane and Isopar-L as pressure increases. Consequently, the CT number of oil in the core is close to the CT number of CO_2 in the rock. To calculate saturations accurately, adding dopant to the oil phase increases significantly the difference in CT number of pure fluids. The same method also works for water phase, when its CT number close to that of oil and gas.

Table 3 Fluid properties at laboratory temperature 15 ^{o}C

	Isopar-L		n-Decane		Water		CO_2	
Pressure (bar)	Density (g/ml)	Viscosity (cp)	Density (g/ml)	Viscosity (cp)	Density (g/ml)	Viscosity (cp)	Density (g/ml)	Viscosity (cp)
1.013	0.779	1.290	0.734	0.987	0.999	1.001	1.80E-3	0.015
65	—	—	0.739	1.065	1.002	0.998	0.848	0.080
100	—	—	0.742	1.108	1.004	0.996	0.890	0.089

Usually, sodium iodide (NaI) or potassium iodide (KI) is used as water dopant, and iodododecane ($CH_3(CH_2)_8CH_2I$) is added to the oil phase. In our experiments, sodium tungstate dihydrate ($Na_2WO_4 \cdot 2H_2O$) is chosen as an alternative dopant in water phase, which had been applied in the previous experiments with chalk cores [75]. The unit of the concentration of dopants applied in this thesis is weight-based.

3.4.3 Experiment #1

Visualization of flow experiments with three mobile phases by dual-energy scanning was first presented by Vinegar et al. [25]. By scanning the core materials in two different energies (90 kV and 140 kV), they showed that the equations for water and oil saturations are linearly independent. This technique is known as the dual-energy technique for three-phase saturation measurements. In the paper, they demonstrated the use of iodododecane ($CH_3(CH_2)_8CH_2I$) as dopant for oil phase in the CO_2 flooding. Sahni et al. [12] measured three-phase relative permeability during the gravity drainage by using X-ray CT. This work was conducted at low pressure condition, and the density difference between oil and gas is significant. Consequently, difference between their CT numbers is large enough to obtain accurate saturations, and only brine was doped with Sodium Bromide (NaI). Akervoll et al. [75] was successful on performing history matching on water-alternated-gas (WAG) experiment with in situ saturation measurements at reservoir conditions. In this work, Sodium tungstate dihydrate and iodododecane were used to dope water and oil respectively. The comparison of core properties and experimental conditions for above experiments from literature is shown in Table 4.

Table 4 An overview of Experimental conditions for previous three-phase experiments

	Rock type	Permeability (md)	Porosity (%)	Temperature Pressure	Doped fluids	Dopant (weight%)
Vinegar et al. [25]	Berea sandstone	280	20	76 °C 207 bar	Soltrol	40% Iodododecane
Sahni et al. [12]	Berea sandstone	79	13.4	Room temperature & atm. Pressure	Brine	10% Sodium bromide
Akervoll et al. [75]	North Sea rock	892	26.8	100 °C 300 bar	Stock tank oil	25% Iodododecane
					Brine	7% Sodium tungstate dihydrate

In Table 4, the experiments conducted by Akervoll et al. [75] used the North Sea rock and had similar experimental conditions to ours. However, the permeability of their core sample is much higher than ours. Therefore, the aim of Exp. #1 is to test their methods in our low permeable chalk sample. Sodium tungstate dihydrate and iododododecane were chosen as dopants for water and oil respectively, with concentration as 7 wt% and 5 wt% separately. The solubility of Sodium tungstate is 41g/100g H_2O at 0 ^{o}C [28], which indicates that the doped water is far from its saturated solution.

In the Exp. #1, all general procedure was followed. To detect the influence of experimental pressures on the CT number of CO_2 saturated core, different pressures were applied when CO_2 was injected into the core. The density of CO_2 varies with pressures at 15 ^{o}C, which indicates that the vapor pressure is 50.87 bar (Figure 11 [25]).

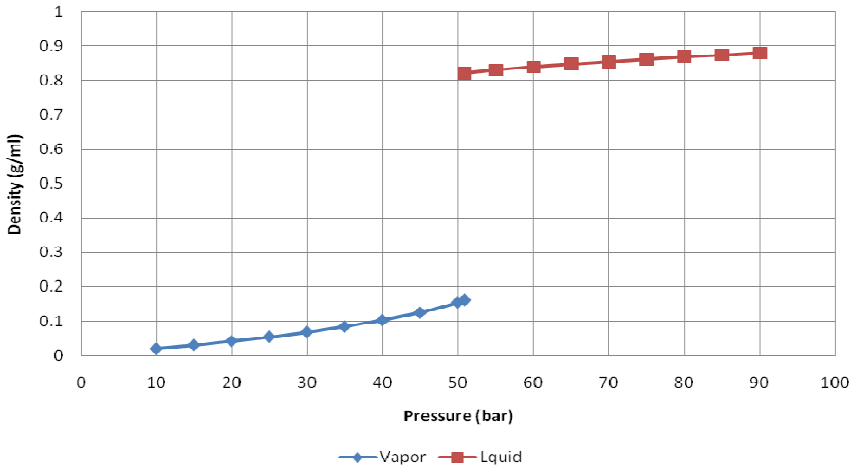

Figure 11 Effect of pressure on CO_2 density

In Figure 12 and Figure 13, the CT number does not vary significantly with pressures, which are above vapor pressure. This probably indicates that the small variation of density has little influence on the change of CT number. However, the CT number jumps considerably over the vapor pressure due to the large density difference. The CT number of CO_2 saturated core at 70 bar is more homogeneous than those at 60 bar and 65 bar, which probably suggests that enough time is needed for liquefied CO_2 to becomes homogeneous along the core sample.

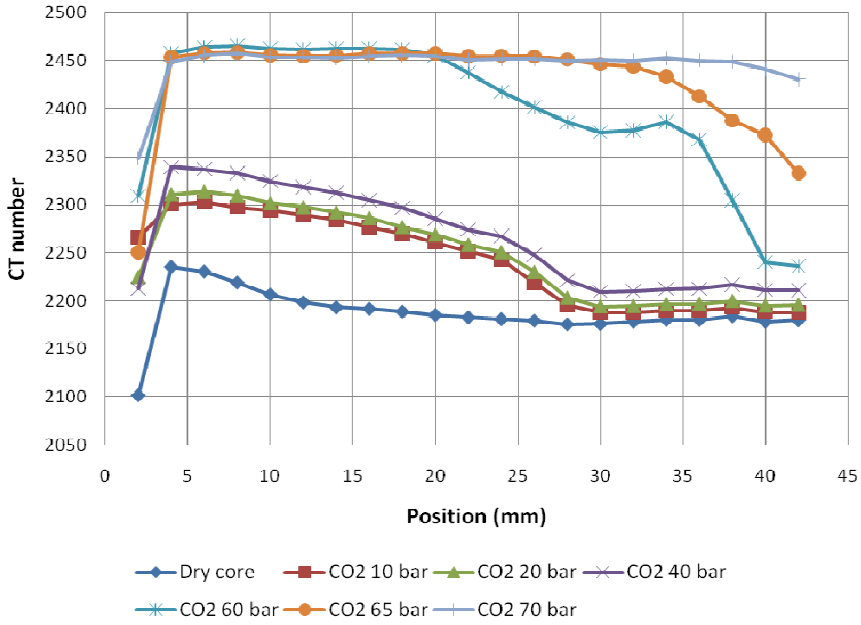

Figure 12 CT number of CO_2 sat. core at 80 kV (core #1)

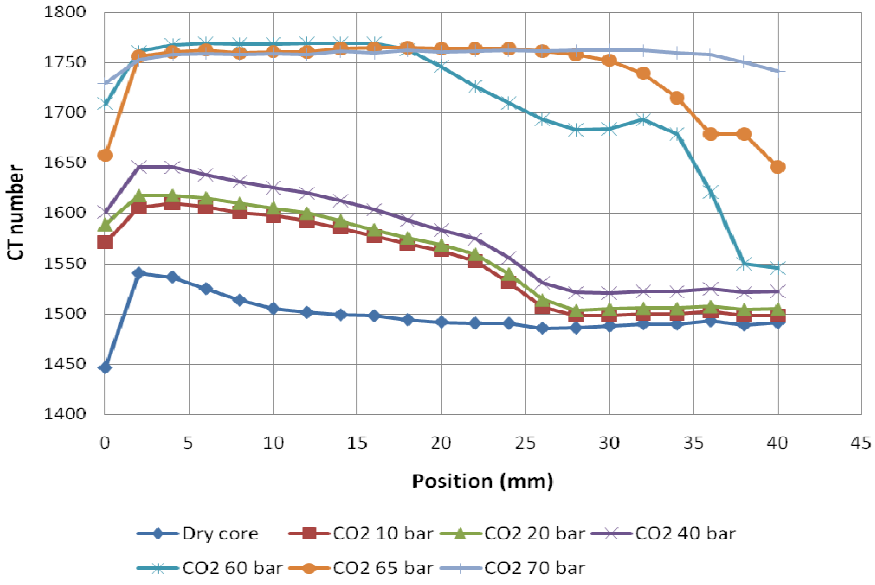

Figure 13 CT number of CO_2 sat. core at 120 kV (core #1)

Figure 14 and Figure 15 show the CT number of various fluid saturated core from position 2 mm to 40 mm (the CT numbers at the very ends of the plug are omitted due to the noise created by the

filters). Since the penetrating power of X-rays through the material increases with the potential difference across the tube, the CT number at 80 kV is always higher than that at 120 kV from the fluids used in our experiments. In the experiment with core #1, the core was saturated with CO_2, doped water and doped oil in sequence, and the corresponding CT numbers at two energy levels are shown in Figure 14 and Figure 15. At both energy levels, the CT numbers from dry core and CO_2 saturated core indicate that the core #1 is homogeneous chalk and CO_2 is well-distributed in the core. However, the CT number from doped water saturated core and doped oil saturated core are non-distinguishable around the inlet, and approach the upper limit of the CT scanner, 3071, which indicate that doped fluids or dopants themselves probably have inhomogeneous distribution along the sample. In the flooding experiments, 5-7 pore volumes were injected to guarantee that the sample is fully saturated injected fluids. Therefore, the inhomogeneous distribution is probably caused by the adsorption of the dopant from water phase in the core.

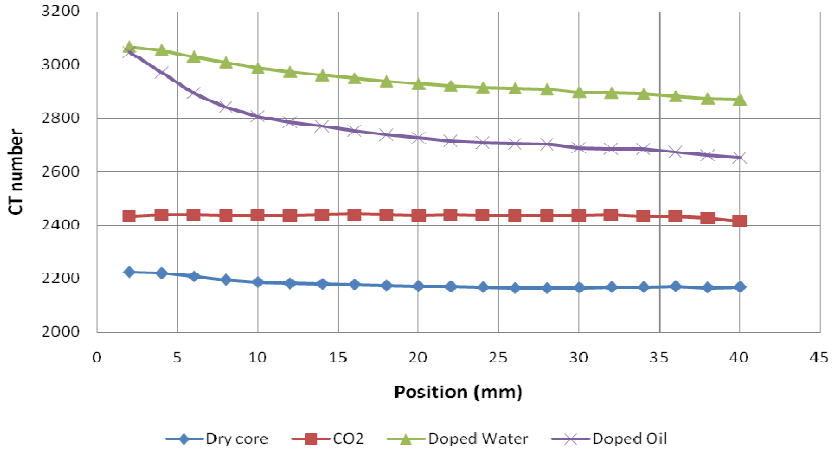

Figure 14 CT number of various fluid saturated core at 80 kV (core #1)

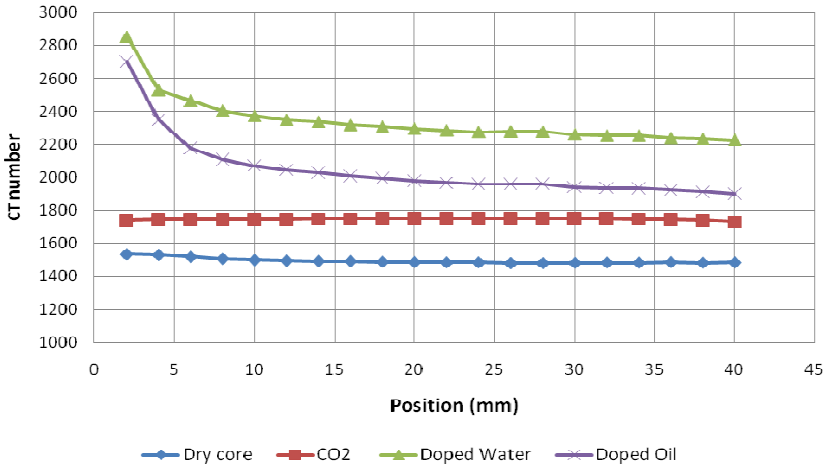

Figure 15 CT number of various fluid saturated core at 120 kV (core #1)

In Figure 16, CT number distribution of ROI (region of interest) at each position along doped water saturated core is displayed in sequence. The image at top left is from position 2 mm (inlet) and the one at bottom right from position 40 mm (outlet). The CT number is well distributed in the ROI at different positions and approaches to the upper limit of CT scanner at the inlet, where most areas are in dark red.

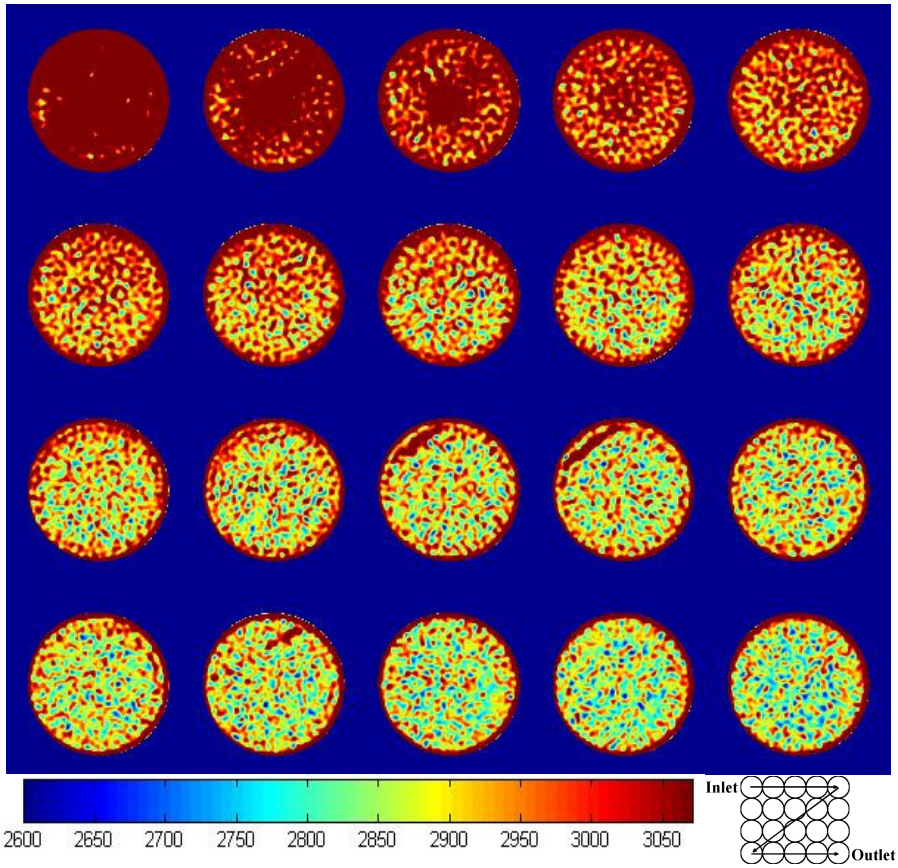

Figure 16 CT number distribution along doped water saturated core at 80 kV (core #1)

After the core was fully saturated with doped oil, water flooding and gas flooding were performed directly in sequence without creating S_{wi} (irreducible water saturation) conditions. The CT number of water-oil saturated core and water-oil-gas saturated core are shown in Figure 17and Figure 18. As the low density gas injected into the water-oil saturated core, the CT number decreased along the core, which has been proved at both energy levels. However, the CT number from water-oil saturated core and water-oil-gas saturated core at inlet positions are still close to each other, which also indicate that the adsorption of dopants in the rock matrix has happened.

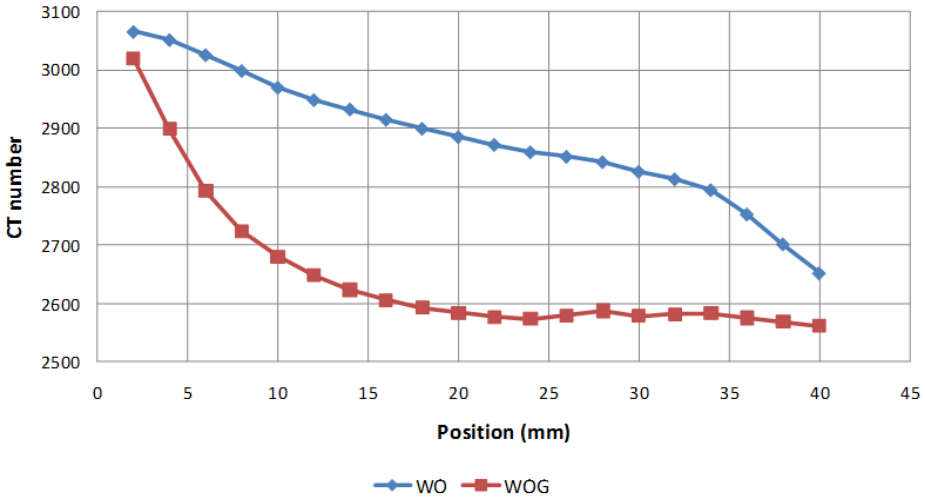

Figure 17 CT number of flooded core at 80 kV (core #1)

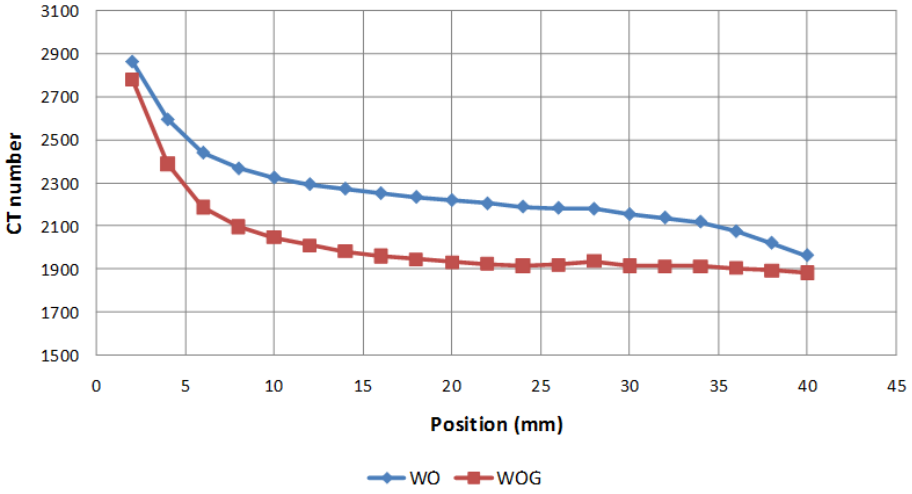

Figure 18 CT number of flooded core at 120 kV (core #1)

During water flooding, dynamic scanning was taken at the position 40 mm every 20-30 min (Figure 19). As shown in Figure 19, the injected doped water reached the outlet after 60 min, around 0.51 PVI (pore volume injected). The CT number did not change after 200 min, around 2.28 PVI, which indicates that the water saturation does not change anymore.

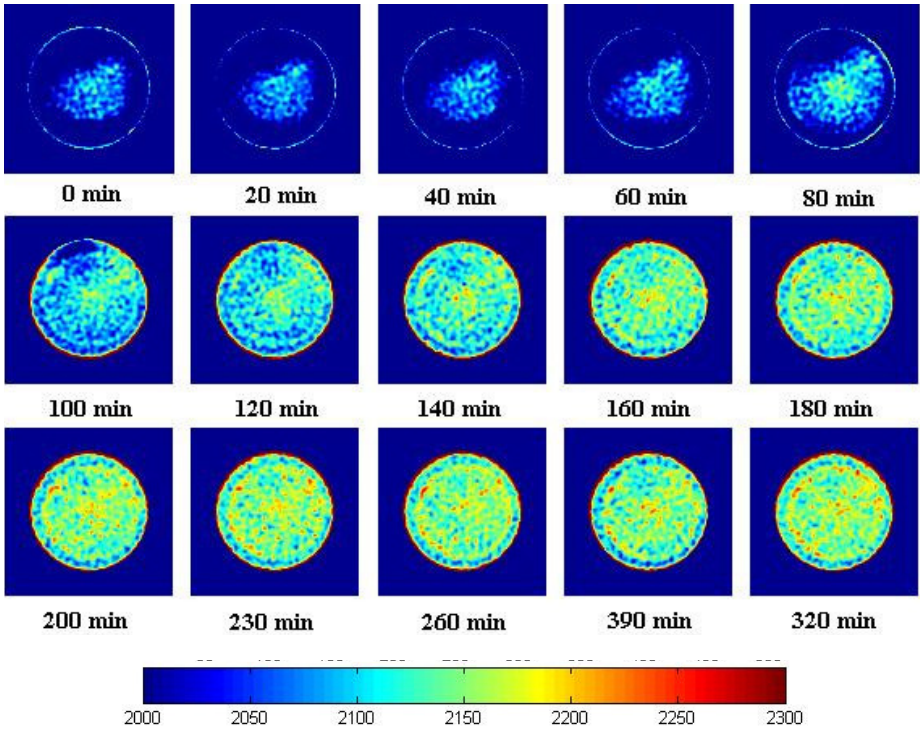

Figure 19 CT number distribution at position 40 mm during water flooding, 80 kV (core #1)

The phase saturations calculated by using eqs. (24)-(26) are shown in Figure 15. The average gas saturation, 64.4%, is close to the value, 61%, calculated from mass balance. But the average water and oil saturations are not in a reasonable range, exhibiting even negative values. The water saturation at inlet is much higher than the rest of the core, which is probably due to the adsorption of dopants at inlet positions.

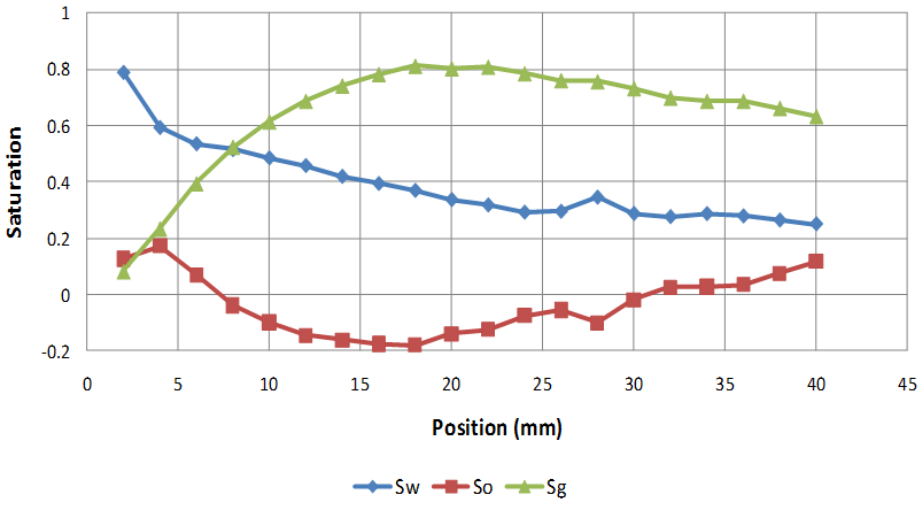

Figure 20 Three-phase saturation (core #1)

From the mass balance, the calculated oil saturation and water saturation are 21.2% and 17.8% respectively and all production profiles are in Table 5.

Table 5 Production profiles (core #1)

	Before water flooding	Water flooding	CO_2 flooding
Oil volume (ml)	7.87	3.07	1.67
Water volume (ml)	0	4.8	1.4
Sw	0	0.69	0.18
So	1	0.31	0.21
Sg	0	0	0.61
Oil recovery	0	0.55	0.18

The core sample was cleaned and scanned after the whole set of experiment finished to confirm the adsorption of dopant. As shown in the 3-D reconstruction image and direct scanning image (Figure 21), the CT numbers at the inlet of the dry core after the experiment are much higher than those before the experiment and almost reach the upper limit of the CT scanner. This indicates that strong adsorption of the dopant happened during the experiment, which ruins the results on three-phase saturations, and neither properties nor the concentration of dopant is favorable for the experiment.

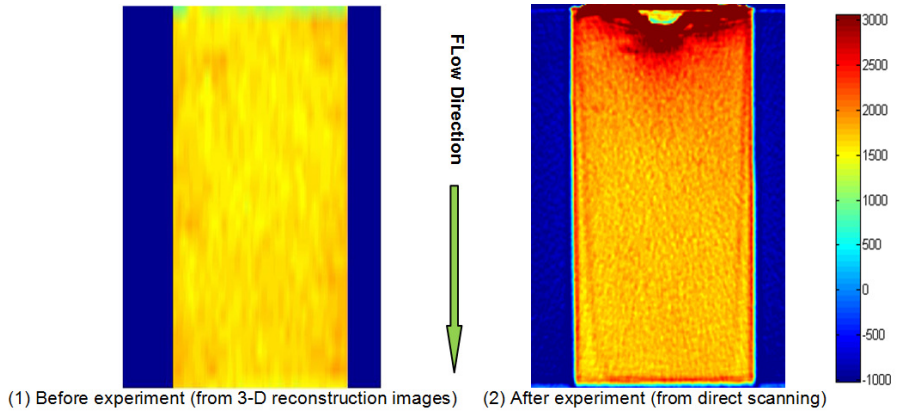

Figure 21 Comparison of CT images from dry core before and after the experiment (core #1)

3.4.4 Experiment #2

In the Exp. #1, the adsorption of dopant in water phase (7 wt%) happened and spoiled the final calculated saturation. Therefore, low concentrations of dopant, 1 wt% and 3 wt% $Na_2WO_4 \cdot 2H_2O$, were used to dope distilled water in the experiment with core #2. The CT number of CO_2, Isopar-L and water saturated core at 65 bar and 15 ^{o}C was also compared to investigate the necessity of doping two phases at the same time.

Figure 22 and Figure 23 show the CT number of various fluids saturated core at both energy levels. The CT number of Isopar-L and CO_2 are close to each other with average difference around 9, and the average difference between the CT number of water and Isopar-L is less than 50. This indicates that water and Isopar-L should be doped to identify three phases individually, and the three-phase flooding can be considered as pseudo two-phase flooding with doped water phase and CO_2-Isopar-L phase. Water doped with 3 % $NaWO_4$ was considered as water phase in the flooding process, since it has enough contrast to CO_2 and Isopar-L. However, the adsorption of dopant happened again, even with low concentration, as shown in Figure 24. The CT number of pure water saturated core after experiment has enhanced 100 more than that after experiment, especially at the inlet, where significant increasing was observed. This result is similar to that obtained in the experiment with core #1. Therefore, the Na_2WO_4 is not considered as choice of dopant for water phase in the later experiments on low permeable chalks.

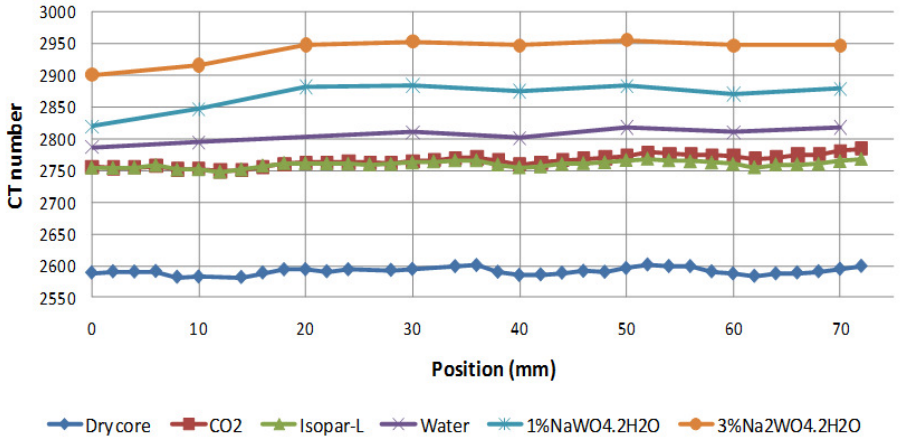

Figure 22 CT number of various fluid saturated core at 80 kV (core #2)

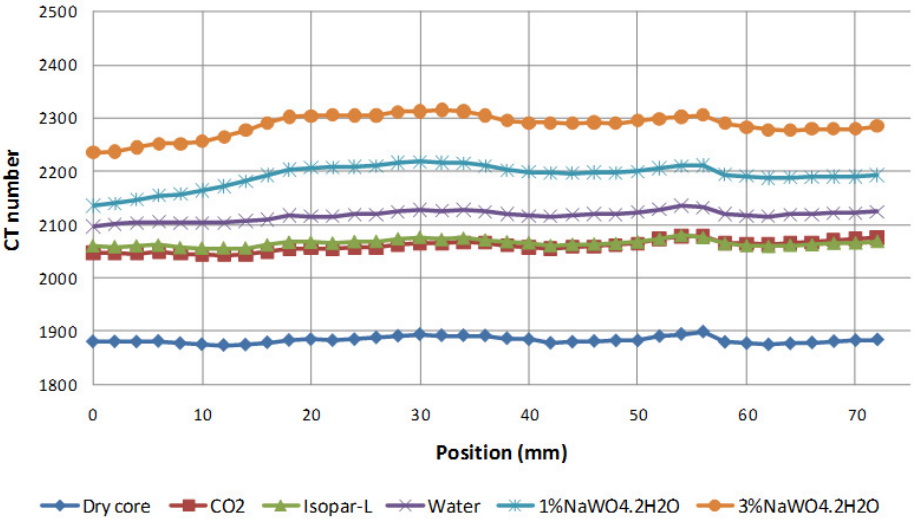

Figure 23 CT number of various fluid saturated core at 120 kV (core #2)

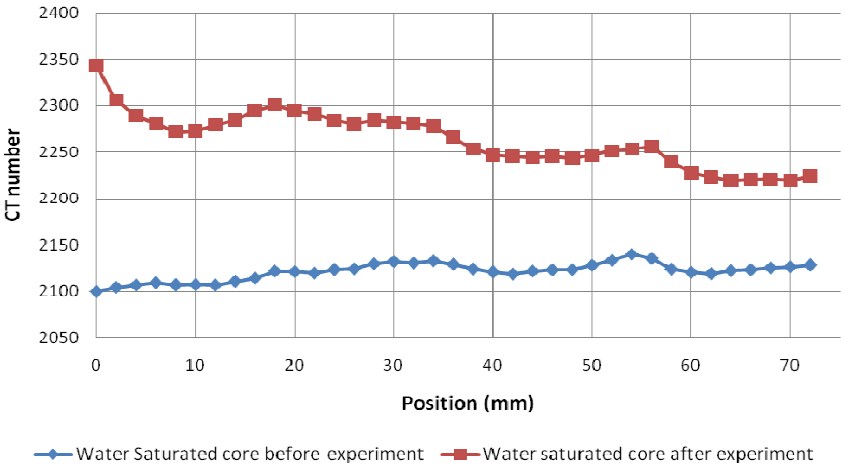

Figure 24 Comparison of pure water saturated core before and after doped water flooding at 120 kV (core #2)

3.4.5 Experiment #3

In Exp. #2, the idea of pseudo two-phase flooding has been proposed. Since Isopar-L and CO_2 have similar CT number at 65 bar and 15 °C, the saturation of water phase can be accurately decided under three-phase condition. In this experiment, Isopar-L was deliberately not doped to take advantage of its similar CT numbers to the high pressure CO_2 at 65 bar and 15 °C. Since Isopar-L and CO_2 can be treated as one pseudo phase in CT visualization, only the water saturation was measured here and the other two saturations were not determined. Based on the suggestions from literature [60] [12] [61] [30] and Reslab (now with Weatherford®) [31], KI (potassium iodide) was chosen as dopant for water, due to its stability under various flooding conditions. At the same time, with the comparison of water saturation before and after CO_2 flooding, it is possible to examine whether dissolved CO_2 would mobilize water phase under S_{wi}.

Step 3 in the general procedure was deliberately skipped in this experiment to investigate if CO_2 can mobilize the irreducible water and only single energy level 120 kV was used during Exp. #3. In Figure 25 and Figure 26, CT number of various fluid saturated core is plotted at both energy levels and it can be seen that the CT number of CO_2 saturated core and Isopar-L saturated core are close to each other, especially at 120 kV.

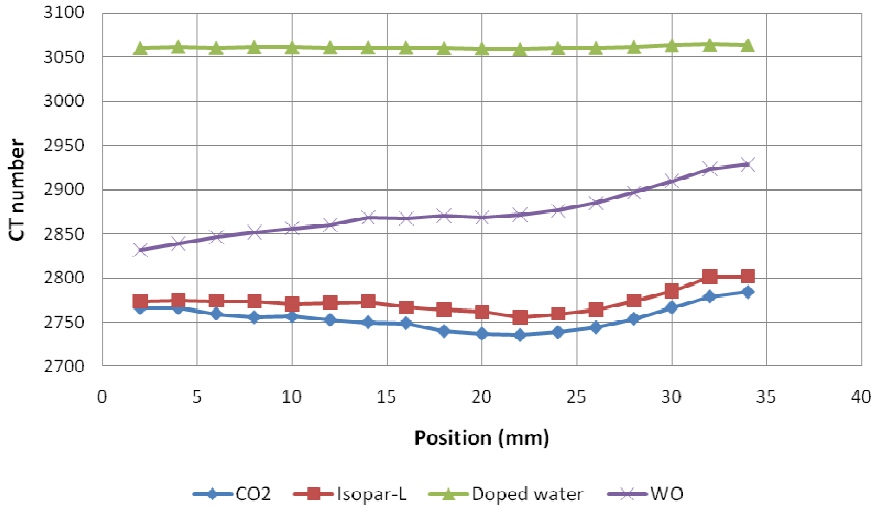

Figure 25 CT number of various fluid saturated core at 80 kV (core #3)

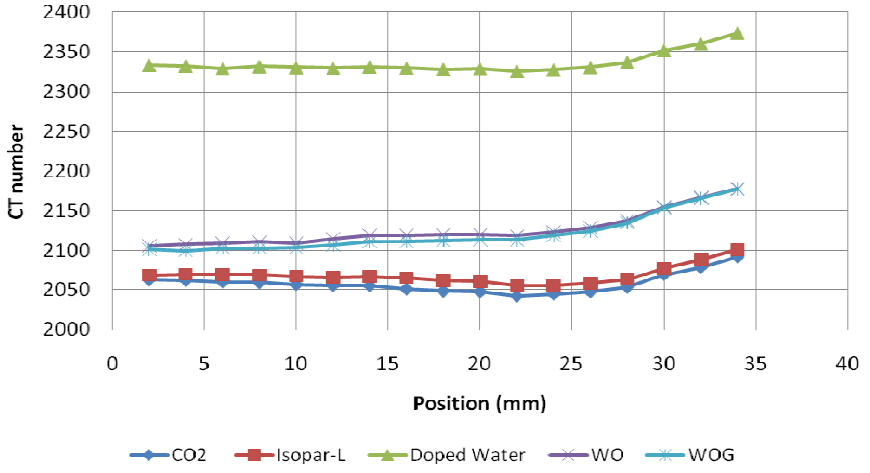

Figure 26 CT number of various fluid saturated core at 120 kV (core #3)

The difference of CT numbers between CO_2 and Isopar-L induces at maximum ± 0.003 error in the CO_2/Isopar-L saturations calculated by using eq. (1.21). Figure 27 shows fluid saturations calculated by using CT numbers at 120 kV, whose average value is in a good agreement with those calculated from mass balance (Table 6). Compared with the water saturation before CO_2 flooding, the water saturation at the end of the core has increased by around 0.03. Meanwhile, no water production was observed during the CO_2 flooding. It seems that the water mobilized by the injected CO_2 is captured at the end of the core by capillary pressure.

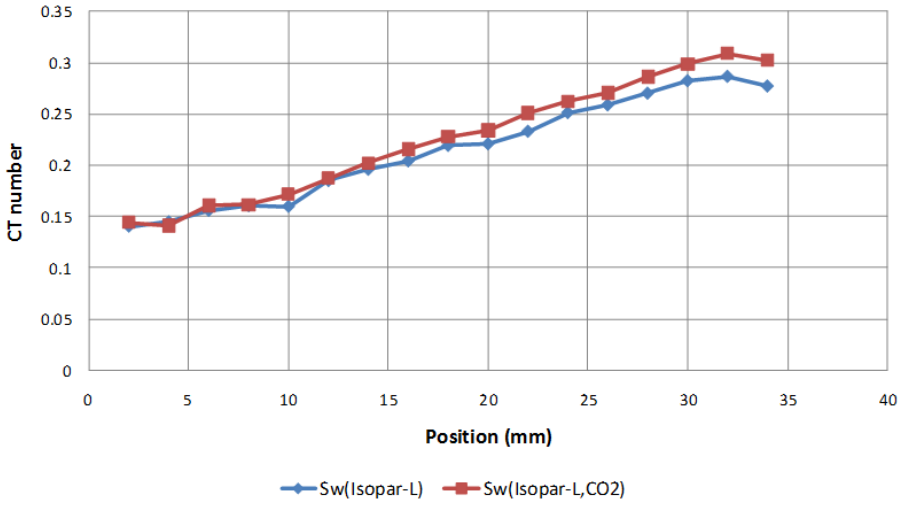

Figure 27 Water saturation at two-phase and three-phase conditions (core #3)

Table 6 Production profile (core #3)

	Original core	At Swi	CO2 flooding
Oil volume(ml)	0	4.46	—
Water volume(ml)	5.14	0.68	—
Sw	1	0.13	—
So	0	0.87	—
Sg	0	0	—

Figure 28 shows the distribution of pixel CT numbers in the region of interest on the CT image (The region of interest excludes bright circle area, which is characteristic of high CT number and induced by the beam hardening effect.). Normally, the CT number of ROI is the average value from that of all pixels in the region. The histograms from Exp. #1, Exp. #2 and Exp. #3 indicate that the CT number distribution is very close to normal distribution, which is usual for a homogeneous sample. Both software FPImage® and ImageJ® provided the same result.

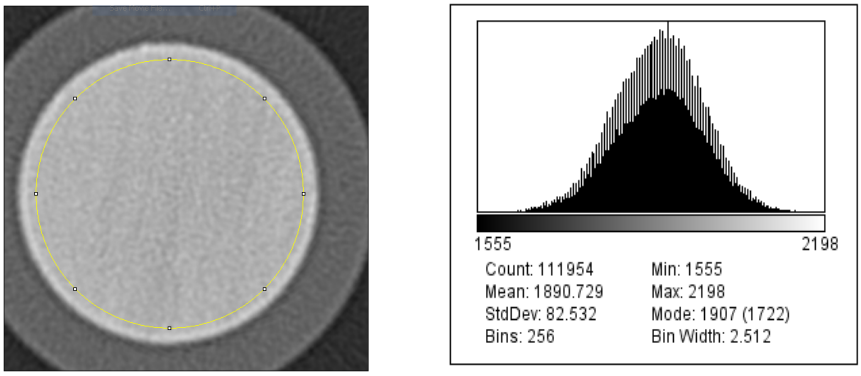

Figure 28 CT number distribution in the region of interest of dry core (core #3)

In Figure 29, by using the statistical data provided by the ImageJ®, shown in Figure 28, the reconstructed normal distribution fits the shape of CT number in the histogram. Correspondingly, the CT number of ROI is the average value of the normal distribution and is representative of the distribution of CT number from individual pixels. However, the CT number provided by the software is not corrected in two situations.

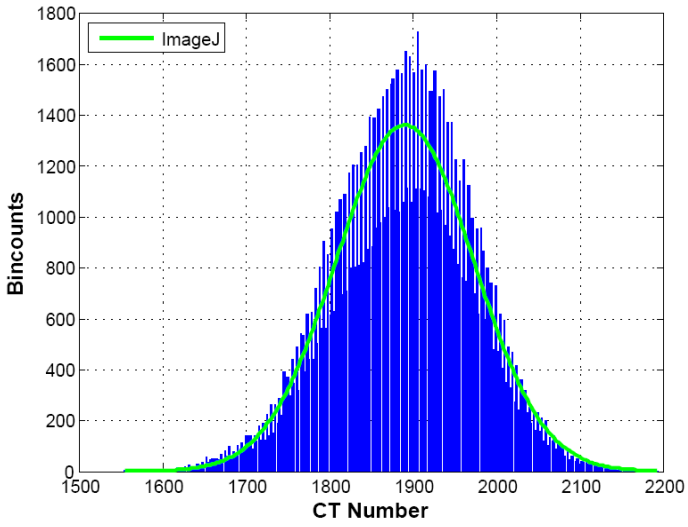

Figure 29 Normal distribution of CT number in the ROI

In Figure 30, both the reconstructed 3-D image and 2-D image at 120 kV indicate that there was high density substance existing in core #3, which has higher CT number than surrounding area. These substances are non-porous solid particles, which have no contribution to the flooding experiments

and should be excluded for calculating the average values. Obviously, the average value and standard deviation provided by the ImageJ® was influenced by these substances.

As indicated in Figure 25 and Figure 26, by using dopant, a decent contrast in CT numbers for different fluids was obtained at 120 kV. However, at 80 kV, there is a danger that some CT numbers will be beyond the upper limit of the CT scanner. In Figure 31, the 3-D image and 2-D image, fully saturated with bright color, indicate that most CT number of the core #3 saturated with 5 % KI doped water at 80 kV is over the upper limit. ImageJ® does not account for that effect and thus provide erroneous average CT numbers (as shown in the histogram). This error should be partly responsible for the inaccuracy in the three-phase saturation obtained by using dual energy scanning with core #1.

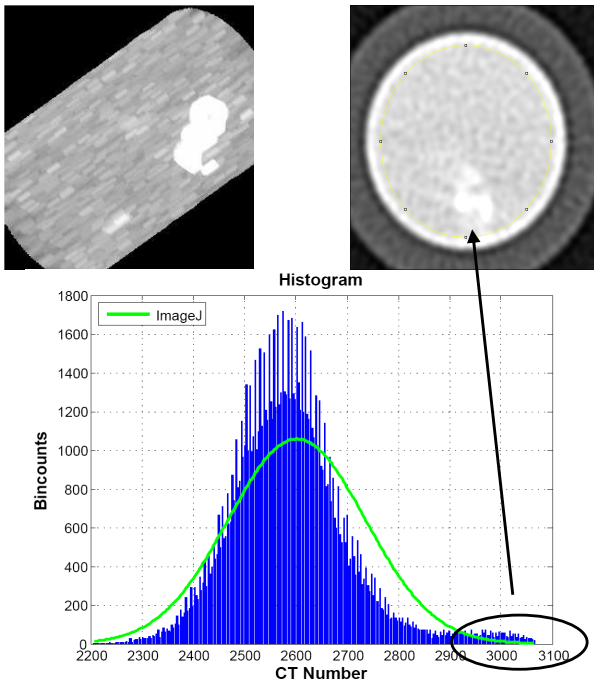

Figure 30 limitations of ImageJ® (1) Inhomogeneity of the core (core #3)

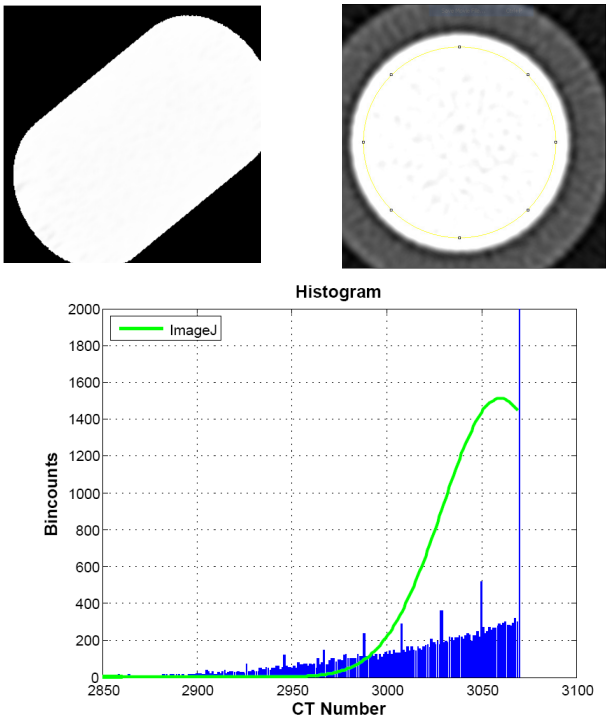

Figure 31 limitations of ImageJ® (2) Upper limit of CT scanner (core #3)

To obtain the correct CT numbers, an optimization method, the nonlinear Huber estimation, was used. Comparing with the Levenberg - Marquardt (LM) method, a damped Newton type's method with the least square estimator [32][33], the nonlinear Huber estimation (NHE) is a combination of the least square estimator and L_1-estimator, and this application offers the capability of faster convergence for NHE than LM. This kind of method can be Gauss-Newton model with a trust region approach, or LM like method [34]. In NHE's method, the application of the threshold γ is introduced to distinguish the magnitudes of residuals and further confine the influence of wild points in fitted data.

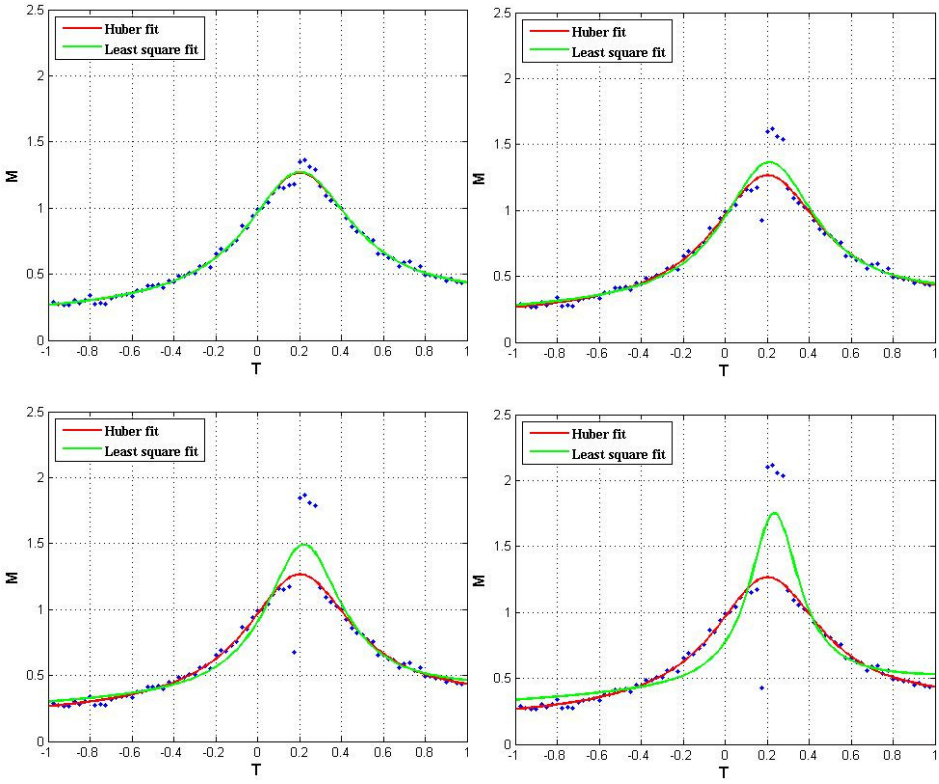

Figure 32 Comparison of LM and NHE

In Figure 32, comparison of the LM method (green line) and the NHE method (red line) on controlling the influence of wild points in fitted data is shown. By tuning the parameters in the numerical model **M**, its results should fit the experimental data **T** (details about the model available in the report by Ben et al. [35]). When the experimental data become wilder, results from LM are influenced more seriously and cannot represent the trend of most data. However, NHE has much better performance than LM in avoiding wild data. Therefore, NHE is considered as our main method applied in processing data.

Figure 33 and Figure 34 show the application of nonlinear Huber estimation. The differences between the average CT numbers from ImageJ® and from our method are 25 and 101 for two cases respectively. Considering the fact that average difference between the CT number of water phase and CO_2-Isopar-L phase is around 250 and 300 at 120 kV and 80 kV respectively, therefore, the errors induced by the limitations of CT scanner could affect the results calculated by data directly from ImageJ® significantly.

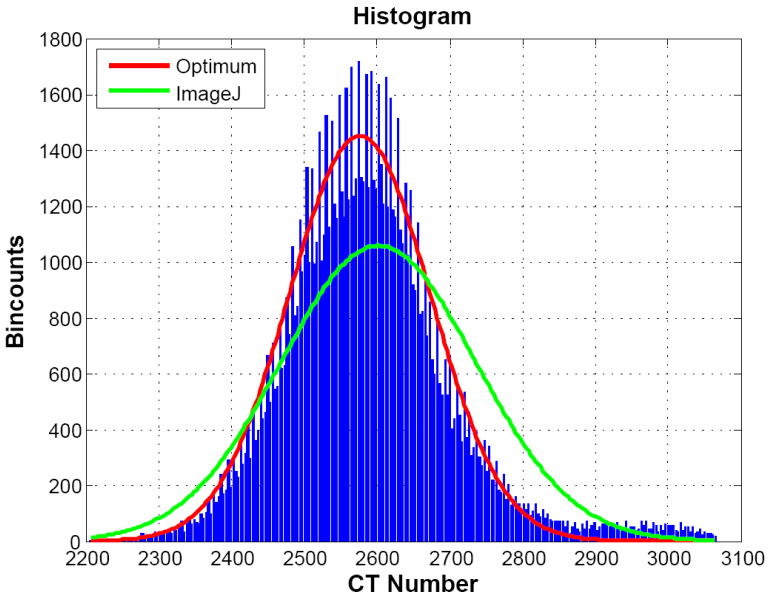

Figure 33 Application of NHE in limitation 1

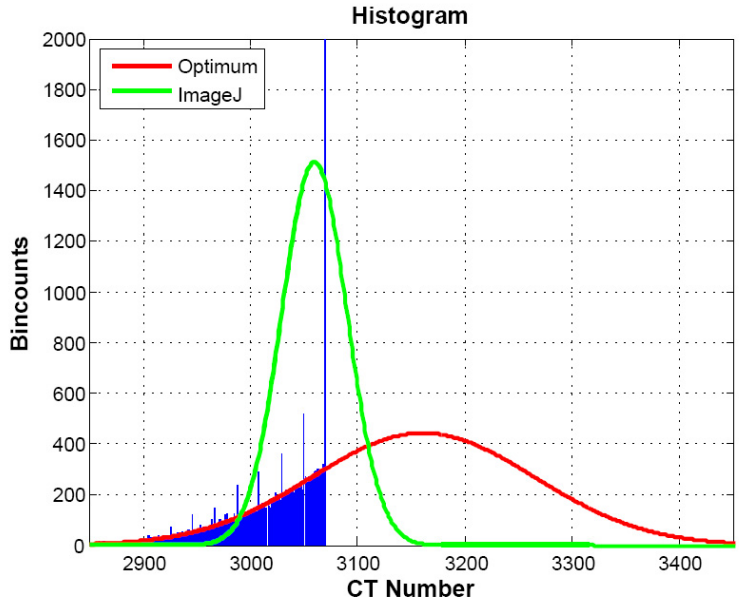

Figure 34 Application of NHE in limitation 2

Figure 35 compares the water saturation determined using data at 80 kV and 120 kV. It can be seen that if the 80 kV data were not corrected using our method, a significant deviation could be resulted.

Therefore, re-estimation of the average CT number using the nonlinear Huber estimation is necessary when there are a lot of data points beyond the upper limit of the CT scanner.

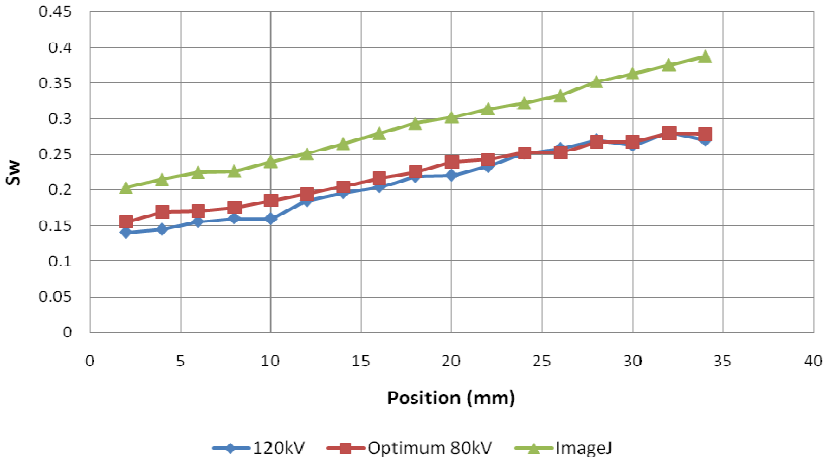

Figure 35 Comparison of water saturation (core #3)

3.4.6 Experiment #4

In Exp. #4, a complete set of experiment following the general procedures with dual energies scanning was performed. The obtained CT numbers were corrected using the method described in section.

To perform the dual energy scanning under high pressure, core #4 was initially used to determine the necessary concentration of dopant (iodododecane) in oil phase to distinguish it from CO_2. Then, dual energy scanning experiment following general procedures was conducted on core #5 to identify three phases. The back pressure was set to 100 bar where full miscibility between oil and gas can be achieved.

Figure 36 and Figure 37 indicate that 5% iododdecane could provide enough contrast between decane and CO_2 at experimental conditions.

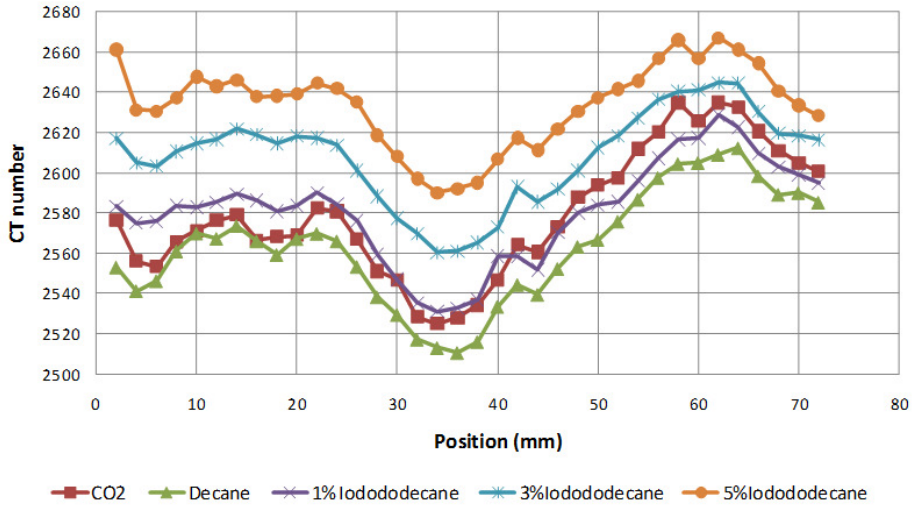

Figure 36 CT number of various fluid saturated core at 80 kV (core #4)

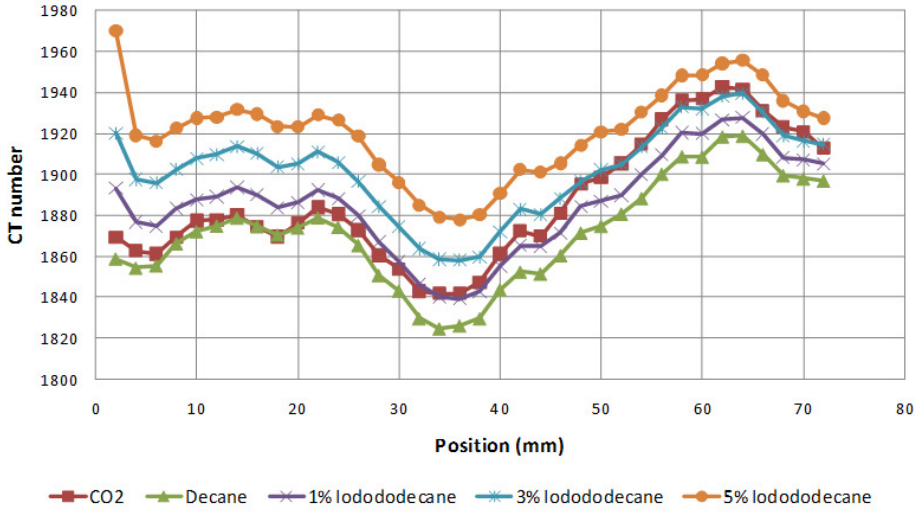

Figure 37 CT number of various fluid saturated core at 120 kV (core #4)

Therefore, 5% iodododecane and 3% KI were used to dope decane and water respectively. CT number of the core plug saturated by various fluids at both energy levels was plotted in Figure 38 and Figure 39. These data indicate that the core was well-saturated by various fluids and a decent contrast between them is obtained. In Figure 40 and Figure 41, the dynamic scanning of gas flooding is shown. The CT number decreases with time, which reveals that gas is invading into the core. The

CT number of gas flooding after 1 hour and S_{or} condition cannot be distinguished from each other, because the time is needed for building up the pressure gradient along the core.

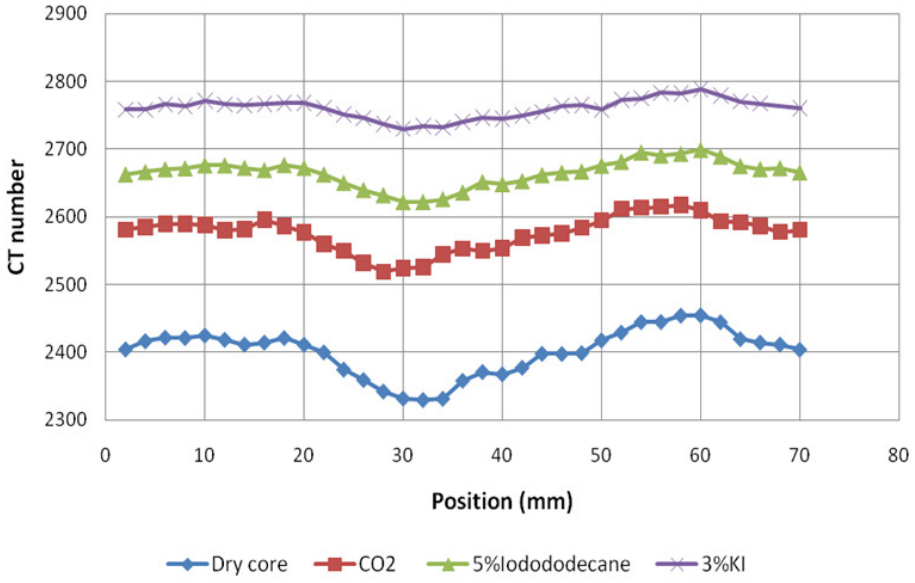

Figure 38 CT number of various fluid saturated core at 80 kV (core #5)

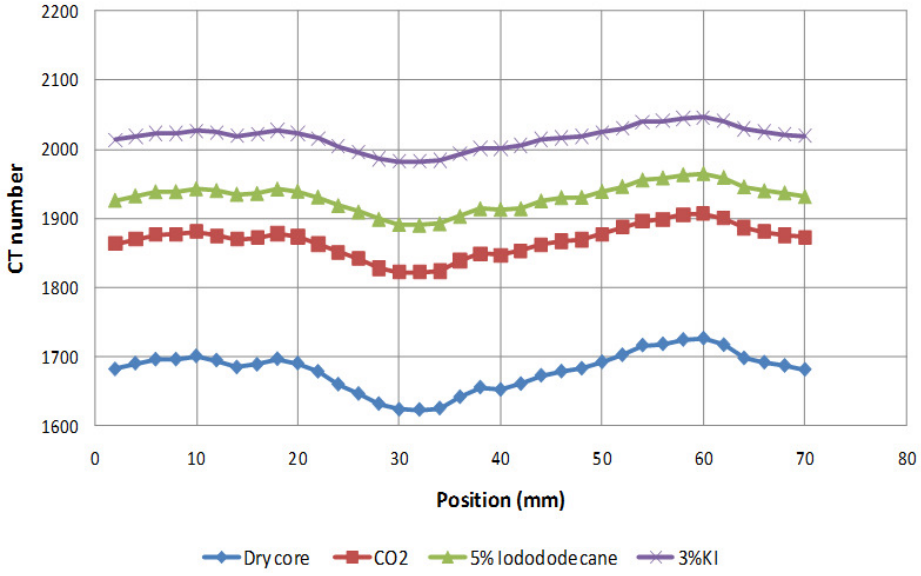

Figure 39 CT number of various fluid saturated core at 120 kV (core #5)

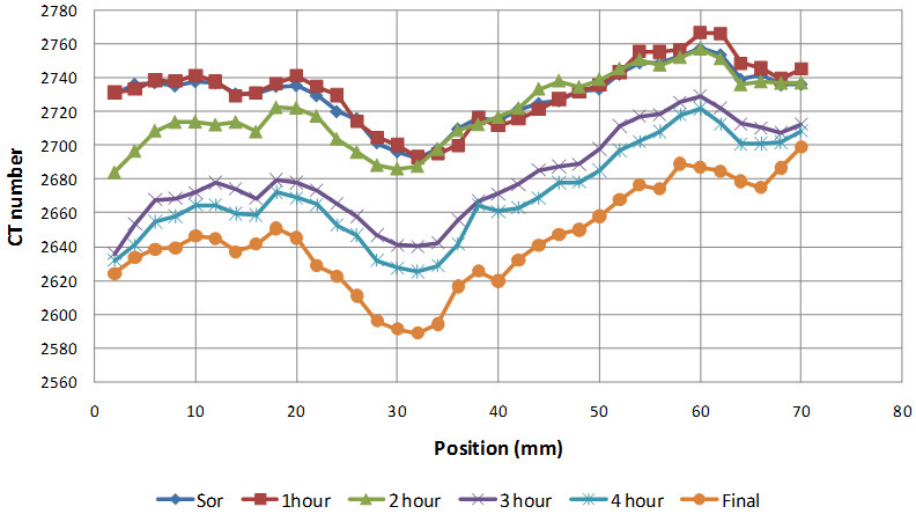

Figure 40 Dynamic scanning in gas flooding at 80 kV (core #5)

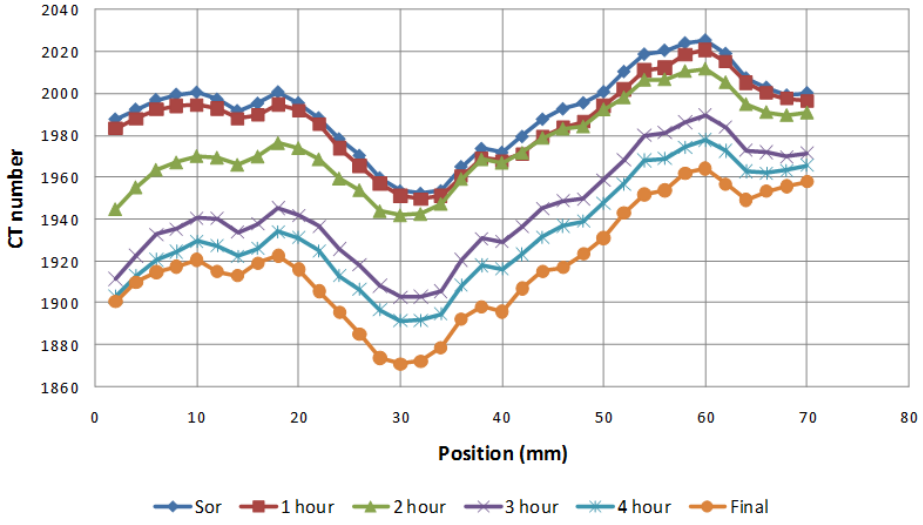

Figure 41 Dynamic scanning in gas flooding at 120 kV (core #5)

By using eqs. (24)-(26), (30) and (31), the three-phase saturation from position 2 mm to 70 mm is calculated, plotted and analyzed in Figure 42 and Table 7. For the results at 80 kV, to account for pixels with CT numbers higher than the upper limit of the CT scanner, the Huber estimation was used to get the correct average CT numbers.

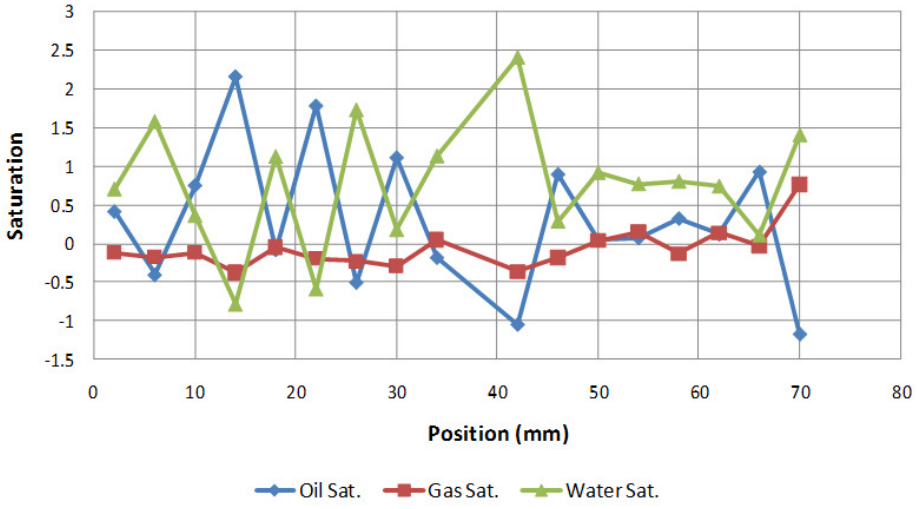

Figure 42 Saturation profiles (core #5)

Table 7 Three-phase saturation and error estimation for experiment with core #5

Position (mm)	Oil sat.	Gas sat.	Water sat.	det(A)	$\frac{\delta S_o}{\delta CT_{wr1}}$	$\frac{\delta S_o}{\delta CT_{or1}}$	$\frac{\delta S_o}{\delta CT_{gr1}}$
2	-0.120	0.704	-0.044	-0.026	-0.050	0.008	-0.120
6	-0.175	1.580	-0.058	-0.018	-0.062	0.012	-0.175
10	-0.116	0.363	-0.091	-0.010	-0.036	0.005	-0.116
14	-0.376	-0.789	-0.073	-0.003	-0.099	0.028	-0.376
18	-0.047	1.127	-0.096	-0.011	-0.042	0.002	-0.047
22	-0.196	-0.588	-0.111	-0.004	-0.076	0.013	-0.196
26	-0.228	1.732	-0.096	-0.005	-0.125	0.024	-0.228
30	-0.292	0.178	-0.058	-0.004	-0.107	0.025	-0.292
34	0.046	1.134	-0.027	-0.012	-0.033	-0.002	0.046
42	-0.367	2.413	-0.067	0.008	-0.127	0.032	-0.367
46	-0.186	0.289	-0.052	-0.001	-0.058	0.009	-0.186
50	0.036	0.920	-0.092	-0.007	-0.037	-0.002	0.036
54	0.155	0.772	-0.125	-0.012	-0.038	-0.009	0.155
58	-0.131	0.805	-0.083	0.009	-0.096	0.010	-0.131
62	0.137	0.743	-0.136	-0.001	-0.052	-0.008	0.137
66	-0.038	0.108	-0.085	0.011	-0.115	0.004	-0.038
70	0.764	1.407	-0.085	-0.042	0.011	-0.102	0.764

In Figure 42 and Table 7, the calculated saturations are clearly unsatisfactory since some values are out of the range [0, 1]. The large error can be explained by the determinant of matrix **A** in eq. (31). The system of equations is well-conditioned if the determinant is far from zero. This can be easily achieved in two-phase scanning where CT_{or} is much smaller than CT_{wr}. Furthermore, the scanning is

often performed at the high energy level, 120 kV, where the CT number can be more accurately measured and the upper limit of the CT scanner is not a problem. For three-phase scanning, however, the determinant becomes far from zero if a_{12} and a_{22} in matrix A are largely different from each other. Although CT_{ir1} and CT_{ir2} (i=o, w, g) are strongly different at two energy levels, the differences between a_{12} and a_{22} are not that large, especially for liquefied CO_2. As shown in Table 7, det(**A**) approaches to zero, which indicates that eq. (31) is ill-conditioned. In addition, the CT numbers obtained at 80 kV have larger errors compared to those at 120 kV due to the upper limit of the CT scanner as explained in the experiment with core #3 and the poorer image quality at lower energy scanning. This further affects the determination of three-phase saturations.

By differentiating eq. (24) with respect to CT_{wr1}, CT_{or1}, and CT_{gr1}, similar to eq. (30), the sensitivity of S_o to the individual CT numbers can be calculated (Table 7). It is clear that S_o is most sensitive to the change of CT_{or1}, e.g., if δCT_{or1}=1, the maximum absolute change on the S_o can be as large as 0.127. The error estimation reveals the reasons for inaccurate three-phase saturations.

As mentioned in the Chapter 2, Vinegar and Wellington suggested selecting a K_{edge} dopant for determining three-phase saturations [25]. CT scanning just above the K_{edge} energy will see a sudden increase in the attenuation coefficient. Therefore, if two dopants are used and one of the dopants has K_{edge} between the two scanning energy levels, it is possible to make (CT_{or}-CT_{wr}), or a_{12} and a_{22}, have opposite signs at two energy levels. And if the absolute values of a_{12} and a_{22} are not too close to zero, **A** will become well-conditioned. In the possible dopants with K_{edge} between our energy levels 120 kV and 80 kV[25], as shown in Table 1, most of them are compounds containing heavy elements, such as lead nitrate ($Pb(NO_3)_2$) and thallium fluoride (TlF). Those dopants are rarely used in core analysis perhaps due to their toxicity. And one also should be aware of the potential adsorption problem if a new dopant is used.

To investigate the possibility of applying K_{edge} of specific dopants under dual energy levels of our CT scanner, 80 kV and 120 kV, two dopants, lead disodium ethylene-diaminetetraacetate (PbEDTA) and lead nitrate ($Pb(NO_3)_2$), were chosen. The K_{edge} for these two salts is 88 kV, according to Table 1(Chapter 2). Since there is no PbEDTA available in the market, it was made by using $Pb(NO_3)_2$ and Disodium edetate (Na_2EDTA),

$$Pb(NO_3)_2 + Na_2EDTA \longrightarrow PbEDTA + 2NaNO_3$$

In Figure 43 to 45, the CT images of pure water, 1% PbEDTA doped water and 6% ($Pb(NO_3)_2$) doped water under two energy levels are shown. The difference of pure water under two energy levels is 10.8. For PbEDTA and ($Pb(NO_3)_2$) doped water, the differences are 31 and 122 respectively. Therefore, the added dopants increase the difference of doped fluids, which indicates that K_{edge} does not work in our case. Based on the available reference in the medical CT scanning and applied physics [36][37][38], the possible reason for this failure is the intensity and spectra of X-ray at different energy levels. As shown in Figure 5, X-ray beams from a medical CT scanner are polychromatic with a moderately broad energy spectrum. Therefore, at 120 kV, the spectrum of X-ray probably covers the K_{edge}, and results in no sudden increase in CT number as expected. In the successful applications, the narrow spectrum of X-ray produced at different energy levels should be close to K_{edge} to get enough contrast [36]. This can be realized either by using photons from single energy bin [37] or by selecting photon energy and controlling energy width from polychromatic X-rays to perform monochromatic energy discriminating radiography [38]. Compared with the application of above two methods in medical diagnosis, it is more difficult to use them in core flooding experiments, because outside the core material, there are rubber sleeve, surrounding water or gas, and core holder, all of which could attenuate passed X-ray and affect the quality of reconstructed images.

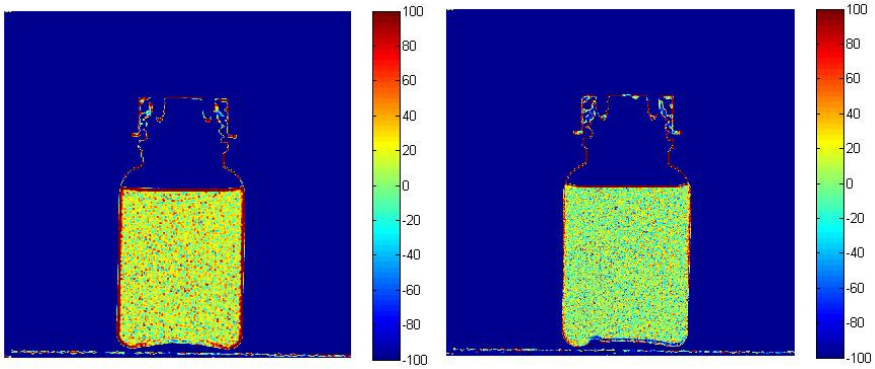

(1) 80 kV **(2) 120 kV**

Figure 43 CT number of pure water

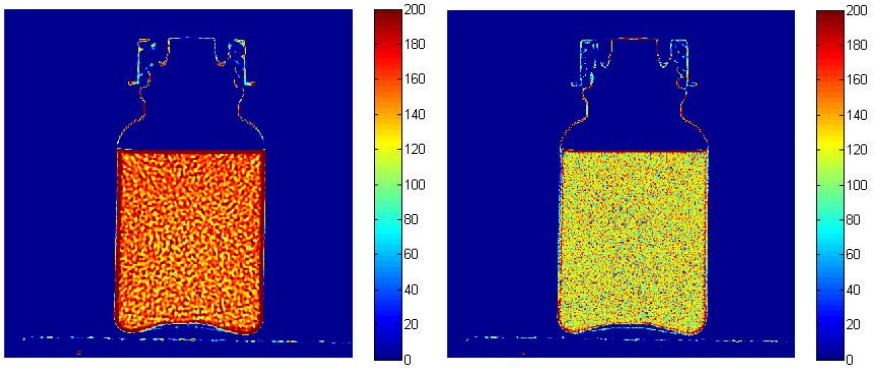

(1) 80 kV **(2) 120 kV**

Figure 44 CT number of 1 weight% PbEDTA

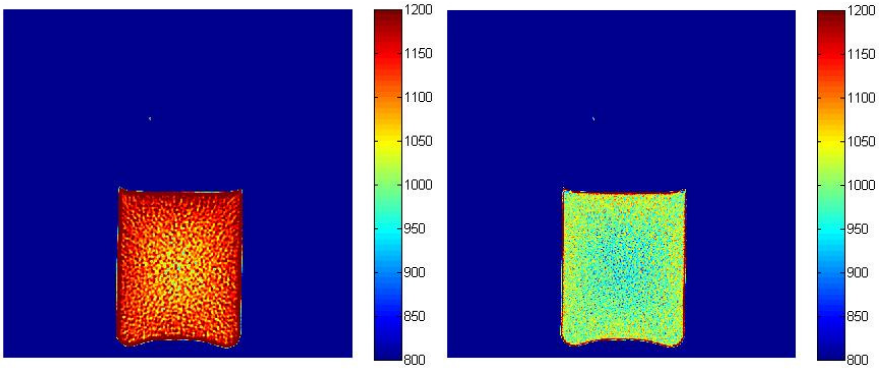

(1) 80 kV **(2) 120 kV**

Figure 45 CT number of 6 weight% $Pb(NO_3)_2$

During water flooding, production data were recorded every hour (Figure 46). The oil production stopped soon after water breakthrough. In Figure 47, the cumulative production profiles of gas flooding are plotted. There was no oil production until gas breakthrough, which started after 0.45 PVI. The oil production reached the peak after 1.4 PVI. In Table 8, the oil recovery information is listed. The oil recovery of water flooding is around 28% and that of gas flooding is 38%, which indicates that gas flooding is an effective method in getting more oil from water flooded reservoir. Compared with oil recovery from Exp. #1, the total oil recovery by water flooding and gas flooding are similar in these two experiments, around 70%, although water flooding could recover more oil in Exp. #1.

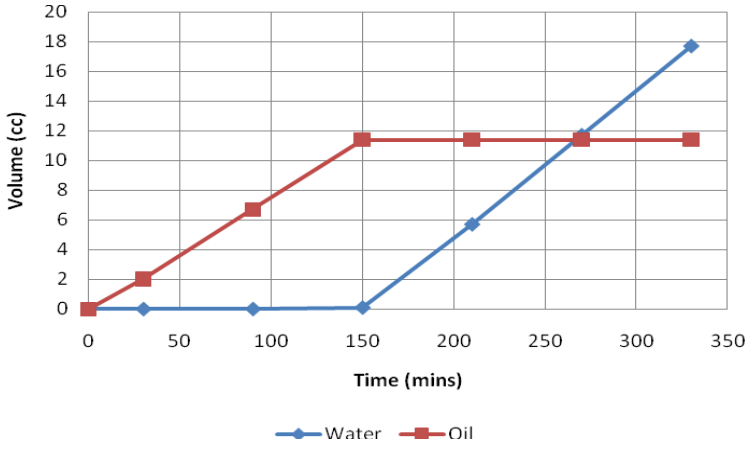

Figure 46 Cumulative production profiles for water flooding (core #5)

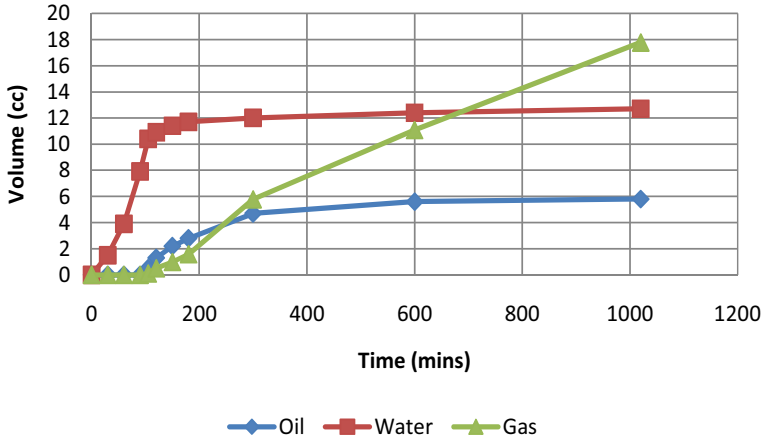

Figure 47 Cumulative production profiles for gas flooding (core #5)

Table 8 Oil recovery (core #5)

	Initial condition	Water flooding	Gas flooding
S_w	0.308	0.502	0.253
S_o	0.693	0.499	0.236
S_g	0	0	0.512
Oil Recovery	—	28%	37%

3.4.7 New experimental method

Based on the previous literature and our trial experiments, the application of CT in the saturation determination in a core with three fluid phases were conducted in three different ways: (1) keep one of the fluid phase immobile, and determine the saturation of the other two phases using single energy scanning; (2) determine the three-phase saturations using dual energy scanning and all three phases can be mobile, and (3) match the CT numbers of two fluid phases and treat them as a single phase.

Coles et al. [39] employed the first method by maintaining S_{wi} (irreducible water saturation) constant and immobile within a Berea core and flooding with oil and gas in sequence, and further calculated their in situ saturation. Yu et al. [26] applied the same strategy in the high temperature and pressure experiments with live oil and saline water. They also kept S_{wi} constant and performed two complete gas and oil injection cycles to investigate the relative permeability hysteresis in gas injection process. However, this method is not suitable for CO_2 flooding in the water flooded cores, where three phases are mobile.

Visualization of flow experiments with three mobile phases by dual-energy scanning was first presented by Vinegar and Wellington [25]. The introduction of this method has been stated in section 3.1. There are two main disadvantages of dual energy scanning: (1) the choice of dopant and its adsorption on the core, and (2) the high concentration of dopants in the doped phase. In our previous trial experiments with core #1, the same dopants as those in the experiment of Akervoll et al. [75] have been tested. The adsorption of dopants used for water phase has been observed in the rock, as shown in Figure 21. Compared with the images before experiment, areas with high CT number at the inlet on the images after experiment indicated that the sodium tungstate has been adsorbed. In the Exp. #3 and Exp. #4, Potassium iodide (KI), a kind of stable dopant, was chosen for water phase. However, the results were not satisfied due to the linear increase of CT number under different energy levels, as shown in the Exp. #4. As indicated in Table 4, the concentration of dopants in the reservoir conditions are usually higher than those in low pressure and temperature experiments to obtain enough contrast between different phases, due to the close CT numbers between various phases [25]. On the other hand, high concentration of dopant could change the physical properties of the oil phase significantly, including its density, bubble point and minimum miscible pressure (MMP). As the concentrations of dopants increases, the beam hardening effect also become more and more profound, which could further affect the image quality [34]. Furthermore, because the CT number of materials under low energy level is higher than that at high

energy levels, the high concentration of dopants may give CT numbers higher than the upper limit of the CT scanner during the low energy level scanning and thus induce errors in the saturation calculation, as indicated in the Exp. #1 and Exp. #3. Therefore, the dual energy scanning requires that the type of dopants and their concentration levels must be carefully selected for given fluid systems and rock types [41]. It is not always possible to obtain maximum sensitivity for all concentration ranges for a given system, such as the low permeable chalk at reservoir conditions.

The third method has been adopted by Siddiqui et al. [42] and Al-wadah et al. [43] to verify the Buckley-Leverett three-phase theory and investigated three-phase counter-current flow respectively. In their work, water doped with sodium iodide, decane doped with iodododecane and benzyl alcohol were used as three immiscible phases. By changing the concentration of dopants, any two of three phases could have similar CT numbers and be treated as one phase in the flooding experiment on the glass bead packs with very high permeability. There is no literature about the use of this idea on real reservoir fluids in reservoir conditions.

In Exp. #3, Isopar-L and CO_2 were found to have similar CT number at 65 bar and 15 ^{o}C, Therefore, they were treated as one pseudo phase in CT visualization, and only water saturation was determined to investigate if CO_2 can mobilize the irreducible water. Although, this method could only identify the most desired phase in the three-phase flow experiments, it has no special constraints on the application of dopants and its high concentrations in any desired system, and the abundant experience on two-phase flow experiment with the use of X-ray CT can also be used for reference. The results from measuring CT number of PbEDTA and $Pb(NO_3)_2$ show the limits of current medical CT scanner and the complexity of application of K_{edge} in practice.

As indicated from the previous studies, because the limits of dual energy scanning techniques applied in the low permeable chalk and the gas phase is our most interesting phase during the tertiary CO_2 flooding, a new experimental method has been proposed as follows: After water flooding, the water phase without dopant is replaced by the doped water which could have similar CT number as the doped oil. Therefore, in tertiary CO_2 flooding, water phase and oil phase can be treated as non-gas phase, and only single energy scan is needed to quantitatively identify the in situ saturation of CO_2. In section **3.5**, the application of this method with live oil at reservoir condition is discussed in details.

3.5 Flooding experiments on North Sea chalk with live oil under CT scanning

Exp. #5-7 were conducted at reservoir conditions to measure in situ CO_2 saturation quantitatively during the CO_2 flooding. Section 3.5.1 presents the general procedures for these three experiments, and variations in the detailed steps for each experiment are introduced in the subsequent subsections.

3.5.1 Experimental procedure

As a preparation for the flooding experiment, short chalk core (core #6), which has similar properties to those of cores #7, #8 and #9, was selected in Exp. #5 to tune the dopants concentrations in the distilled water and doped oil. On the one hand, the dopants concentrations should be high enough to provide enough contrast in CT numbers; on the other hand, their concentrations should be kept as low as possible so as not to change phase properties and phase equilibrium too much.

All the water injection and tertiary gas flooding experiments were carried out in restored chalk core from a Danish North Sea reservoir at the reservoir temperature 115^{o}C and a pressure (385 bar) higher than the bubble point pressure, where the calculations showed that the system is fully multicontact miscible with CO_2. The long core (core #7, core #8 and core #9) used in the flooding experiment were aged for three weeks in the live oil and water at reservoir temperature and pressure to obtain realistic wetting conditions.

The experimental procedure is as follows, where the short core trial experiment only followed step 1 and the long core experiments followed all the steps:

1. Scan dry core, CO_2 saturated core, doped oil saturated core, and pure water saturated core at a single energy level. If necessary, clean the core with toluene and ethanol before changing the saturating fluid;
2. Flood the core with doped oil until S_{wi} is reached;
3. Age the core for three weeks to restore the reservoir conditions;
4. Flood the core with pure water until S_{or} is reached;
5. Flood the core with doped water to replace the pure water;
6. Flood the core with CO_2 until no fluid is produced;
7. Clean and dry the core.

In addition to the scan in step 1, CT scan was taken at the end of each step. All the scans uses single energy level 120 kV and a composite factor of 330 mA·s. During the flooding produced oil, water and gas were separated at atmospheric condition and their volumes were recorded.

In the tertiary CO_2 flooding, where water and oil were doped to the same CT number and treated as a pseudo single phase, the CO_2 saturation is given by

$$S_g = \frac{CT_{wogr} - CT_{wor}}{CT_{gr} - CT_{wor}} \tag{32}$$

In eq. (32), S_g is expressed in terms of the measured CT numbers of various fluid saturated cores. Subscripts o, w, g and r represent oil, water, gas and rock respectively. Their combinations, wor and wogr represent the existence of the corresponding phases in the core.

3.5.2 Fluids

The recombination GOR of live oil was 216.8 sm^3/sm^3 and the oil formation volume factor is 1.63 rm^3/sm^3. The bubble point of the live oil is around 360 bar. The density and viscosity of fluids before adding dopant at reservoir conditions are listed in Table 9. No asphaltene were observed in the swelling test. The live oil was doped with iodododecane. The distilled water was used instead of synthetic water for the sake of simplicity and the focus on phase identification. The application of distilled water could increase the solubility of CO_2 and further the dissolution of calcite, since less ions appears in the water phase comparing with the case of synthetic water. The distilled water was doped with KI. The unit of the concentration of dopants is weight-based.

Table 9 Fluid properties at experimental conditions

	Live oil	Distilled water	CO_2
Density (g/ml)	0.633	0.966	0.708
Viscosity(cp)	0.251	0.253	0.061

3.5.3 Experiment #5

Short core #6 was initially used to tune the concentration of dopant in live oil and water, with injection rate at 6 ml/h. This injection rate was chosen based on the mechanical properties of core sample and the conditions of experiments. Since doping live oil needs high pressure operations and tuning the dopant concentration until the live oil reaches a desired CT number can be time

consuming. An effective way to avoid the high pressure trial-and-error is to use dead oil instead to get information about how the CT number will change with the dopant concentration. After that, doping the live oil can be completed just for once. The CT number of doped oil saturated core was in Figure 48. The doped oil with 0%, 5% and 10% iodododecane flooded the core in sequence. The difference of CT number between CO_2 and 10% doped dead oil is more than 250, which is considered to be enough for the calculation of in situ saturations. Consequently, 10% iodododecane is chosen to dope the live oil phase.

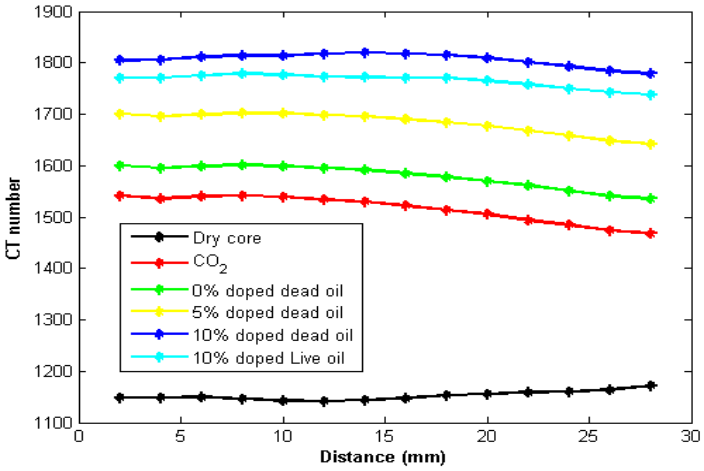

Figure 48 CT number along core #6 saturated with the doped oil

The difference between the CT number of the core saturated by the doped live oil and CO_2 is 200. To tune the concentration of KI in the water and match the CT number of doped live oil, 0%, 2% and 2.5% KI doped water have been injected into the core in sequence, and the CT numbers are shown in Figure 49. By assuming a linear dependence of the CT number on the concentration of dopant in the fluid, the optimum concentration of KI, 3.04%, was chosen, as shown in Figure 49. The selected concentrations of dopants provide enough contrast to get accurate average saturations on a scanning slice. However, it should be noted that, to calculate the saturation accurately for each pixel, a larger contrast in CT number is needed. Oshita et al. [60] and Oseto et al. [61] have 15% NaI (sodium iodide) in their CT scanning. For such a high concentration of the dopant in water, the concentration of iodododecane in live oil will reach about 40% in tertiary CO_2 flooding, which willchange the live oil properties significantly (With our oil sample, the added 10% iodododecane could decrease bubble from 360 bar to 340 bar). Therefore, the low concentrations of dopants, 10%

iodododecane and 3.04% KI for live oil and water respectively, are preferred to keep original properties of fluids in our experiment.

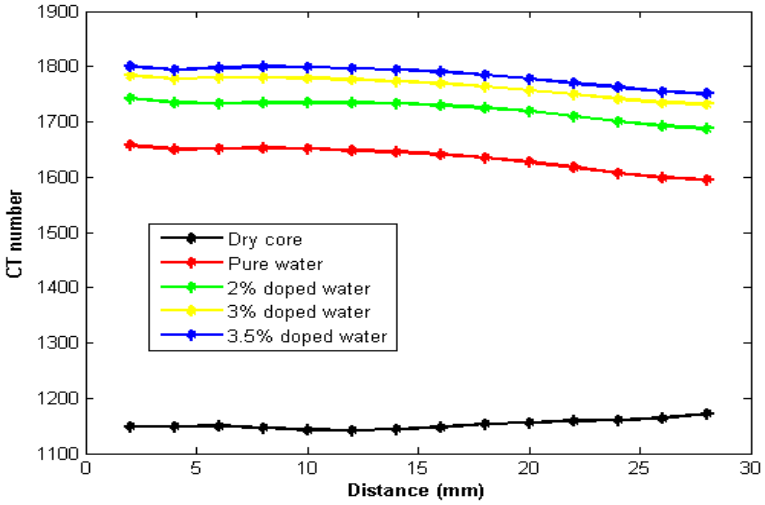

Figure 49 CT number along core #6 saturated with doped water

Then, core #7 was used to perform the complete set of the water injection and tertiary gas flooding experiment with 6 ml/h for both water flooding and gas flooding. Before putting the core into the core holder, small fractures were observed at the outlet, as indicated in Figure 50. In the first step of general procedures, the dead oil was used to flood the core to replace the CO_2 and then doped live oil was injected, which could reduce the amount of doped live oil used to saturate the core. 10% iodododecane and 3.04% KI were chosen for live oil and water respectively. In Figure 51, the CT number of various fluids saturated core is plotted. There is a high density area close to the inlet of core.

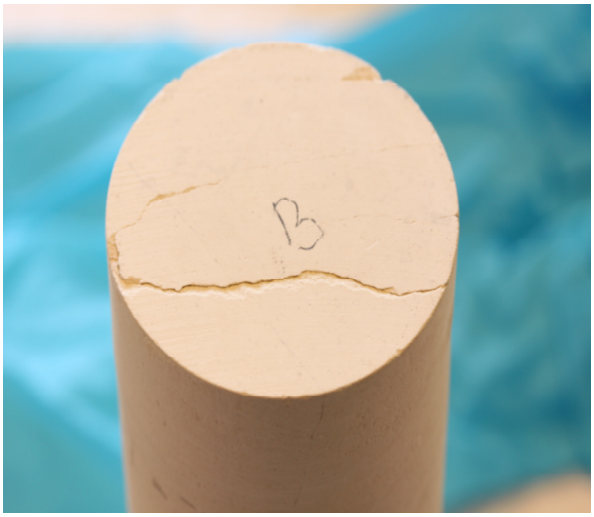

Figure 50 Photo of core #7 before experiment

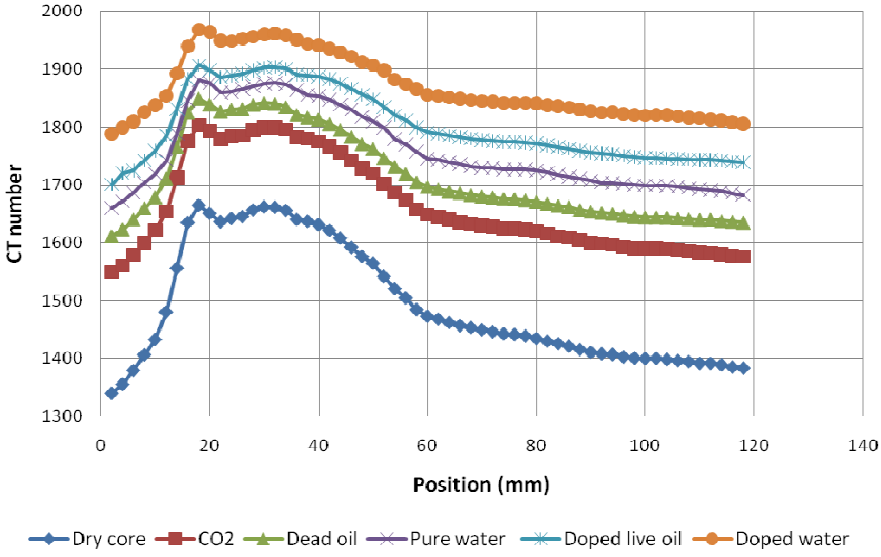

Figure 51 CT number of various fluids saturated core (core #7)

The production profiles of water flooding are plotted in Figure 52. The water breakthrough happens at 0.4 PVI. Based on the data from mass balance, the oil recovery for water flooding is 23.4%. After water flooding, the leakage of sleeve rubber was detected and the experiment had to be stopped. The broken sleeve was shown in Figure 53, which could probably be induced by high temperature and pressure and CO_2 diffusion. The whole period of experiment with core #7 took around 1.5 month,

during which high temperature and pressure could soften and furthermore, outside water could penetrate the rubber sleeve (a hole was found in the red circle area.). By consulting specialists from Weatherford®, special rubber was used in the later experiments.

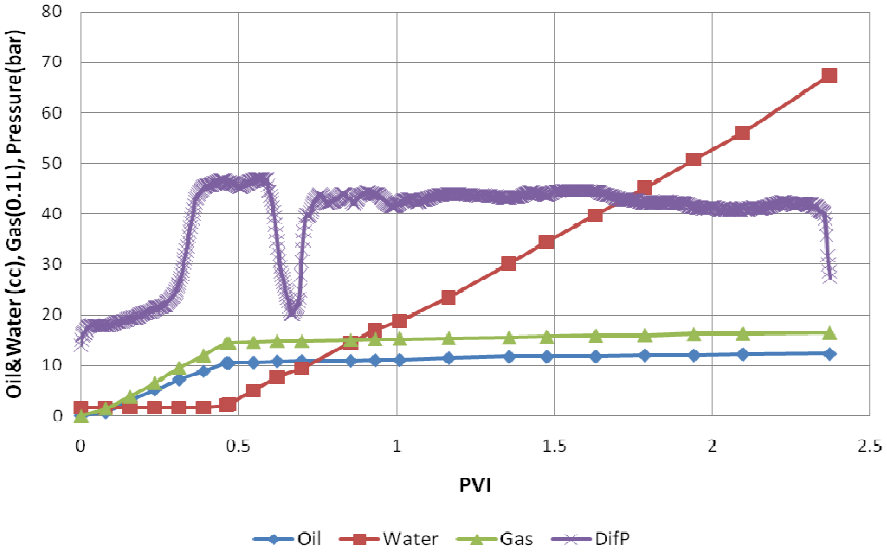

Figure 52 Production profiles of water flooding (core #7)

Figure 53 Broken rubber sleeve (core #7)

3.5.4 Experiment #6

In Exp. #6, core #8 was used to perform the complete set of the water injection and tertiary gas flooding experiment, with injection 2 ml/h and 4 ml/h respectively. The distribution of porosity in each cross section image is displayed every 4 mm along the core in Figure 54. The number on each image represents its position along the core. In the region of interest (white circle), there is a high

porosity channel starting at 34 mm from the inlet. To analyze quantitatively the water propagates in the core, the CT data is converted into saturation profiles by using eq. (16). The saturation distribution in the sample at different times for water injection is shown in Figure 55. In the saturation profiles corresponding 2 hours, 4 hours and 6 hours, an oil bank built up ahead of water front can be seen. This phenomenon probably was induced by the inhomogeneous distribution of oil and water in the core. The inconsistency of injection rate is probably another reason, because in step 2 of the general procedures, 6 ml/h was used to inject oil into the core to create S_{wi} condition, and however, lower injection rate, 2 ml/h was used for water flooding.

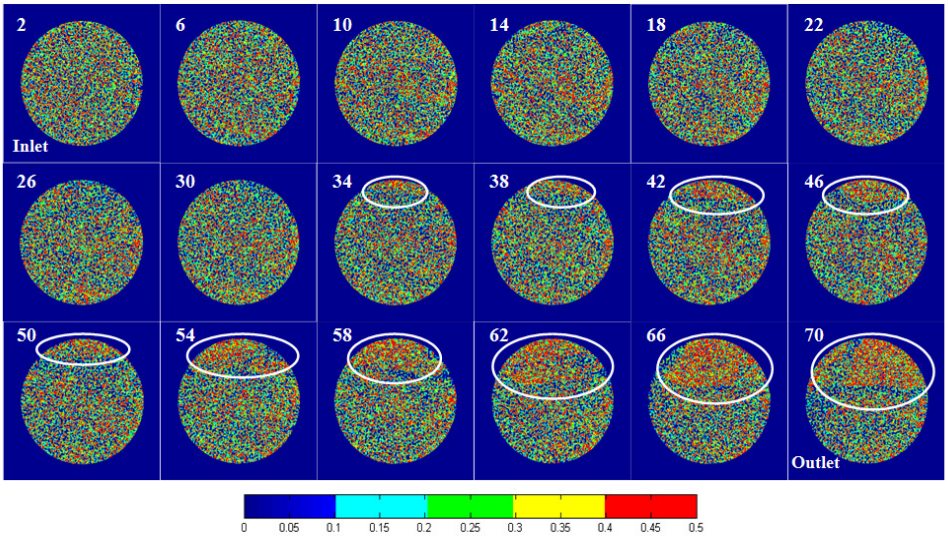

Figure 54 Distribution of porosities along the core (core #8)

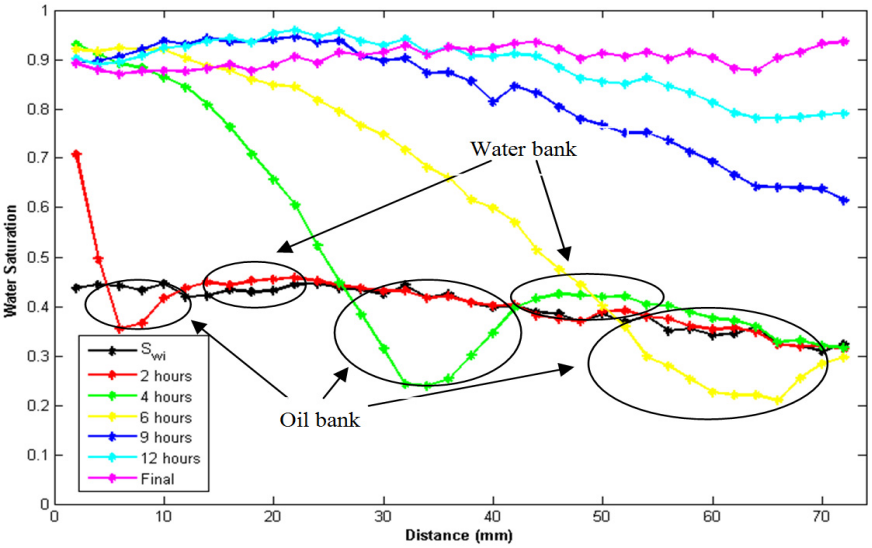

Figure 55 Distribution of water saturation in the core at different times (core #8)

During water flooding, the production data was recorded every 30 minutes. The production profiles and the differential pressures along the core are plotted in Figure 56. In total 3.4 pore volumes was injected until no oil production can be observed. The water breakthrough happened after 0.5 PVI (pore volumes injected), and little oil was recovered after the breakthrough. The changing of differential pressure also clearly indicates that the flow becomes stable after water breakthrough. The data about the oil recovery in water flooding will be discussed together with those in CO_2 flooding later.

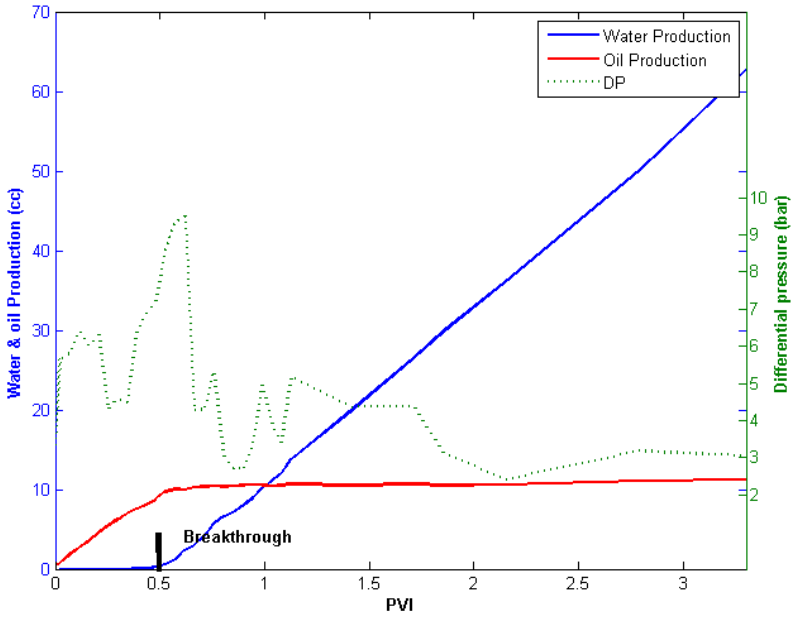

Figure 56 Production profiles for water flooding (core #8)

The CO_2 saturation profiles converted from CT data using eq. (32) is presented in Figure 57. The whole injection period lasted for 2 days, and more than 4 PVI has been injected until no fluid produced. The strong water end effect can clearly be observed, the difference between lowest and highest saturation reaches to 50%. The variation of CT number at different times along the core is demonstrated in Figure 58. The invasion of gas in the sample core is uniform at positions x= 2mm and x= 20mm. However, at the position x=38mm and x=56 mm, the injected gas invades the large porosity area first, as shown in the region of interest (white circle). The high porosity channel might cause early gas breakthrough. The quantitative measurement of in situ gas saturation is the main aim of our experiments, the results from the CT scanning will be compared with those from productions.

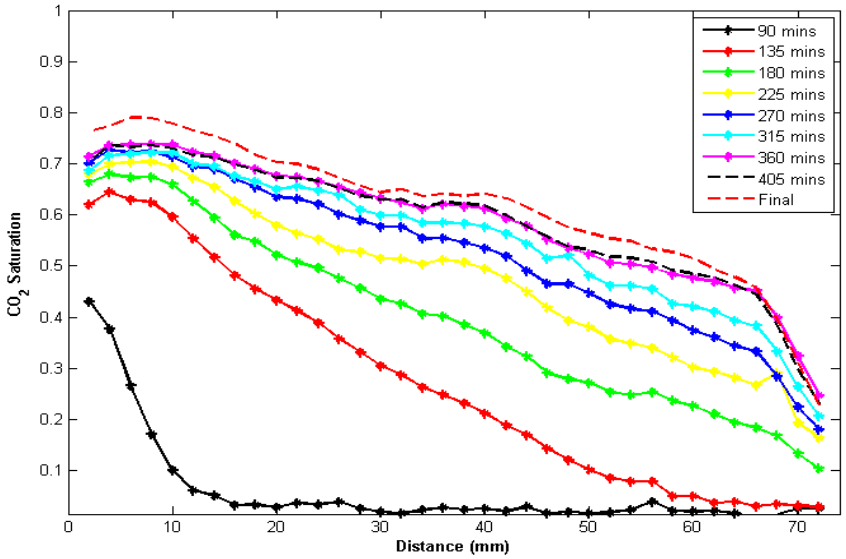

Figure 57 Distribution of CO_2 saturation in the core at different times (core #8)

In gas flooding, the production data was recorded every 15 minutes. The production profiles and the differential pressures along the core are plotted in Figure 59. During the CO_2 injection, there was no oil produced until 0.48 PVI. The oil production lasted for a short period, which indicated that the oil bank was formed in tertiary CO_2 flooding and produced quickly after gas breakthrough. 0.88 PVI injected gas is enough for producing mobilized oil. The oil recovery information compared with data derived from CT scanning is shown in Table 10. The oil recovery from water flooding is more than 80%, which proves that water flooding is an effective recovery method for the particular chalk reservoir. The oil recovery from the CO_2 tertiary flooding reaches 13.4%, which indicate that most of oil in the core has been recovered by injecting water and gas.

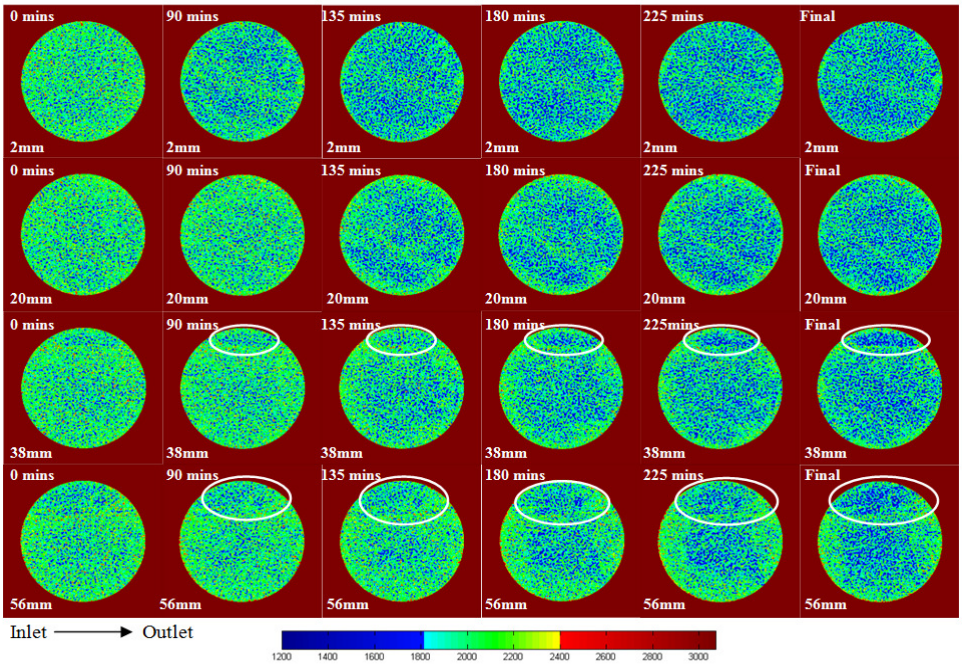

Figure 58 Distribution of CT numbers along the core at different times (core #8)

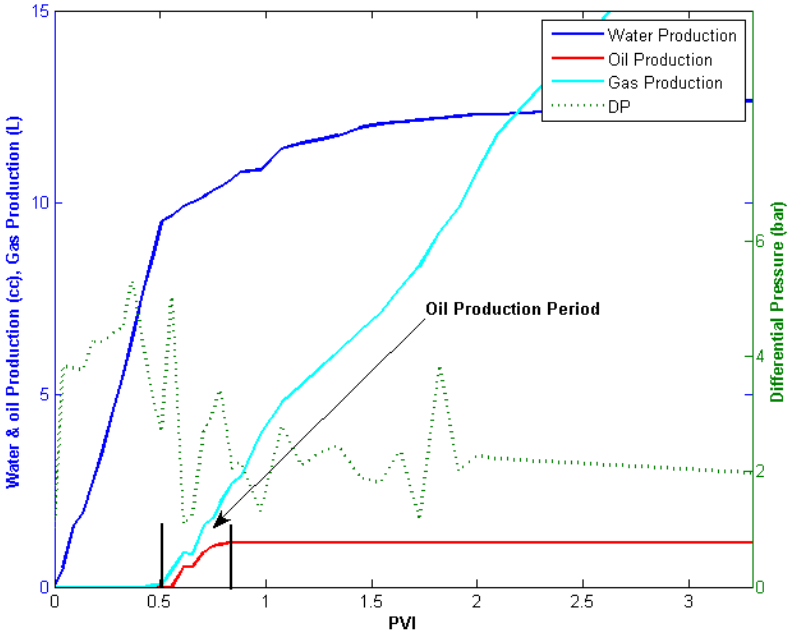

Figure 59 Production profiles for tertiary CO_2 flooding (core #8)

All the dead volumes in the equipment were carefully measured and included in all the mass balance calculations. The average saturations from mass balance and CT scanning agree each other well and the absolute difference between them ranges from 0.8% - 4.3%. Besides the influence from dead volume, there are two more possible reasons for these errors. Firstly, the injected CO_2 could dissolve in the water and live oil, and the calculated CO_2 saturation from CT data is not the saturation of free CO_2, but as the weight of CO_2 in the pore volume. Saturation from mass balance mainly represents the pore volume occupied by free CO_2. As a result, CO_2 saturation from CT scanning could be smaller than that obtained by mass balance. Secondly, although more than 5 PV of the doped water has been injected to replace the pure water after water flooding, 100% replacement may have not been realized which could lead to the fact that CO_2 saturation from CT scanning could be larger than that obtained by mass balance.

Table 10 Comparison of data from mass balance and CT scanning

	S_{wi} (%)	S_{or} (%)	Final S_g (%)	EOR_w (%)	EOR_g (%)
Mass balance	35.7	10.4	57.2	83.7	13.4
CT scanning	38.8	9.6	61.5	84.3	13.4

The core before and after the experiment are compared in Figure 60. A lateral fracture was created close to the outlet. During the experiment, the influence of lateral fracture could be negligible, since it is perpendicular to the flooding direction, the differential pressure across the core could keep the core as whole and there is no clear fracture can be observed, as indicated in Figure 58.

(1) Before the experiment

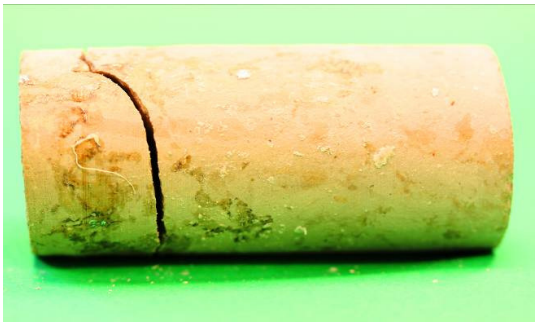

(2) After the experiment

Figure 60 Comparison of the core #8 before and after the experiment (core #8)

3.5.5 Experiment #7

To further improve and validate our proposed method, Exp. #7 with core #9 was used to perform the complete set of the water injection and tertiary gas flooding experiment, with injection 3 ml/h and 3.6 ml/h respectively. To tune the concentration of dopants in the distilled water and live oil and to determine the CT numbers of pure fluids under the reservoir conditions, an artificial core plug made of PTFE glass fabrics was used, which has an outer diameter of 38 mm and a length of 60 mm, as in Figure 61. A hole was drilled in the centre along the core plug. Three different inner diameters (10, 15 and 20 mm) were deliberately used to evaluate the influence of the Teflon thickness on the CT number of high pressure fluids. During the measurement of CT number of different fluids, the core holder was vertically placed and fluids were injected in sequence based on their density to guarantee the fully displacement of each other.

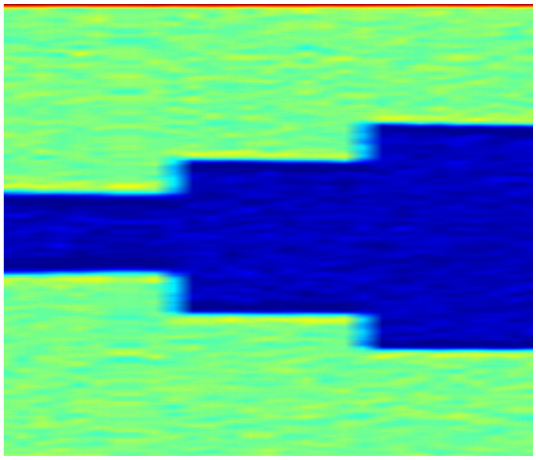

Figure 61 The cross section image of artificial core along the length direction

The CT numbers of pure CO_2, pure water, doped oil and doped water at the experimental conditions were measured as -270, 45, 473 and 476, respectively. The concentrations of dopants in live oil and water were 14 wt% and 3 wt%, respectively. Compared with Exp. #8, which takes several weeks to tune the concentration of dopants with real chalk core, the use of artificial core could shorten this period to several days and improve the accuracy of results.

The average S_{wi} is 35% before water flooding. The production profiles for water flooding and CO_2 flooding are plotted in Figure 62 and Figure 63 respectively. In water flooding, 1.4 pore volume was injected until no oil production can be observed. The water breakthrough happened after 0.35 PVI (pore volume injected), and little oil was recovered after the breakthrough. The average S_{or} is 43.2% after water flooding. During the CO_2 injection, the oil production started immediately after CO_2 breakthrough. The oil production was fast in the beginning and most mobilized oil was produced at 0.72 PVI. After that, only several data point has been recorded, therefore, the oil production curve has a sharp change.

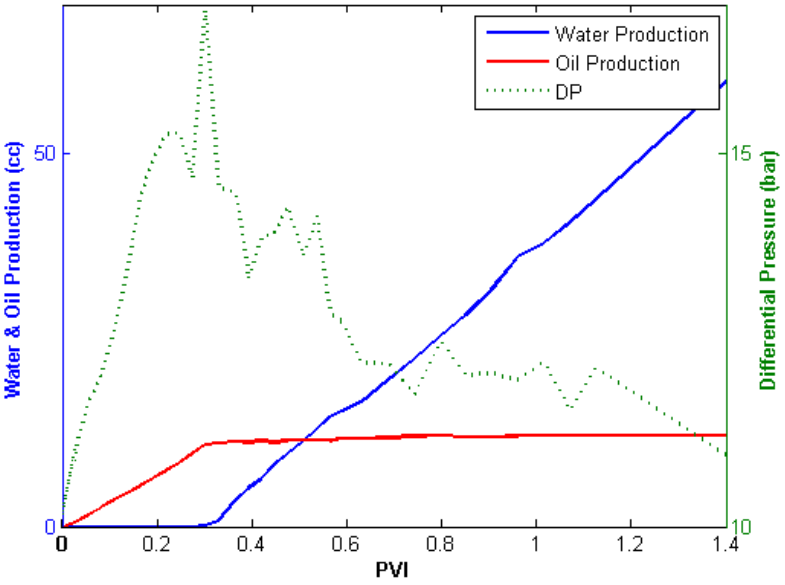

Figure 62 Production profiles for water flooding (core #9)

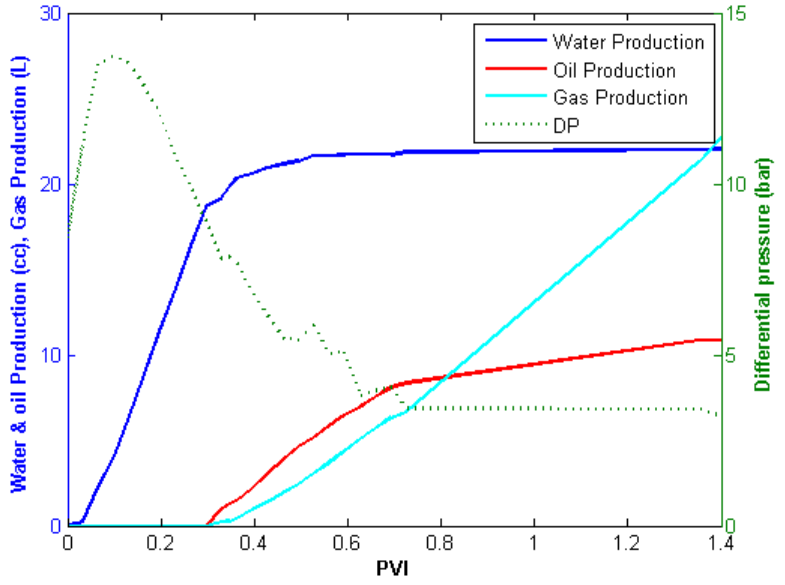

Figure 63 Production profiles for gas flooding (core #9)

The CO_2 saturation converted from CT data using eq. (32) is presented in Figure 64, which quantitatively describes the dynamical propagation of CO_2 in the core. Table 11 provides the saturations after the water flooding and after the CO_2 flooding obtained from mass balance and from CT scanning. The oil recovery factors after the water flooding and the CO_2 flooding are 33.5% and 77.7%, respectively, showing that CO_2 flooding is an effective recovery method for the particular chalk reservoir and most of oil in the core has been recovered by injecting water and CO_2.

In Exp. #6 and Exp. #7, core#8 and core#9 origin from two different formations in the North Sea section. As shown in Table 10, Water flooding in Exp. #6 gives very high recovery, while that in Exp. #7 gives just moderate recovery (in Table 11). This indicates that two formations have different responses to water flooding, although their permeability and porosity are similar. CO_2 flooding into the water flooded cores has produced a lot of additional oils in both cases. This shows that the potential of tertiary CO_2 flooding to extract the remaining oils after water flooding, especially for formations where water flooding is not very efficient.

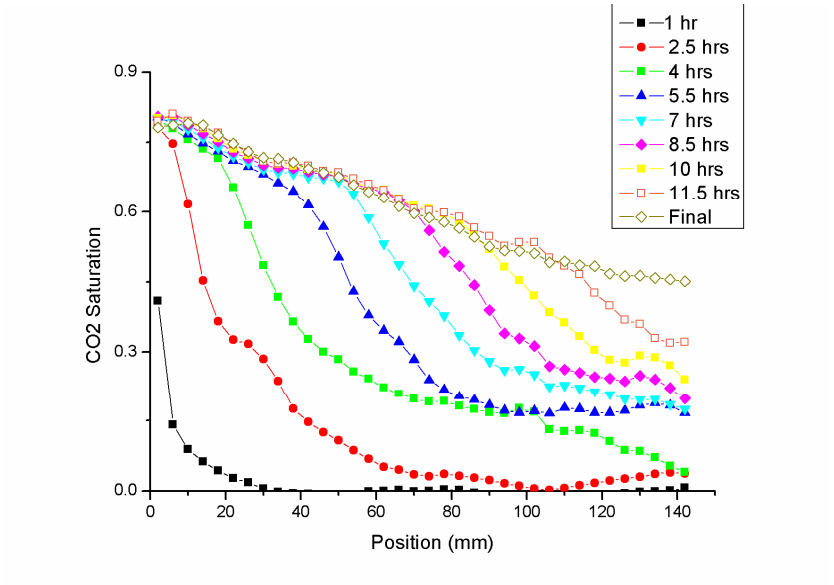

Figure 64 Distribution of CO_2 saturation in the core at different times (core #9)

In Figure 57 and Figure 64, the end effect has different influence on the distribution of CO_2 saturation in core#8 and core#9 respectively. More liquid phase has been capatured at the end of the core#8 than in the core#9, due to the fact that the length of core#8 is smaller and it is more water-wet than core#9.

Table 11 Comparison of data from mass balance and CT scanning (core #9)

	Initial S_o (%)	Water flooding S_{or} (%)	Gas flooding S_g (%)	RF_w (%)	RF_g (%)
Mass balance	65.0	43.2	57.5	33.5	77.7
CT scanning	66.5	-	61.4	-	-

All the dead volumes in the equipment were carefully measured and included in all the mass balance calculations. The average saturations from mass balance and CT scanning agree each other well and the absolute difference between them ranges from 1.5% - 3.9% (Table 11). Similar as in Exp. #7, besides the influence from dead volume, the dissolution of CO_2 in water and the incomplete replacement of the pure water by the doped water after water flooding, are main reasons for the errors in the CO_2 saturation.

Reference

[1] D. M. Beeson and G. D. Ortloff, "Laboratory Investigation of the Water-Driven Carbon Dioxide Process for Oil Recovery," *Journal of Petroleum Technology*, vol. 11, no. 2, pp. 63–66, April 1959.

[2] E. Manrique, V. Muci, and M. Gurfinkel, "EOR Field Experiences in Carbonate Reservoirs in the United States," *SPE Reservoir Evaluation & Engineering*, vol. 10, no. 6, pp. 667–686, December 2006.

[3] A. Espie. (2005, 21-23 November) A New Dawn for CO_2 EOR. Paper SPE 10935 presented at the International Petroleum Technology Conference, Doha, Qatar.

[4] A. Zick. (1986, 5-8 October) A Combined Condensing/Vaporizing Mechanism in the Displacement of Oil by Enriched Gases. Paper SPE 15493 presented at the SPE Annual Technical Conference and Exhibition, New Orleans, Louisiana.

[5] E. A. Turek, R. S. Metcalfe, and R. E. Fishback, "Phase Behavior of Several CO_2/West-Texas-Reservoir-Oil Systems," *SPE Rreservoir Engineering*, vol. 3, no. 2, pp. 505–516, May 1988.

[6] J.G. Shyeh-Yung. (1991, 6-9 October) Mechanisms of Miscible Oil Recovery: Effects of Pressure on Miscible and Near-miscible Displacements of Oil by Carbon Dioxide. Paper SPE 22651 presented at the SPE Annual Technical Conference and Exhibition, Dallas, Texas.

[7] L. W. Holm and V. A. Josendal, "Effect of Oil Composition on Miscible-type Displacement by Carbon Dioxide," *SPE Journal*, vol. 22, no. 1, pp. 87–98, February 1982.

[8] R. Metcalfe and L. Yarborough, "The Effect of Phase Equilibrium on the CO_2 Displacement Mechanism," *SPE Journal*, vol. 19, no. 4, pp. 242–252, August 1979.

[9] A. Rosman. (1977, 9-12 October) Experimental Studies of Low IFT Displacement by CO_2 Injection. Paper SPE 6723 presented at the SPE Annual Fall Technical Conference and Exhibition, Denver, Colorado.

[10] S. Ghedan. (2009, 19-21 October) Global Laboratory Experience of CO_2-EOR Flooding. Paper 125581 presented at SPE/EAGE Reservoir Characterization and Simulation Conference, Abu Dhabi, UAE.

[11] S. L. Wellington and H. J. Vinegar, "X-Ray Computerized Tomography," *Journal of Petroleum Technology*, vol. 39, no. 8, pp. 885–898, August 1987.

[12] S. L. Wellington and H. J. Vinegar. (1985, 22-26 September) CT Studies of Surfactant-Induced CO_2 Mobility Control. Paper SPE 14393 presented at the SPE Annual Technical Conference and Exhibition, Las Vegas, Nevada.

[13] Y. Junji, S. Tohru, I. Hiroshi, and O. Komei. (1997, 14-16 April) An Analysis of CO_2 WAG Coreflood by Use of X-Ray CT. Paper SPE 38068 presented at the SPE Asia Pacific Oil and Gas Conference and Exhibition, Kuala Lumpur, Malaysia.

[14] O. Izgec, B. Demiral, H. Bertin, and S. Akin. (2005, 30 March-01 April) CO_2 Injection in Carbonates. Paper SPE 93773 presented at the SPE Western Regional Meeting, Irvine, California.

[15] P. L. Zitha, Q. P. Nguyen, and P. K. Currie. (2003, 9-11 September) Effect of Flow Velocity and Rock Layering on Foam Flow: An X-Ray Computed Tomography Study. Paper SPE 80530 presented at the SPE Asia Pacific Oil and Gas Conference and Exhibition, Jakarta, Indonesia.

[16] D. Du, P. L. Zitha, and M. G. Uijttenhout, "Carbon Dioxide Foam Rheology in Porous Media: A CT Scan Study," *SPE Journal*, vol. 12, no. 2, pp. 245–252, June 2007.

[17] T. Oshita, H. Okabe, and T. Namba. (2000, 25-26 April) Early Water Breakthrough—X-ray CT Visualizes How It Happens in Oil-Wet Cores. Paper SPE 59426 presented at the SPE Asia Pacific Conference on Integrated Modelling for Asset Management, Yokohama, Japan.

[18] A. Hove, J. Ringen, and P. Read, "Visualization of Laboratory Corefloods with the Aid of Computerized Tomography of X-Ray," *SPE Reservoir Engineering*, vol. 2, no. 2, pp. 148–154, May 1987.

[19] H. J. Vinegar and S. L. Wellington, "Tomographic Imaging of Three-Phase Flow Experiment," *Rev.Sci.Instrum.*, vol. 58, pp. 96–107, January 1987.

[20] A. Kantzas, "Investigation of Physical Properties of Porous Rocks and Fluid Flow Phenomena in Porous Media Using Computer Assisted Tomography," *In Situ*, vol. 14, no. 1, pp. 77–132, 1990.

[21] I. Chatzis, A. Kantzas, and F. A. L. Dullien. (1988, 2-5 October) On the Investigation of Gravity-Assisted Inert Gas Injection Using Micromodels, Long Berea Sandstone Cores, and Computer-Assisted Tomography. Paper SPE 18284 presented at the SPE Annual Technical Conference and Exhibition, Houston, Texas.

[22] A. Lackner, G. Haaskjold, and O. Torsaeter. (2005, 20-23 June) Selecting X-Ray Energy Levels for Three-Phase Saturation Measurements. Paper SPE presented at the SPE Latin American and Caribbean Petroleum Engineering Conference, Rio de Janeiro, Brazil.

[23] A. Sahni, F. Gadelle, , M. Kumar, L. Tomutsa, and A. Kovscek, "Experiments and Analysis of Heavy-Oil Solution-Gas Drive," *Reservoir Evaluation & Engineering*, vol. 7, no. 3, pp. 217–229, June 2004.

[24] http://www.temcoinstruments.com/PDF/X Ray%20Core%20Holder.pdf.

[25] http://webbook.nist.gov/chemistry/.

[26] I. Akervoll, M. Talukdar, S. Midtlyng, J. Stensen, and O. Torsaeter. (2000, 3-5 April) WAG Injection Experiments with In Situ Saturation Measurements at Reservoir Conditions and Simulations. Paper SPE 59323 presented at the SPE/DOE Improved Oil Recovery Symposium, Tulsa, Oklahoma.

[27] A. Sahni, F. Gadelle, M. Kumur, A. Kovscek, and L. Tomusta. (2001, 30 September-3 October 2001) Experiments and Analysis of Heavy Oil Solution Gas Dirive. Paper SPE 71498 presented at the SPE Annual Technical Conference and Exhibition, New Orleans, Louisiana.

[28] http://www.proscitech.com/cataloguex/msds/c142.pdf.

[29] K. Oseto, A. Al-Amoudi, and M. Suzuki. (2006, 5-8 November) Comprehensive Approach of Core Analysis to Predict Waterflooding Performance in a Heterogeneous Carbonate Reservoir, Offshore Abu Dhabi. Paper SPE 101287 presented at the Abu Dhabi International Petroleum Exhibition and Conference, Abu Dhabi, UAE.

[30] B. C. Sharma, W. E. Brigham, and L. M. Castanier, “CT Imaging Techniques for Two-Phase and Three-Phase In Situ Saturation Measurements,” Stanford University, CA, USA, Tech. Rep., June 1997. [Online].

[31] ResLab, GEUS, CALSEP, and SINTEF, “Joint Chalk Research - vi,” Tech. Rep., 2007.

[32] K. Levenberg, “A Method for the Solution of Certain Problem in Least Squares,” *Quarterly of Applied Mathematics*, vol. 2, pp. 164–168, 1944.

[33] D. Marquardt, “An Algorithm for Least Squares Estimation of Nonlinear Parameter,” *SIAM Journal on Applied Mathematics*, vol. 11, pp. 431–441, 1963.

[34] K. Madsen and H. Nielsen, “Finite Algorithm for Robust Linear Regression,” *BIT Numerical Mathematics*, vol. 30, pp. 682–699, 1993.

[35] B. Niu and R. R. Boesen, “Compulsory Assignment C on Course 02610 Optimization and Data Fitting,” Department of informatics and Mathematical Modelling, Tech. Rep., 2007.

[36] J. P. Schlomka, E. Roessl, R. Dorscheid, S. Dill, G. Martens, T. Istel, C. Bumer, C. Herrmann, R. Steadman, G. Zeitler, A. Livne, and R. Proksa, “Experimental Feasibility of Multi-Energy Photon-Counting K-Edge Imaging in Pre-Clinical Computed Tomography,” *Physics in Medicine and Biology*, vol. 53, no. 15, pp. 4031–4047, 2008.

[37] S. Feuerlein, E. Roessl, R. Proksa, G. Martens, O. Klass, M. Jeltsch, V. Rasche, H. J. Brambs, M. H. K. Hoffmann, and J. P. Schlomka, “Multienergy Photon-Counting K-edge Imaging: Potential for Improved Luminal Depiction in Vascular Imaging,” *Radiology*, vol. 249, pp. 1010–1016, 2008.

[38] H. Matsukiyo, M. Watanabea, E. Sato, A. Osawa, T. Enomoto, J. Nagao, P. Abderyim, K. Alzawa, K. Hitomi, E. Tanaka, H. Mori, T. Kawai, A. Ogawa, K. Takahashi, S. Sato, and J. Onagawa, “Energy-Discriminating K-Edge X-Ray Computed Tomography System,” *Japanese Journal of Applied Physics*, vol. 49, pp. B–1 –B–5, 2010.

[39] M. E. Coles, E. L. Muegge, and B. F. Marek. (1992) Use of Attenuation Standards for CAT Scanning Applications within Oil and Gas Production Research. Paper 9223 presented at the Society of Core Analysts Conference.

[40] S. YU, I. Akervo, O. Torsaeter, J. Stensen, J. Kleppe, and S. Micftlyng. (1998, 2-6 November) History Matching Gas Injection Processes with In Situ Saturation Measurements and Process Hysteresis. Paper SPE 488421 presented at the SPE International Oil and Gas Conference and Exhibition in China, Beijing, China.

[41] P. Z. Wong, *Methods in the Porous Media*, R. Celotta and T. Lucatorto, Eds. Academic Press, 1999, vol. 35.

[42] S. Siddiqui, P. J. Hicks, and A. S. Grader, “Verification of Buckley-Leverret Three-Phase Theory Using Computerized Tomography,” *Journal of of Petroleum Science and Engineering*, vol. 15, pp. 1–21, 1996.

[43] M. Al-Wadah, A. S. Grader, and T. Ertekin. (2000, 1-4 October) An Investigation of Three-Phase Counter-Current Flow Using X-Ray Computerized Tomography and Neuro-Simulation Modelling. Paper SPE 63146 presented at the SPE Annual Technical Conference and Exhibition, Dallas, Texas.

Chapter 4. Geochemical Transport in Porous Media for CO_2 Injection into Aquifers and CO_2 EOR Process

4.1 Introduction

Geochemical transport in porous media is determined by various processes of physical and chemical types, such as advection and dispersion of fluids, geochemical reactions between ions and rock matrix, redox processes and biochemical process with bacteria, etc. It has always been an important topic in the groundwater study, due to its various applications, as ore body deposition [1], heavy metal migration [2], interaction between ground water, contamination of aquifer [3] and surface water [4] and water quality monitoring network [5]. At the same time, geochemical reactive transport is also a common topic in petroleum engineering. Alkaline flooding[6], acidizing wells [7] and non-equilibrium seawater injection [8] etc. are typical reactive transport processes among enhanced oil recovery (EOR) methods.

Recently, to reduce the excessive greenhouse gas in the atmosphere, especially CO_2, which is considered as the major contributor to global warming, sequestration of CO_2 from large industrial sources, such as natural gas processing and power stations [9], has become a key research area. The sequestration of CO_2 means that the disposal of CO_2 in the places, which have sufficient capacity and are isolated from atmosphere, such as deep ocean [10] and geological formations [11]. The former option might temporarily store CO_2 with high environmental risks linked to sudden release of CO_2 and also represents a technological challenge [12]. The latter option include various situations, e.g. coal beds, in which CO_2 will be adsorbed on the surfaces of coal particles and replace the adsorbed CH_4, oil and gas reservoir, where the injected CO_2 can enhance the recovery of hydrocarbons, or deep saline aquifers. A comprehensive literature review has been given by Orr [13] on storage of carbon dioxide in geologic formations, which includes both theoretical description of mechanisms and comparison of field cases.

In practice, geological storage of CO_2 in oil reservoirs and aquifers are considered as most efficient and feasible ways. The former is easier to implement thanks to the plentiful experience accumulated in the oil industry. The process also provides additional benefit by enhancing the oil recovery. The world's largest CO_2 EOR is carried out in Permian basin, USA, with the first project started in 1972. There are more than 23 mtCO_2/yr delivered to more than 50 active projects in the basin, and at the same time, more than 145,000 bpd of incremental oil produced [2]. However the oil and gas reservoir are not uniformly distributed geographically, and anthropogenic CO_2 is generated in many

locations that are not close to potential storage sites in oil reservoirs [13]. Therefore, the widely distributed deep saline aquifers with huge storage capacity are also considered as ideal candidates. The reservoir simulators for CO_2 flooding and the geothermal simulators for CO_2 sequestration usually have different focuses. The former focuses on three-phase flow and phase equilibrium, while the latter focuses on geochemical reaction in the aqueous phase, with only two phases (gas and aqueous) flow included.

Multiphase reactive transport models, that can treat any combination of transport and geochemical process, date back to mid-1980s [15]. Lichtner [16] presented a time-space continuum model for transport of hydrothermal fluids in porous media involving simultaneous, reversible and irreversible reactions among liquids, gases and minerals. His work outlined much of the basic theory of a continuum model for reactive transport [15]. The analytical techniques used in solving reactive transport with equilibrium and kinetic controlled geochemical reactions have also been developed at the same time, including the method of characteristics [17] [18] [19] and the theory of precipitation/dissolution waves [20] [21]. By discussing the existing approaches on formulating reactive transport problems, Yeh and Tripathi [22] also presented the theoretical and numerical basis for simulating subsurface solute transport. Steefel and Lasaga [23] presented a coupled model for transport of multiple chemical species and kinetic precipitation/dissolution reactions with application of reactive flow in single phase hydrothermal systems. Currently, the simulator TOUGHREACT, which is developed in the Lawrence Berkeley National Laboratory (LBNL), represents the state of the art in modelling reactive transport referring to CO_2 injection into aquifers. These studies were largely focused on developing the theoretical and numerical tools for simulating reactive transport in a range of environments [15].

Usually, most models on CO_2 flooding in oil reservoir mainly focus on the multiphase flow without considering geochemical reactions, since the phase behavior is very complex during the process and the accurate prediction of oil recovery is the priority. Nghiem and Li [24] investigated the effect of multiphase phenomena on flow behavior, recovery efficiency and the prediction of minimum miscible pressure (MMP) by performing slim-tube simulations. Chang et al. [25] discussed the effect of CO_2 solubility in brine on the oil recovery of CO_2 flooding by using three-phase compositional model. The influence of the possible fourth phase in CO_2 EOR on oil recovery was reported by Guler et al. [26], with using a 2-D compositional model.

However, except the complex interaction between oil, water and CO_2 in the coexisting three fluid phases, such as mutual solubility, change of acidity, and oil swelling, CO_2 flooding process also involves geochemical reactions between aqueous phase and rock, similar to CO_2 injection into aquifers. The three-phase fluid flow and geochemical process also influence each other. The former determines how solutes are transported; the latter changes the flow by changing porosity and permeability due to mineral dissolution and precipitation. Therefore, there is a strong coupling between transport and geochemical reaction. Furthermore, in order to predict the overall process of CO_2 flooding in oil reservoir accurately and to evaluate the efficiency of CO_2 storage during and after this process, the gap between the above two kinds of simulators should be filled.

In this section, the classification and application of geochemical and solute transport modelling on CO_2 injection into aquifers and CO_2 EOR process is discussed first, which includes the mechanisms of CO_2 storage, various focuses of existing models and their application in different aspects. Then, both analytical and numerical techniques, used in simulating geochemical transport systems, are introduced. Finally, the investigation on how to simulate CO_2 flooding including both three-phase flow and geochemical reaction by using COMSOL Multiphysics (hereafter called COMSOL) is conducted, and the detailed simulation results at reservoir scale and lab core scale are presented.

4.2 The classification and application of geochemical and solute transport modelling in CO_2 injection into aquifers and CO_2 EOR process

4.2.1 Importance of evaluating geochemical impacts during CO_2 storage in aquifers and oil reservoirs

CO_2 can be sequestrated in geological formation as oil reservoir and aquifers by four mechanisms: hydrodynamic trapping, solubility trapping, capillary trapping and mineral trapping. CO_2 can be trapped as gas or supercritical fluid under a low-permeability cap rock, similar to the way natural gas is trapped in gas reservoirs [27]. This mechanism is called hydrodynamic trapping, which is the most important for short term sequestration. Considerable experience with CO_2 and hydrocarbon gas injection projects obtained in oil industry and the detailed geological information about the injection site from both oil industry and earth science are ready for future application in CO_2 sequestration.

Similar as gas dissolved in oil, CO_2 can also dissolve into the fluid phase, and this mechanism is called as solubility trapping. The relative importance of solubility trapping in CO_2 storage depends on

various factors, such as sweep efficiency, formation heterogeneity and hydrodynamic instabilities due to displacement between gas and fluid phase with different viscosity [79]. The dissolved CO_2 could increase the density of formation brine, and as a consequence, the CO_2 dissolved water will sink gradually, while the CO_2 phase will move up due to the buoyant force. In most cases of practical interest, the longest timescale for the complete dissolution of the carbon dioxide could be thousands of years, mainly depending on the vertical permeability [29].

Capillary trapping is considered as the most rapid method to immobilize the CO_2, which happens when non-wetting gas phase is displaced by the water phase in water wet media and capillary-dominated flow regime due to the phenomenon of snap-off and cooperative filling [30]. Capillary trapping influences the efficiency of CO_2 storage in two ways: (1) after CO_2 has been injected into aquifers, CO_2 plume will move up due to the buoyant forces. At the trailing, water displaces gas in an imbibitions process, which leads to snap-off and trapping CO_2 phase [31]. (2) since there is a possibility that the cap rock could leak, react with CO_2 and brine, have gaps, or be penetrated by wells, which could induce leakage of CO_2, water flooding is suggested after the injection of CO_2 to render the CO_2 immobile by capillary trapping before it moves up to cap rock [32].

CO_2 can react either directly or indirectly with the minerals and organic matter in the geological formations leading to the precipitation of secondary carbonates and the solubilisation of organic matter [27]. This mechanism is called mineral trapping. Although this process takes thousands of years to immobilize CO_2, it could sequestrate CO_2 in subsurface environment permanently and prevent CO_2 easy return to the atmosphere [33]. A study of simulation on CO_2 disposal in Gulf Coast sediment [34] shows that CO_2 is trapped by secondary carbonate minerals such as calcite ($CaCO_3$), dolomite ($CaMg(CO_3)_2$), siderite ($FeCO_3$), and dawsonite ($NaAlCO_3(OH)_2$) and the CO_2 mineral trapping capability after 10000 years is comparable to CO_2 dissolution in pores water. The reactive behaviour of supercritical CO_2 under conditions relevant to geological storage and sequestration of CO_2 is largely unknown, especially at high pressure and temperature conditions [35]. Kaszuba et al. [35] performed experiments at 200 ^{o}C and 200 bar to investigate geochemical reactions in a model brine aquifer and observed that silicate precipitation happened next to carbonate precipitation, pointing out that transfer of H_2O from brine to supercritical CO_2 may have substantial influence on mineral reactions.

When CO_2 reaches the lower section of cap rock, it might trigger geochemical reactions, which could affect the porosity, permeability, and therefore the sealing capacity of the cap rock [36]. Both

seismic surveys and reservoir simulation prove that CO_2 reaches the base of the thick shale layer close to the top of the Utsira sand approximately 3 years after injection at the Sleipner site [37]. The simulation to evaluate major geochemical reactions between CO_2, the formation water and the clay cap rock mineralogy indicates that a slight decrease of the porosity might improve the sealing capability of the cap rock after thousands of years [38]. At the same time, the concept of forced mineral trapping for sequestration of CO_2 has also been proposed. McGrail et al. [39] suggested that portlandite $Ca(OH)_2$, the principle constituent in concrete from construction/demolition (C&D) waste, could be injected together with CO_2 to control the location of a calcite precipitation front and thus to maximize utilization of reservoir capacity for permanent carbon sequestration via mineral trapping.

The direct evidences from fields on the geochemical impact of injecting CO_2 were discussed by Kharaka et al. [40] and Wilson et al. [41]. By comparing fluids samples from injection and observation wells before injection with those after injection from the Firo formation, sharp drops in pH and pronounced increases in both alkalinity and iron concentration were found [40], indicating that the rapid dissolution of carbonate and mobilize toxic trace metals happened in the injection area. By analyzing the brine composition from observation well of the Weyburn project, Wilson et al. [41] also found the evidence of CO_2 dissolution and H_2CO_3 dissociation.

Besides the far field regions, as introduced above, which are facing long term geochemical reactions during CO_2 storage, the near wellbore regions could also be subjected to serious increase/decrease of the injectivity induced by mineral dissolution/precipitation [42]. Both experimental work and field cases indicated that the well injectivity issue is complex, since many factors are combined in this process, such as rock fabric, flow region, thermodynamic conditions and fluid compositions [43]. Some evidence has been found in experimental investigation of reaction-transport phenomena during CO_2 injection by Egermann et al. [44]. They concluded that the high flow rates could limit the permeability reduction due to the precipitation [44]. However, Rogers et al. [45] investigated the injectivity behaviour in various CO_2 flooded reservoir cases by reviewing more than 100 papers, and indicated that dissolution/precipitation, and particle invasion/migration during the injection of CO_2 and WAG (water-alternating-gas) process have not been proved or disproved conclusively. Therefore, the gap between experimental work and practical cases shows that this area still needs more efforts on both theoretical and experimental point of view.

In conclusion, geochemical reactions not only serve as an important mechanism on trapping CO_2 for long term, but also act as an influential factor on well injectivity for short term which clearly needs more theoretical and practical investigations.

4.2.2 The classification of geochemical and solute transport models on CO_2 injection into aquifers and CO_2 EOR process

Numerical modelling of CO_2 injection in aquifers and oil reservoir can provide further understanding of various mechanisms and predict the short and long-term fate of injected CO_2. These models can have different emphases based on their functions, and can be divided into three catalogues:

Reaction path model: The reaction path model, also called the batch model, is mainly used to simulate a wide range of geochemical reactions and investigate geochemical fluid-rock interactions with complex mineralogical assemblages and dissolution and precipitation kinetics without considering any flow aspects [46]. Pruess et al. [47] conducted a survey of minerals commonly encountered in crustal rocks to identify possibilities for mineral trapping of CO_2 through the formation of carbonates, and performed batch reaction modelling of the geochemical evolution of reprehensive aquifer mineralogies. Xu et al. [48] used batch reaction modelling to evaluate the geochemical evolution of three different aquifer mineral compositions in the presence of CO_2 at high pressure and found that the trapping capacity at various sites depends significantly on the mineral composition. Marini et al. [12] gave comprehensive discussion on the thermodynamics, kinetics and reaction path modelling about geological sequestration of CO_2, and illustrated water-CO_2-rock interactions with appearance of different minerals by using reaction path model, EQ3NR®. Although no flow transport is considered, reaction path model is still a powerful tool in evaluating interactions of water-CO_2-rock, since the problems concerning geochemical reactions are very complex and case dependent and careful evaluation of simulation results could provide further insights into sequestration mechanisms and controlling geochemical conditions [47].

Hydrodynamic model: The hydrodynamic model is mainly used to study the flow of multiphase fluids in various dimensions, including hydrodynamic trapping, solubility trapping and capillary trapping, without considering geochemical reactions. Various simulation tools have been developed to describe multiphase transport in geological formations, such as black oil/compositional reservoir simulators used in the oil industry and simulators used for geothermal, nuclear waste and groundwater studies. To predict the distribution of injected CO_2 in the Utsira sand, Sleipner,

Lindeberg et al. [37] used ECLIPSE to predict the growth and migration of CO_2 accumulations, and the results are quite similar to seismic images. Ulker et al. [49] investigated the effect of phase behaviour on the performance of the CO_2 trapping in depleted gas reservoir and aquifers, and found that the solubility trapping strongly depends on brine salinity, density between gas and brine, and critical gas saturation. Jessen et al. [50] used Eclipse 300 to simulate various schemes, which could increase CO_2 storage during the EOR process, and they suggested that the application of horizontal wells and partial completion of both injection and production wells could improve the contact of gas with the entire reservoir volume in the presence of buoyancy and mobility effects. Spiteri et al. [51] discussed the influence of relative permeability hysteresis on geological CO_2 sequestration by performing 3-D simulation with in-house simulator and figured out that accounting for trapping and relative permeability hysteresis of the non-wetting CO_2 phase is essential in order to correctly characterize the migration and final distribution of the injected CO_2. Oldenburg et al. [52] investigated the large scale deployment of carbon sequestration with enhanced gas recovery by using TOUGH2. The simulation results showed that significant amounts of CO_2 can be injected to produce significant quantities of additional natural gas and injection of CO_2 at the bottom of reservoir could inhibit the mixing of CO_2 and natural gas due to density effects. Although hydrodynamic models do not consider the geochemical reactions, they are still the main tools used in the oil industry concerning with EOR processes and CO_2 injection into aquifers. Because abundant experiences on commercial reservoir simulators can be directly used to the projects related to CO_2 storage and mineral trapping is a relatively long-term effect compared with the other mechanisms.

Reactive transport model: The reactive transport model is a combination of the previous two models, which is used to quantify the long-term fate of CO_2 as well as other aspects during geological storage and the most challenging to perform [46]. There are two families of simulators that are most widely used nowadays: TOUGHREACT, the enhancement of the multiphase fluid and heat flow code TOUGH2 by introducing geochemistry [53], and the commercial simulator, GEM-GHG, a combination of a black oil simulator and a geochemical batch code designed for simulating CO_2 trapping mechanisms [54]. Both simulators have integrated the dissolution and precipitation processes with their feedback on porosity and permeability [46]. Xu et al. [55] presented a 1-D radial model to simulate CO_2 disposal in deep saline aquifers at Gulf Coast sediment with TOUGHREACT. In this case, a detailed mineralogy was selected representative of the Gulf Coast formations, and porosity modification due to the mineral reactions was estimated for 10000 years [55]. Pruess et al. [47] evaluated the capacity of different rock-forming minerals to sequester CO_2 with TOUGHREACT and concluded that for most cases with practical interest in aquifer disposal of CO_2, the total amount

of CO_2 that can be sequestrated is of the order of 30 kg per m^3 of aquifer volume. Audigane et al. [56] simulated the injection scenario and storage period of CO_2 injection at the Sleipner site by using TOUGHREACT, and figured out that solubility trapping, other than mineral trapping, is the dominant storage mechanism at the Utsira sand formation. Calabrese et al. [57] evaluated the CO_2 storage in a depleted gas reservoir with GEM-GHG, and found that the key determinants of storage capacity are injection rate and purity of gas. Thibeau et al. [58] studied specific mineralization pathways and their CO_2 mineralization potential in Utsira sand formation with CEM-GHG. Their results [58] showed that carbonates path way first have net dissolution of dolomite, and then the dissolution of illite leads to the precipitation of chalcedony and kaolinite, and the CO_2 mineralization takes 10000 years to reach a stable state. Kumar et al. [59] used GEM-GHG to investigate the migration and growth of CO_2 plume in the deep aquifers and performed a detailed risk analysis about the CO_2 leakage based on reservoir and operation parameters. Reactive transport model is an ideal tool to simulate CO_2 sequestration in aquifers with considering all trapping mechanisms. However, there is almost no reactive transport model suitable for the CO_2 EOR process, which includes multiphase flow (oil, gas and water), and geochemical reactions simultaneously.

4.2.3 The application of geochemical and solute transport models on CO_2 injection into aquifers and CO_2 EOR process

In 2008, Gaus et al. [46] have conducted a comprehensive literature study on the domains concerning geochemical and solute transport modelling for CO_2 storage. In their study, four areas have been proposed as experiment, well integrity, near well injectivity and long-term CO_2 storage. However, the short-term CO_2 storage, especially aiming at CO_2 EOR process, is not included. In this section, all of the above five domains are addressed, and previous plot regarding the catalogue of four domains, based on their own spatial scale and timeframe of interest [46] has been extended, as shown in Figure 65. Based on the individual focus of each application domain, various models should be adopted and improvements are still needed.

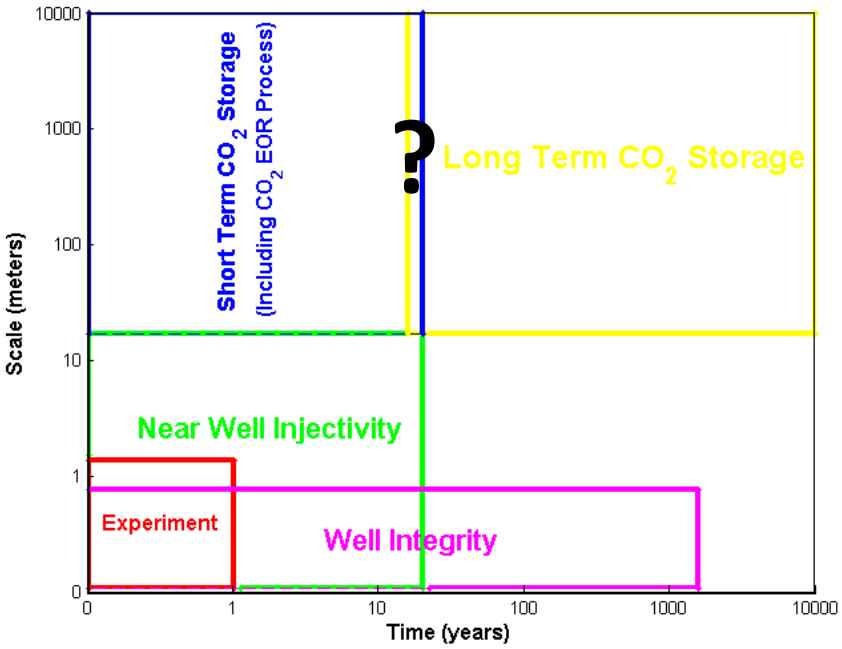

Figure 65 Application domains of CO_2 injection into aquifers and CO_2 EOR process

Experiment: modelling of laboratory experiments allows for the calibration and validation of newly developed model and acquirement of specific chemical or physical parameters. Due to the duration and time scale of experiments and the complexity of geochemical reaction, the developed model can be only calibrated with the interactions which have short-term impacts (in Figure 65) [42].

Batch experiments, which access the mineral trapping capability and change of porosity in porous media, are usually conducted and modelled to further understand trapping mechanisms and importance of various minerals under different reservoir conditions. Gunter et al. [60] conducted and modelled a batch experiment, containing reactions between CO_2 rich solution and glauconitic sandstone. After one month experiment, little reaction was observed, which occurred due to the fast-reacting carbonate minerals and the simulation results indicated that reactive surface area is an essential parameter in accurately predicting experimental results [60]. The differences between the model and observations in batch experiments highlight the need for thermodynamic and kinetic data with respect to CO_2 induced geochemical reactions at relevant P-T conditions [46].

Core flooding experiments focusing on geochemical reactions are modelled with emphasizing the variation of sample's porosity and permeability, but not the propagation of dissolution patterns, mainly because of difficulty in modelling the formation of worm hole. Wellman et al. [61] calibrated their reactive transport model with experimental data. In their study, CO_2 and water were injected simultaneously into the core sample, with recording the periodical change of sample's porosity and permeability, and the whole experiment lasted for 111 days. Afterwards, the data has been used to calibrate their model, developed from TOUGH2. Izgec et al. [79] carried out similar experiments on carbonate core, and used CMG-STARS to simulate the change of permeability in the sample.

Well integrity: To develop a well for production, cement would be filled in the annular space between the casing and rock, and when the well is abandoned, the open hole would typically be filled with a series of cement plugs [62]. The cement, used to ensure the wellbore and formation integrity during the injection and long-term storage, is threatened in acidic environment caused by CO_2 injection [42]. The well failure (possible leakage paths, shown in Figure 66), induced by deterioration on cement, is considered as one of the major risks for release of CO_2 to the surface during the CO_2 storage [63]. Therefore, the geochemical impacts of CO_2 injection on well integrity must be precisely evaluated and defined by both experiments and modelling.

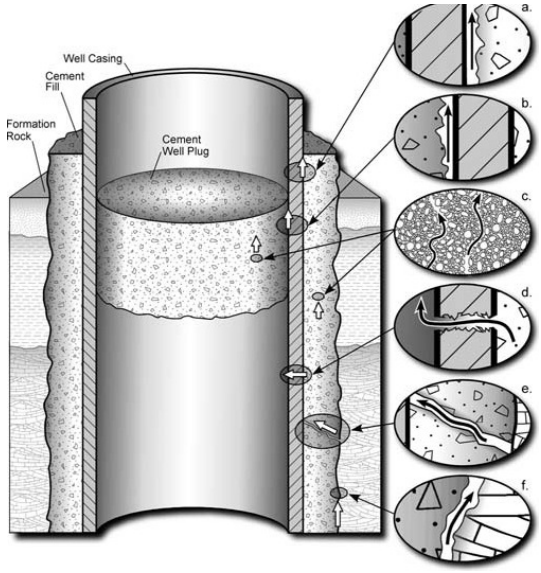

Figure 66 Potential leakage pathways along existing well: between cement and casing (paths a and b), through the cement (c), through the casing (d), through fractures (e), and between cement and formation (f) [63]

Benge [64] discussed the current selections, identified industrial methods to enhance the seal, and reviewed material selection methods that include stress modelling of the wellbore environment. Barlet et al. [65] performed a comprehensive study on the degradation of cement with injected supercritical CO_2 under downhole conditions. In their study, based on the data relating cement-strength loss, CO_2 penetration and the evolution of cement chemistry and porosity with time, it was found that Portland cement is not resistant enough to wet supercritical CO_2 and new CO_2 resistant material must be adopted. There are few studies dealing explicitly with well cement degradation modelling for CO_2 storage applications [46]. Jacquemet [66] performed experimental analysis and numerical simulations on the reactions between brine-CO_2-H_2S and cement-steel system under high temperature and pressure conditions. In his study, the cement carbonation and the steel sulphidation were found to be the main reactions, and 1-D simulations without considering well geometry were performed to reproduce the experimental results.

Near well injectivity: Modelling on well injectivity mainly focuses on the large pressure variation due to the geochemical reaction occurring near wellbore zones during the injection period. After the start of CO_2 injection, reservoir rocks near well bore zone are seriously flushed by large quantities of supercritical CO_2. The brine acidified by dissolved CO_2 could cause carbonate dissolution, which will increase the porosity and permeability. On the other hand, dry CO_2 also induces desiccation of the brine remaining in the pore space, which will lead to the precipitation of salts and sulphate minerals, blocking pore, and diminishing injectivity [46]. These two reserve processes could result in large pressure variation near wellbore zone.

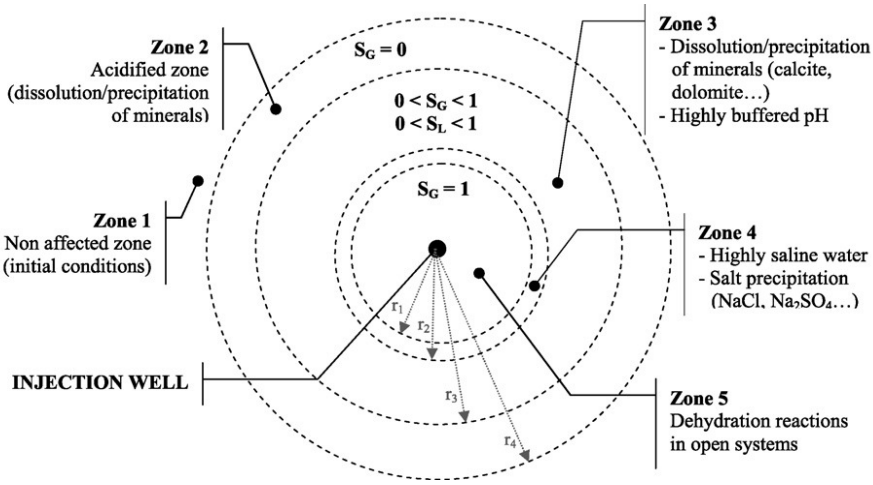

Figure 67 Conceptual diagram of the reactive zones around the injection well as derived from coupled modelling. The different radius (r1, r2, r3, r4) are dependent on CO_2 injection flow rate and rock properties. [67]

In Figure 67, the conceptual diagram of the reactive zones around the injection well is shown. Closest to the injection well, Zone 5 is fully saturated with dry CO_2, which could react directly with minerals [66]. Zone 4 is a transition zone, which is featured with low saturation of high saline pore water. With continuous CO_2 flow from the upstream (Zone 5), massive salts could precipitate in the pores, where saline water stay. In Zone 3, the pH of saline water is buffered by pressure of CO_2 phase, and mineral dissolution-precipitation happens at the same time. There is no CO_2 phase available in Zone 2, and only acidified aqueous CO_2 rich solution existing and reacting with rock matrix. Finally, Zone 1 is still in initial conditions.

To date, comprehensive simulation on investigating near well injectivity under reservoir conditions is still few, and the impact of brine desiccation process on well injectivity has not been thoroughly addressed [35]. André et al. [68] used TOUGHREACT to perform simulations on both CO_2 saturated water and pure supercritical CO_2 injection into deep aquifers in the Paris Basin with considering desiccation process. Their results [68] indicated that CO_2 saturated water is more reactive than supercritical CO_2 and can dramatically damage the reservoir structure. When the pressure is sufficiently high and under a continuous dry (without water vapor) CO_2 flux, an evaporation process starts leading to the precipitation of salts and possible another secondary minerals [68]. They also found that although dissolution could induce around 5% increase of porosity in the most part of

reservoir, the mineral precipitation during desiccation process appears to be the main important factor on the limited modification of well injectivity [68].

Long-term CO_2 storage: CO_2 long-term storage with considering the geometry of reservoir has been the most successful application of reactive transport modelling. Most of the models focus on the prediction of the ultimate fate of injected CO_2, the change of chemistry in water and the effect of CO_2 on the cap rock. The compromise between the number of geochemical reactions and complexity of geometry decides most models are performed in 1 or 2 dimensions. Xu et al. [69] performed 1-D simulation to predict ultimate fate of CO_2 after long-term storage and reproduce the change of water chemistry obtained from selected observation wells during CO_2 injection. In their study, more than 17 minerals have been considered and the model can be successful in reproducing the observed increases in aqueous Fe concentration. Bacon et al. [70] simulated CO_2-SO_2 injection into deep saline formations in 2-D, and concluded that addition of SO_2 in the injection could lead to the precipitation of anhydrite near the well and mineral trapping mechanisms had no significant effect on the rate of carbon sequestration in 100-year period.

When the number of model grid increases due to the complexity of layers and geometry, the identification of dominant geochemical reactions becomes more difficult and the resolution of gridding should be reduced. White et al. [71] simulated CO_2 injection into San Rafael Swell, Utah. In their study, a complex geological model has been introduced with considering 40 different layers in sedimentary sequence including potential reservoir and seal formation. They developed 2-D reactive transport model which consider time period up 100000 years with two different meshes [71]. The model with fine gridding mesh was mainly used to simulate flow transport without geochemical reactions. The one with coarse gridding was applied to modelling selected CO_2-brine-rock interactions due to the requirement of computing time.

For modelling on long-term CO_2 storage, the number of geochemical reactions considered and the parameters regarding kinetically controlled reaction are essential to the accuracy and validity of simulations results. Several researchers have performed simulations based on the same case, Sleipner CO_2 project. However, their results are different or even contradictory with respect to certain conclusions on the long-term behaviour [46]. Both Thibeau et al. [58] and Franeul et al. [72] performed simulation on CO_2 injection in Utsira aquifer at Sleipner in 3-D with geochemical compositional simulator GEM-GHG. However, they have different conclusions about the importance of mineral trapping mechanisms. Thibeau et al. [58] considered a comprehensive mineralogical

description and concluded that significant amount of CO_2 could be trapped in mineral. However, Franeul et al. [72] only considered the carbonate mineralogy in the geochemical reactions, and claimed that no obvious precipitation was detected.

Both Johnson et al. [73] and Gaus et al. [74] evaluated the security of CO_2 storage at Sleipner and modelled the change of porosity of caprock by simulating the migration of CO_2 to the top of reservoir. Johnson et al. [73] found that after 20 years, the decrease of porosity in the shale cap rock is an important mechanism for its self-seal and maximizing local carbonate cementation. However, this conclusion was proved by Gaus et al.'s results after 3000 years [74]. The uncertainty in their results is due to the fact that they used different values for specific surface area and further reactive surface area of minerals, which are difficult to measure or estimate.

Short-term CO_2 storage: As shown in Figure 65, CO_2 EOR process in oil industry can be considered as short-term CO_2 storage, since its duration could be more than 30 years (CO_2 EOR projects has been conducted in the Permian Basin of Texas for three decades.). There are several ways to increase the capacity of CO_2 sequestration during the CO_2 EOR process [50] [11]: (1) Partial completion of injection and production wells, (2) Using horizontal wells, (3) CO_2 could be injected into the aquifer instead of into the oil zone above, (4) Using WAG (water-alternating-gas) scheme, and (5) Repressurizing reservoir with continuous injection of CO_2 after oil production until the initial reservoir pressure is reached. The simulation of above five methods in the CO_2 EOR process can be handled by the hydrodynamic models with existing reservoir simulator as ECLIPSE 1000 without considering any issues in geochemical reactions [50].

However, the introduction of geochemical reactions into the simulation of CO_2 EOR process is significantly important. Firstly, as shown in Figure 65, during the whole period of CO_2 EOR process, water and CO_2 are continuously injected through wells. Therefore, near well injectivity could affect the efficiency of CO_2 EOR process in practice. Secondly, the alternation of porosity and permeability in reservoir formation owing to the geochemical reaction could possibly influence the fluid flow in porous media. Finally, the long-term monitoring of reservoirs after CO_2 EOR requires the information regarding to the change of mineral assemblage during that process. The question mark in Figure 65 indicates that there is a gap between CO_2 EOR process and long-term CO_2 storage. Because the former excludes the geochemical reaction, while the later considers it in predicting mineral trapping.

In Table 12, the importance of geochemical reaction in short-term CO_2 storage, as CO_2 EOR process is discussed based on the literature research (conducted by the author). The literatures are mainly based on the CO_2 injection into aquifers, since the geochemical reactions could be similar to those in CO_2 EOR process. Although the simulation results are very case dependent due to their differences in mineral assemblage, geological formation and storage time, the importance of geochemical reactions in short-term CO_2 storage still can be evaluated by the parameter, "30 years /Total", in the last column.

Table 12 The importance of geochemical reactions in short-term CO_2 storage

Reference	Formation	Temperature Pressure	Total simulation time (years)	maximum consumed mineral	30 years /Total
White et al.[71]	San Rafael Swell,Utah	54 °C ***	10000	Feldspar	15%
Bacon et al. [70]	Rose Run formation, West Virginia	54 °C ***	100	Calcite	82%
	Copper bridge formation, West Virginia	63 °C ***	100	Calcite	76%
Xu et al. [69]	Firo formation, Gulf Coast	59 °C 152 bar	100	Calcite	>67%
				Siderite	>70%
Thibeau et al. [58]	Sleipner, Norway	28.5-37.6 °C 81.1-108.31 bar	1000	Calcite	>15%
				Dolomite	>20%
Nghiem et al. [54]	***	50 °C 118 bar	100	Calcite	>65%
Calabrese et al. [57]	***	45 °C 140-170 bar	200	Calcite and dolomite	>18.5%

In Table 12, the name of formations and their temperature and pressure are listed. Since there are more than 15 minerals involved in each case and they have individual kinetic reaction rate, only the mineral consumed most in the first 30 years is selected as criteria. The last column, "30 years/total", represents the percentage of the amount of minerals consumed in first 30 years in the amount used during the whole simulation interval. 30 years is chosen as longevity of Short-term CO_2 storage project, since CO_2 EOR projects have been conducted in the Permian Basin of Texas for three decades.

In Table 12, although the parameter, "30 years /Total", ranges from 15%-82% percent for different minerals in various cases, it still indicates that geochemical reactions, especially regarding to calcite and dolomite, are necessarily considered in Short-term CO_2 storage project, because their consumptions in first 30 years could significantly affect the quantification of mineral trapping in long-term storage.

In conclusion, all five application domains are important when it comes to evaluating the impact of geochemical reactions on CO_2 storage, such as CO_2 injection in aquifers and CO_2 EOR process. Especially, the introduction of geochemical reactions into modelling on CO_2 EOR process is essential for the long-term monitoring of the reservoir and evaluation on the impact of mineral trapping mechanisms during the CO_2 storage.

4.3 Mathematical modelling on coupling miscible flow and geochemistry for CO_2 EOR process

4.3.1 Introduction

In 2004 [2], the data on the utilisation of EOR processes in US indicated that thermal methods and gas injection are the two most common techniques in EOR, and more than 60% of gas injection is applied with CO_2. Due to the global warming, the need to stabilise CO_2 concentration in the atmosphere will reinforce the trend towards increased use of CO_2 as common injectant for EOR [2].

Mathematical modelling on CO_2 EOR process has been developed for several decades, together with the growth of this EOR technique. Most of models have emphasized on the multiphase flow transport in the porous media, phase equilibrium and its influence on the final oil recovery. Since 1970s [8], the effect of phase equilibrium on the carbon dioxide flooding has been the main focus of modelling on CO_2 EOR process. In 1986, the mechanism on the development of miscibility between CO_2 and oil, through a combined condensing /vaporizing process, was discovered by Zick [4]. Then, the parameters, which could affect the development of miscibility during CO_2 EOR process and further on oil recovery, become main emphases in modelling work. The effect of the aqueous phase on phase behaviour of CO_2-oil system has been addressed by Nutakki et al. [77], Pollack et al. [78], Turek et al. [79] and Chang et al. [25]. Shyeh-Yung [6] discussed the effects of pressure on miscible and near-miscible displacements of CO_2. When the reservoir conditions is close to the critical conditions of CO_2, an extra fluid phase could appear, Guler et al. [26] used a compositional EOS simulator to evaluated the oil recovery for both three-phase and four-phase cases. Kohse et al. [81] used a compositional reservoir simulator to model asphaltene precipitation and deposition during CO_2 EOR, which can result in plugging of the formation, wellbore and production facilities. However, the geochemical reaction in the CO_2–water-rock system has seldom been addressed by previous researchers.

As the CO_2 EOR process has been considered as an important approach for long-term CO_2 sequestration (discussed in Section 4.2.3), the geochemical reaction is necessarily to be considered in the models. Therefore, in this study, the investigation on how to simulate CO_2 flooding including both three-phase flow and geochemical reaction by using COMSOL was performed. First, the development of both analytical and numerical methods used in the reactive transport modelling is discussed. Then, Since COMSOL has been used to simulate EOR process only for immiscible flow [82], to test if COMSOL can be applied to situations with component exchange between phases and reactive transport with multi-species, two simple EOR processes, gas flooding and polymer flooding, and reactive transport with dissolution of carbonate, were tested. Then, we established a model on miscible CO_2 flooding with consideration of mineral dissolution and change of geophysical properties. Finally, the model was applied to simulating CO_2 flooding in chalk both on reservoir scale and lab scale.

4.3.2 The development of both analytical and numerical methods used in the reactive transport modelling

Modelling on flow accompanied by chemical reactions and mass transfer is central to a wide range of applications [83], such as Alkaline flooding, acidizing wells and non-equilibrium seawater injection in the oil industry and remediation of contaminated soils and aquifers in environmental engineering. The analytical methods used in the reactive transport modelling not only offer the further understanding of mechanisms but also provide reliable data to validate numerical models. Numerical methods are most commonly used nowadays to solve reactive transport problem in multi-dimensions and with complex reactions.

Analytical methods: Based on the complexity of problem and the type of reactions, various analytical methods can be used. The method of characteristic (MOC) and the coherent theory are powerful tools to solve the first-order hyperbolic equations, and are most widely used techniques to solve reactive transport equations. MOC provides a way to transform hyperbolic partial differential equations (PDE) into ordinary differential equations (ODE), which can be easily integrated along characteristic directions. The coherent theory was originally developed by Helfferich et al. [84] for chromatographic phenomena. He also used the MOC to show that a state of coherence will ultimately be attained for homogeneous systems of nonlinear equations with arbitrary starting conditions [85]. In practice, especially when solving Riemann problems involving uniform initial and boundary conditions, the coherent theory is easier to use and has boarder application areas. Pope et

al. [17] and Lake et al. [18] discussed the cation exchange in chemical flooding with considering the effect of dispersion and polymer/surfactant adsorption in porous media by using the coherent theory. Later, Helfferich [21] has successfully extended his theory to the reactive transport with precipitation/dissolution waves under local equilibrium assumption (LEA). In his study [21], the system with three ions and two precipitates are considered and the results have been proved by Bryant et al. [6]. However, when more ions are considered, this method becomes too complex and the validity has not been confirmed. At the same time, Novak et al. [86] proposed a new method to solve precipitation/dissolution waves (under LEA) occurring during reactive flow with use of coherent condition and ruled-based mineral sequences. In his methods, although the multi-species and multi-reactions system can be included, the determination of the proper solid sequence is the most difficult task, which becomes worse with more complex system. Araque et al. [8] extended Novak et al.'s work [86] to geochemical reactions with precipitation/dissolution waves under non local equilibrium assumption (NLEA). In their study, the MOC and travelling wave coordination were used to solve the problems regarding to the simple precipitation wave and the dissolution wave individually, and the relationship between problems under LEA and NLEA are emphasized. A simplified approach to geochemical modelling based on their work has also been proposed, which can speed up the calculation 10 to 50 times and trade-off for the simplifications is the need to determine the LEA wave velocities [87]. Later, Zuluaga et al. [88] also use travelling wave to model the experiments on water vaporization for gas injection. Xu et al. [89] use the similar method as Araque et al. [8] to validate the TOUREACT code by analytical solutions on simple dissolution problems. Although the application of analytical methods is seriously limited by the complexity of problems, they are still effective and fast for solving specific problems under certain assumptions without the loss of accuracy, and can provide validity to numerical solutions.

Numerical methods: Due to the complexity of reactive transport processes in porous media, modelling their dynamic behaviour is a challenging task. In the early times, local equilibrium assumption is widely used in transport reactive modelling, which has been one of the most fundamental tenets of hydrothermal and metamorphic geochemistry and petrology [23]. The system of equations with LEA in 1-D can be simultaneously solved with Newton Raphson method [19]. With the development of quantitative models for kinetic controlled reactions and requirement of multi-dimensions, models become more complex, and therefore different numerical approaches are available to model the coupled processes of mass transport and water-rock-gas interactions in porous media [22]. The first is the sequential iteration approach (SIA), which solving flow transport equation and chemical equations separately and sequentially until the convergence is reached [90].

The approach could handle large systems with large set of chemical species, and therefore becomes the most widely used. Steefel et al. [91] discussed the approaches of modelling of reactive transport in porous media including the introduction of system of equations, application of finite difference methods and finite elements methods in 2-D, and use of SIA. They pointed out that SIA could have convergence difficulties in specific problems.

Walter et al. [92] argue that in problems dealing with entirely with LEA, there is no need to iterate between transport and chemical reactions, in which a single time step consists of a transport step followed by a reaction step. This approach is called sequential non iterative approach (SNIA), also called the operator splitting approach. Later, Xu et al. [93] compared the SIA and SNIA approaches and their results indicated that SNIA could substantially save computing time compared to SIA while its accuracy is generally good, although very dependent on space discretization, time increment size and the nature of geochemical reactions. Clearly the potential errors associated with SNIA originate from its assumption that the flow transport is sufficiently rapid and the reactions only begin after the physical transport is complete. Strang et al. [94] proposed his famous method, 'Strang splitting', which involves entering the reaction step between two transport steps. In the geochemical simulator, TOUGHREACT, developed by Xu et al. [95] used both SNIA and SIA as approaches, since the difference between SNIA and SIA are general small, when the stability condition is satisfied (The Courant numbers are smaller than one.).

The last method is called the fully coupled approach, in which all transport and chemical equations are solved simultaneously. Although the fully coupled approach is considered as the most stable approach, it is rejected in the early time [22] as being too CPU time and memory consuming. Relatively little discussion of the fully coupled approach has appeared in the hydro-geochemical literature. Another obstacle is that the required numerical solution method for fully coupled approach is very demanding. In 2004, Nghiem et al. [54] proposed a fully coupled geochemical compositional Equation-of-State (EOS) compositional simulator for the simulation of CO_2 storage in saline aquifers, GEM-GHG. The success of fully coupled approach depends strongly on the application of efficient sparse solution techniques (Incomplete LU factorization) and robust solution method (GMRES iterative method).

4.3.3 Numerical tests with COMSOL

COMSOL Multiphysics is a finite element analysis and solver software package for various physics and engineering applications, especially for coupled phenomena, or multiphysics [96]. It includes a complete environment for modelling any physical phenomenon that can be described by using

ordinary or partial differential equations. COMSOL version 3.5a includes 12 modules organized into a unifying multiphysics simulation environment [96]. At the same time, COMSOL also allows for building coupled systems of PDEs, which can be entered directly by general form and coefficient form or using the so-called weak form. COMSOL also offers an extensive and well-managed interface to MATLAB® and its toolboxes for a large variety of programming, preprocessing and postprocessing possibilities [97].

The applications of COMSOL have been illustrated by various researchers (http://www.COMSOL.com), and there is also a default library of redefined model for specific applications in each module (Acoustics Module, Chemical engineering Module, Earth Science Module etc.). COMSOL has been applied to simulate EOR process in previous study. Diaz et al. [98] build a black-oil model to simulate the water flooding through sandstone by using COMSOL. In their study, for numerical implementation using a finite element method, the black oil model has been reformulated based on phase pressure and total velocity. Bjørnarå et al. [99] tested various equation system formulations for modelling two-phase flow in porous media to find out the fastest and most robust one. Carrizales et al. [100] simulated heavy oil recovery by Electromagnetic (EM) heating with COMSOL. Currently, there is no commercial simulator available to simulate this process. In their study, only oil phase is considered in their model and the temperature and pressure profiles after three years of EM heating was obtained. However, most of them focus on two phases without considering miscibility between them. Therefore, COMSOL must be tested if it can be applied to situations with component exchange between phases.

Gas flooding and polymer flooding were tested in sequence and to evaluate the performance of COMSOL in modelling miscible flow and transport-reactive flow. The two examples are taken from the existing publications [101] [102]. In all the following description, we use subscripts i and j to represent components and phases, respectively. The two examples are input into the COMSOL, by using the PDE Modes and the coefficient form.

4.3.3.1 Gas flooding

In gas flooding, component separation happens while flowing. The transfer of components between flowing phases strongly influences displacement performance. A 1-D two-component gas/oil displacement is studied here. The details of all assumptions and solutions can be found in reference [101]. Here, only main equations and important steps, which could be similar as those used in our own model, are displayed.

The transport equation for the gas component and the saturation equation are,

$$\phi\frac{\partial}{\partial t}(S_g\rho_g x_{g,g} + S_o\rho_o x_{g,o}) + \frac{\partial}{\partial x}(x_{g,g}\rho_g u_g + x_{g,o}\rho_o u_o) = 0 \tag{33}$$

$$S_g + S_o = 1 \tag{34}$$

where, $x_{g,j}$ is the molar fraction of gas component in the gas (g) or oil (o) phase, S_j is the saturation, ρ_j is the molar density. ϕ is the porosity. Without consideration of capillary pressure, phase flow velocity u_j, becomes,

$$u_j = -\frac{kk_{rj}}{\mu_j}\frac{\partial P}{\partial x} \tag{35}$$

In eq. (35), k is the absolute permeability, k_{rj} and μ_j are the relative permeability and viscosity. P is the pressure. The flow velocity can be written in terms of fractional flow functions, f_j, defined by,

$$u_j = f_j u = f_j(u_o + u_g) \tag{36}$$

In eq. (36), u is the total velocity. The relative permeability for oil and gas can be expressed as, for gas,

$$\begin{gathered} k_{rg} = 0, (S_g < S_{gc}) \\ k_{rg} = \left(\frac{S_g - S_{gc}}{1 - S_{gc} - S_{or}}\right)^2, (S_{gc} < S_g < 1 - S_{or}) \\ k_{rg} = 1, (S_g > 1 - S_{wr}) \end{gathered} \tag{37}$$

for oil,

$$\begin{gathered} k_{ro} = 0, (1 - S_g < S_{or}) \\ k_{ro} = \left(\frac{1 - S_g - S_{or}}{1 - S_{gc} - S_{or}}\right)^2, (S_{gc} < S_g < 1 - S_{or}) \\ k_{ro} = 1, (1 - S_g > 1 - S_{gc}) \end{gathered} \tag{38}$$

In eqs. (37) and (38), S_{gc} is the critical gas saturation, S_{or} is the residual oil saturation. By substituting eqs. (35), (37) and (38) into eq. (36), the fractional flow for gas phase f_g becomes,

$$f_g = 0, (S_g < S_{gc})$$
$$f_g = \left(\frac{(S_g - S_{gc})^2}{(S_g - S_{gc})^2 + (1 - S_g - S_{or})^2 / M} \right), (S_{gc} < S_g < 1 - S_{or}) \quad (39)$$
$$f_g = 1, (S_g > 1 - S_{or})$$

In eq. (39), M is the viscosity ratio between oil and gas. For this example, we assume $S_{gc} = 0.05$, $S_{or} = 0.1$ and $M = 2$.

Under the assumption that the molar density of gas component, ρ_{cg}, is constant in two phases and we have,

$$\rho_{cg} c_{g,j} = \rho_j x_{g,j} \quad (40)$$

where $c_{g,j}$ is the volume fraction of gas component in different phases. By substituting eq. (36) and (40) into eq. (33) , we obtain

$$\phi \frac{\partial}{\partial t}(S_g c_{g,g} + S_o c_{g,o}) + u \frac{\partial}{\partial x}(c_{g,g} f_g + c_{g,o} f_o) = 0 \quad (41)$$

By introducing dimensionless parameters,

$$\tau = \frac{u_{inj} t}{\phi L}, \zeta = \frac{x}{L}, u_D = \frac{u}{u_{inj}} \quad (42)$$

and with $u_D = 1$, eq. (41) becomes,

$$\frac{\partial N_g}{\partial \tau} + \frac{\partial F_g}{\partial \zeta} = 0 \quad (43)$$

where N_g is the overall volume faction of gas component, $N_g = S_g c_{g,g} + S_o c_{g,o}$, and F_g is the overall fractional volumetric flow of gas component, $F_g = f_g c_{g,g} + f_o c_{g,o}$. To compare the results with the analytical solution, P is assumed to be constant, and correspondingly $c_{g,g}$ and $c_{g,o}$ are constant in the isothermal process. We assume $c_{g,g} = 0.95$ and $c_{g,o} = 0.2$.

In solving the system of hyperbolic equations, which represents the advection dominated problems, the standard Galerkin schemes used in COMSOL will produce spatial oscillations. Therefore, an artificial diffusion coefficient D=1×10^{-4} is introduced at the seconder-order partial derivative to avoid oscillation. The initial condition for N_g is 0.05, the left boundary condition is N_g=0.975, and the right boundary condition is Neumann type condition with $\mathrm{q} = \mathrm{g} = 0$ (q and g are parameters in COMSOL).

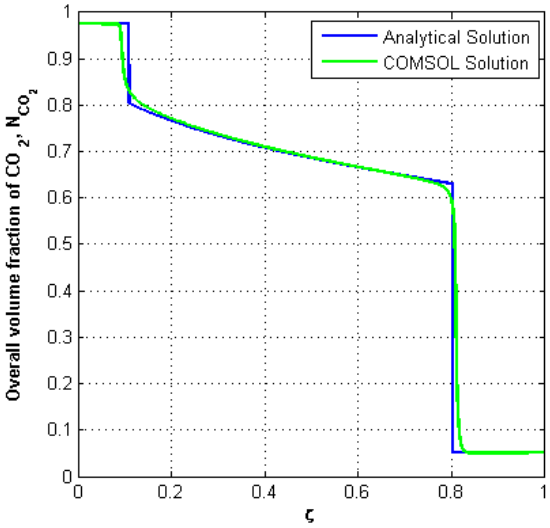

Figure 68 Comparison of analytical solution and COMSOL solution in gas flooding

In Figure 68, the results from COMSOL agrees well with those from analytical solution by using MOC at τ=0.6.

4.3.3.2 Polymer flooding

In polymer flooding, polymer is added to water to increase its viscosity so as to mobilize more oil. However, the polymer can be adsorbed on rock surface, and the decreasing concentration of polymer in water will affect the flow of water phase. The process is characterized by the coupling between adsorption and flow transport. The details of all assumptions and solutions can be found in reference [102].

The transport equations for 1-D polymer flooding are,

$$\begin{aligned} \phi\frac{\partial S_w}{\partial t} + u\frac{\partial f_w}{\partial x} &= 0 \\ \phi\frac{\partial}{\partial t}(S_w c + c_s) + u\frac{\partial}{\partial x}(f_w c) &= 0 \end{aligned} \tag{44}$$

where c is the concentration of polymer in water phase. c_s is the concentration of adsorbed polymer. By using dimensionless parameters in eq. (42) with u_D=1, eq. (44) becomes

$$\begin{aligned} \frac{\partial S_w}{\partial \tau} + \frac{\partial f_w}{\partial \zeta} &= 0 \\ \frac{\partial}{\partial \tau}(S_w c + c_s) + \frac{\partial}{\partial \zeta}(f_w c) &= 0 \end{aligned} \tag{45}$$

The relative permeabilities of oil and water, k_{ro} and k_{rw} are

$$\begin{aligned} k_{ro} &= (1-\psi)^2(1+2\psi) \\ k_{rw} &= 0.25\psi^2 \end{aligned} \tag{46}$$

S_{wr} and S_{or} are the residual saturation of water and oil respectively. Here, S_{wr} and S_{or} are set to 0.2 and 0.3 respectively. The viscosity of water phase is assumed to be a linear function of c,

$$\mu_w = \mu_w^0(1+\beta c) \tag{47}$$

where μ_w^0 is the initial water viscosity, β is constant. The viscosity of oil, μ_o, is constant. f_w can thus be expressed by,

$$f_w = \frac{k_{rw}}{k_{rw} + k_{ro}\mu_w/\mu_o} = \frac{\psi^3}{\psi^3 + \alpha(1+\beta c)(1-\psi)^2(1+2\psi)} \tag{48}$$

where $\alpha = 4\mu_w^0/\mu_o$. The equilibrium relation for the polymer adsorption on rock surfaces is often given by the Langmuir isotherm

$$c_s = \frac{NKc}{1+Kc} \tag{49}$$

where N and K are constant. In eq. (47)-(49), the constants, μ_o is set to 40 cp, μ_w^0 1cp, β 4 L/g, N 0.6 g/L and K 10 L/g.

An artificial diffusion coefficient D=2×10^{-3} is also introduced here. The initial and boundary conditions are

$$\tau = 0: \ S_w = 0.6, \ c = 0 \ \text{g/liter}$$
$$\zeta = 0: \ S_w = 1.0, \ c = 1.0 \ \text{g/liter}$$

Figure 69 and Figure 70 show that the numerical results from COMSOL agree well with those from the analytical solution by using MOC at $\tau = 0.4$, in terms of both the water saturation, S_w, and the polymer concentration in water phase, c.

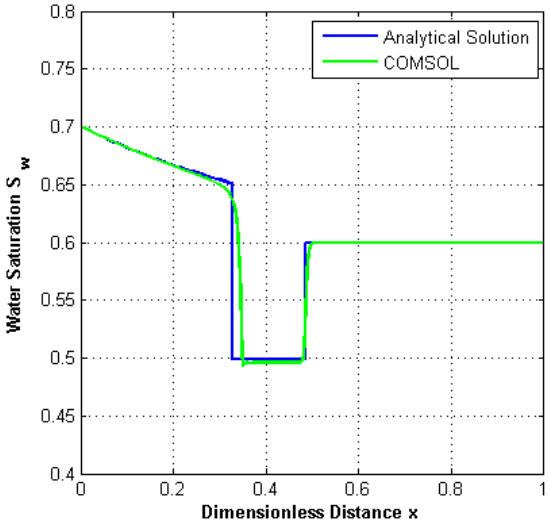

Figure 69 Comparison of analytical solution and COMSOL solution in polymer flooding, S_w

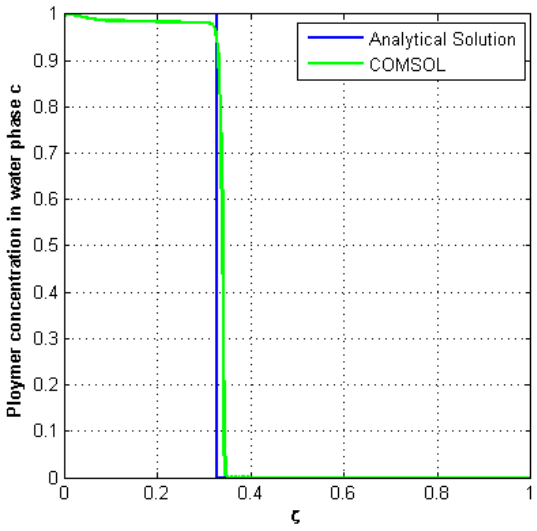

Figure 70 Comparison of analytical solution and COMSOL solution in polymer flooding, c

4.3.4 Modelling of carbon dioxide flooding in North Sea chalk reservoir

4.3.4.1 Description of the system and equations

When CO_2 is injected into oil reservoirs, three phases are present: oil, CO_2 and water. The water phase contains ions and dissolved CO_2. As suggested in the section 4.2.3, the main mineral reaction for calcite considered here is

$$\mathrm{CO_2(aq) + H_2O + CaCO_3(mineral)} \iff \mathrm{Ca^{2+} + 2HCO_3^-}$$

To simplify the system, the following assumptions are used:

1. This process is isothermal;
2. Only $\mathrm{CO_2}$ is dissolved in water;
3. Chemical reaction has no influence on the molar density of water phase;
4. No capillary pressure and diffusion are considered;
5. Molar density of single component in the different phases is same;

The mass conservation equations are Oil component:

$$\frac{\partial}{\partial t}(\phi S_o \rho_o) + \frac{\partial}{\partial x}(u_o \rho_o) = 0 \tag{50}$$

CO_2 component:

$$\frac{\partial}{\partial t}(\phi S_g \rho_g + \phi S_w \rho_w x_{CO_2,w}) + \frac{\partial}{\partial x}(u_w \rho_w x_{CO_2,w} + u_g \rho_g) = -R_m \tag{51}$$

Water component:

$$\frac{\partial}{\partial t}(\phi S_w \rho_w x_{H_2O,w}) + \frac{\partial}{\partial x}(u_w \rho_w x_{H_2O,w}) = -R_m \tag{52}$$

Calcium component:

$$\frac{\partial}{\partial t}(\phi S_w \rho_w x_{Ca^{2+},w}) + \frac{\partial}{\partial x}(u_w \rho_w x_{Ca^{2+},w}) = R_m \tag{53}$$

In the above equations, ϕ is the porosity, S_j ($j = o, g, w$) are the saturation of oil, gas and brine phase, ρ_j is the molar density of different phases, $x_{i,j}$ is the molar fraction of component i in the phase j ($i = CO_2, H_2O, Ca^{2+}, HCO_3^-$), u_j is the Darcy velocity as described by eq. (35). The relative permeability k_{rj} is

$$k_{rj} = S_j^2 \tag{54}$$

The neutrality condition requires

$$2x_{Ca^{2+},w} = x_{HCO_3^-,w} \tag{55}$$

The molar fraction should sum to 1

$$x_{CO_2,w} + x_{Ca^{2+},w} + x_{HCO_3^-,w} + x_{H_2O,w} = 1 \tag{56}$$

The saturations are subject to the constraint

$$S_w + S_g + S_o = 1 \tag{57}$$

The porosity change is given by

$$\frac{\partial(1-\phi)\rho_m}{\partial t} = -R_m \tag{58}$$

where ρ_m is the molar density of mineral. R_m is the reaction term, and can be expressed by $R_m = S_b r_m$, since the r_m is the reaction rate per unit bulk volume of rock when the pore space is filled with water, manipulation by the water saturation S_b is required to obtain the proper rate when part of the pore space is occupied by gas [54]. r_m is expressed as,

$$r_m = k_m A_m (1 - \frac{a_{CO_2,b}^{-1} a_{Ca^{2+},b} a_{HCO_3^-,b}^2}{K_{sp}}) \tag{59}$$

where k_m is the rate constant, A_m is the specific surface of mineral, K_{sp} is the solubility product, and a_i is the activity for aqueous components. Here we assume the activity of water is 1.

The absolute permeability changing with porosity is expressed with the Kozeny-Carman equation [54],

$$\frac{K}{K^0} = \left(\frac{\phi}{\phi^0}\right)^3 \left(\frac{1-\phi^0}{1-\phi}\right)^2$$

where K^0 and ϕ^0 are initial absolute permeability and initial porosity respectively.

In our system, $x_{CO_2,w}$, can be treated as a function of P. Therefore, there are total 8 independent unknowns, S_o, S_g, S_w, P, $x_{H_2O,w}$, $x_{Ca^{2+},w}$, $x_{HCO_3^-,w}$, ϕ for the 8 independent equations, eqs. (50)-(53), and (55)-(58).

4.3.4.2 Solution method

The approach is similar to the one used in the multiphase reactive geochemical simulator, TOUGHREACT [95]. The solution method is shown in Figure 71. At each time step, the pressure equation and the flow equations are solved initially. Then, the solute transport equation is solved with known pressure and saturation. Finally, with updated chemical reaction term, the porosity is calculated.

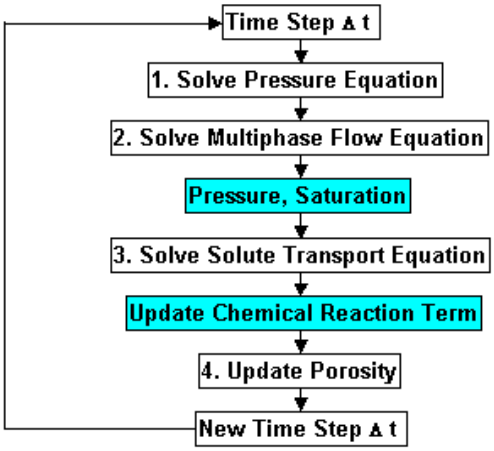

Figure 71 SNIA solution method used in the model

Pressure equation and flow equations

By applying eq. (40), fractional flow functions, f_j, and the assumption that the molar density of single component in various phases is the same and molar fraction of Ca^{2+} and HCO_3^- in eq. (56) are neglected due to their small value , in a way similar to that in gas flooding, eqs. (50)-(52) become

$$\frac{\partial}{\partial t}(G_o) + \frac{\partial}{\partial x}(uH_o) = 0 \tag{60}$$

$$\frac{\partial}{\partial t}(G_g) + \frac{\partial}{\partial x}(uH_g) = -R_m \tag{61}$$

$$\frac{\partial}{\partial t}(G_w) + u\frac{\partial}{\partial x}(uH_w) = -R_m \tag{62}$$

where

$$G_o = \phi\rho_{co}N_o = \phi\rho_{co}S_o,$$

$$H_o = \rho_{co}F_o = \rho_{co}f_o,$$

$$Gg = \phi\rho_{cg}N_g = \phi\rho_{cg}(S_g + S_w c_{CO_2,w}),$$

$$H_g = \rho_{cg}F_g = \rho_{cg}(f_g + f_w c_{CO_2,w}),$$

$$G_w = \phi\rho_{cw}N_w = \phi\rho_{cw}S_w(1 - c_{CO_2,w}),$$

$$H_w = \rho_w F_w = \rho_{cw}f_w(1 - c_{CO_2,w})$$

ρ_{co}, ρ_{cg} and ρ_{cw} are the molar density of oil component, CO_2 component, and H_2O component, respectively. They are constant in the model. $c_{CO_2,w}$ is the volumetric fraction of CO_2 dissolved in the water. G_i is the overall molar concentration of each component based on the grid bulk volume.

By deleting the molar density in eqs. (60)-(62) , and adding them together, we obtain the pressure equation

$$\frac{\partial}{\partial x}\left((\frac{kk_{ro}}{\mu_o}+\frac{kk_{rg}}{\mu_g}+\frac{kk_{rw}}{\mu_w})\frac{\partial P}{\partial x}\right)=-R_m\left(\frac{1}{\rho_{cg}}+\frac{1}{\rho_{cw}}\right) \tag{63}$$

Only two flow equations in eqs. (60)-(62) are chosen to be the flow equations.

Solute transport equation

In the system described here, since $c_{CO_2,w}$ is constant at a certain pressure, molar fraction of CO_2 in water $x_{CO_2,w}$ and the updated molar density of water phase are,

$$\rho_w=\rho_{cg}c_{CO_2,w}+\rho_{cw}(1-c_{CO_2,w}) \tag{64}$$

By substituting eqs. (59) and (55) into eq. (53), and we obtain

$$\frac{\partial}{\partial t}(\phi S_w\rho_w x_{Ca^{2+},w})+\frac{\partial}{\partial x}(u_w\rho_w x_{Ca^{2+},w})=S_w k_m A_m(1-\frac{4\rho_w^2 x_{Ca^{2+},b}^3}{x_{CO_2,b}K_{sp}}) \tag{65}$$

where the activity coefficient of components are assumed to be 1 and thus the kinetic reaction term can be expressed by molar concentration of components.

Porosity equation

With the updated reaction term, R_m, porosity can be solved by eq. (58), and further the permeability can also be updated.

Following the solution method in Figure 71, the above equations are implemented into COMSOL by using the PDE Modes, the coefficient form and solved sequemtially by segregated solver. UMFPACK (Unsymmetric Multifrontal Sparse LU Factorization) is used to solve Jacobian matrix. There are totally 1000 grids has been applied and at each of them, second-order elements was chosen.

4.3.4.3 Validation of the model

A finite difference code for 3-phase immiscible or miscible flooding without chemical reaction is used to validate the model. By using dimensionless parameters in eq. (42), eqs. (61) and (62) become dimensionless:

$$\frac{\partial N_g}{\partial \tau} + \frac{\partial F_g}{\partial \zeta} = 0 \tag{66}$$

$$\frac{\partial N_w}{\partial \tau} + \frac{\partial F_w}{\partial \zeta} = 0 \tag{67}$$

The initial condition is Ng=0, N_w=0.4, and the boundary condition is N_g=1, N_w=0. The parameters are $c_{CO_2,w} = 0.05$, $\mu_g = 0.1cp$, $\mu_o = 0.8cp$, and $\mu_w = 1cp$.

If the injection velocity is constant, the results from COMSOL agree well with those from the 1-D solver, as shown in Figure 72 at $\tau = 0.2$. As before, a diffusion coefficient D=1×10^{-3} has been introduced to avoid oscillation.

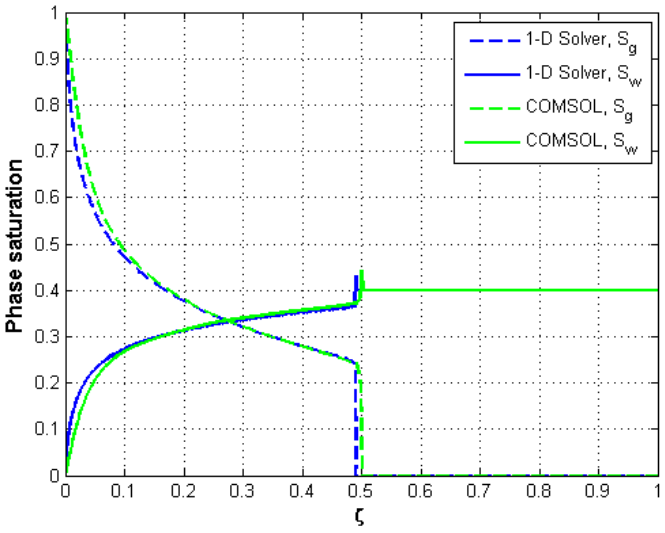

Figure 72 Three-phase flooding without reaction

4.3.4.4 Simulation of reservoir scale flooding

The model is used to simulate field scale CO_2 flooding in a 1-D chalk oil reservoir, which only has water and oil phase initially. The pressure and temperature in reservoir are 385 bar and 115 ^{o}C

respectively. In this case, the CO_2 is injected with constant injection rate and the oil in the reservoir is assumed to be n-decane. The simulation parameters are listed in Table 13. The initial and boundary conditions are listed in Table 14.

Table 13 Parameters used in the simulation

Property	Unit	Value	Description	Property	Unit	Value	Description
$c_{CO_2,w,c}$		0.02	Equilibrium volumetric gas water ratio	k_m [54]	$mol/(m^2 s)$	1.6E-9	Chemical reaction rate
μ_o	cp	0.7	Oil viscosity	A_m[54]	m^2/m^3	10000	Reactive Surface area
μ_w	cp	0.6	Water viscosity	k_{sp}[54]		1E-5	Solubility product
μ_g	cp	0.06	Gas viscosity	K^0	m^2	3E-15	Initial absolute permeability
ρ_{co}	mol/m^3	4900	Molar density of oil	ϕ^0		0.3	Initial porosity
ρ_{cw}	mol/m^3	54000	Molar density of water	ρ_m	mol/m^3	27100	Molar density of calcite
ρ_{cg}	mol/m^3	16000	Molar density of gas				

Table 14 Initial and boundary conditions

	Initial	Boundary (L)	(R)
u	***	5e-7 m/s	***
P	385 bar	***	***
G_g	3.792 mol/m^3	16000 mol/m^3	Same as initial condition
G_w	6467.25 mol/m^3	0 mol/m^3	
$x_{ca^{2+},w}$	0.0001	0	
ϕ	0.3	0	
S_w	0.4	0	
S_g	0	1	

The model has been used to simulate the CO_2 flooding in Chalk reservoir for 400 days. The change of saturation profiles and the molar concentration of calcium in the water phase are shown in Figure 73. The molar concentration of calcium $m_{Ca^{2+},w}$ has increased more than twice than the initial value, indicating the necessary consideration of geochemical reaction in the simulation of CO_2 flooding on reservoir scale, especially when the assessment of long-term storage continues later.

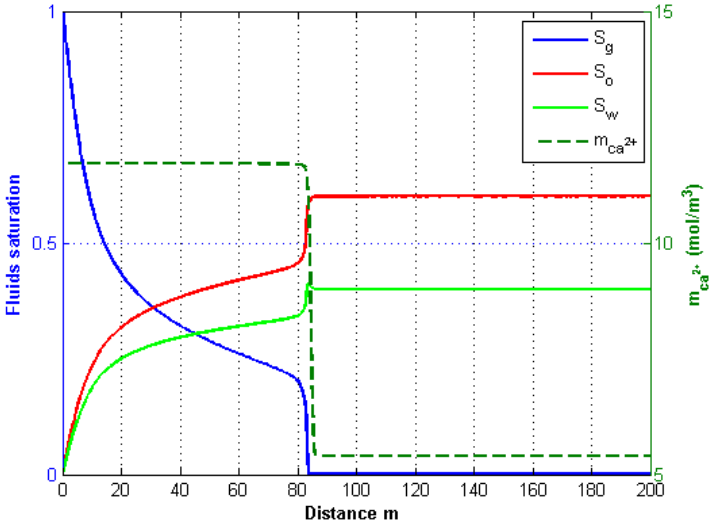

Figure 73 Saturation Profiles and $m_{ca^{2+}}$ at 200 days

Figure 74 and Figure 75 show how the gas saturation profile moves with time and the profile of molar concentration of calcium, $m_{Ca^{2+},w}$ from 100 to 400 days respectively. In Figure 74, the gas front will break through after 500 days. In Figure 75, molar concentration of calcium $m_{Ca^{2+},w}$ becomes constant and the kinetic reaction reaches equilibrium even at early stage, indicating that the dissolution of calcite for reservoir scale flooding can be treated as an equilibrium process.

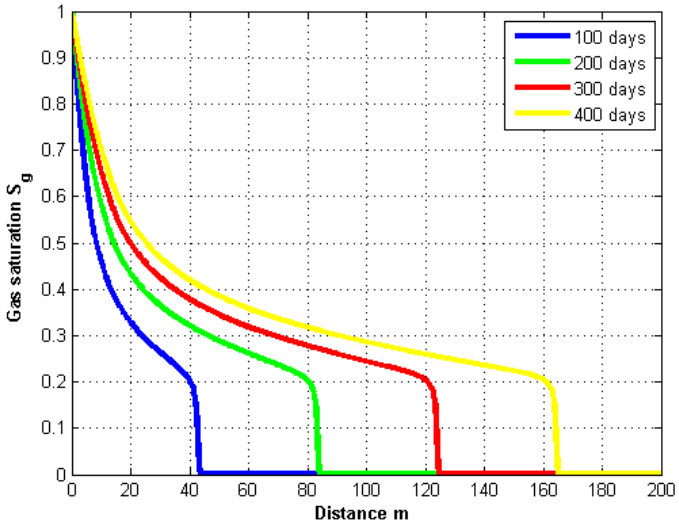

Figure 74 S_g from 100 to 400 days

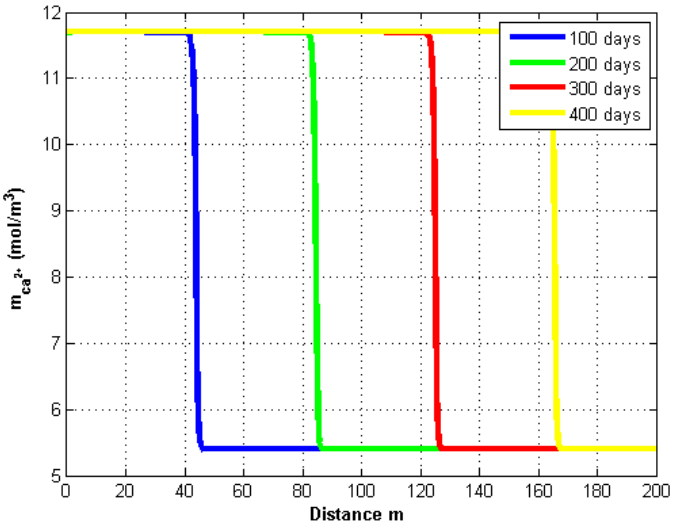

Figure 75 $m_{Ca^{2+},w}$ from 100 to 400 days

Influence of equilibrium phase composition

In Figure 76 and Figure 77, the influence of equilibrium phase composition, $c_{CO_2,w,c}$, on the fluid transport and geochemical reaction are illustrated. $c_{CO_2,w,c}$ represents the critical volumetric ratio between gas component and water component in water phase. The larger $c_{CO_2,w,c}$ indicated that more CO_2 can be dissolved in the water. In Figure 76, the increasing dissolved CO_2 retards the progress of gas front, and further delays the breakthrough of injected CO_2. In Figure 77, the molar concentration of calcium is increasing with larger $c_{CO_2,w,c}$, indicating more calcite has dissolved in the water .

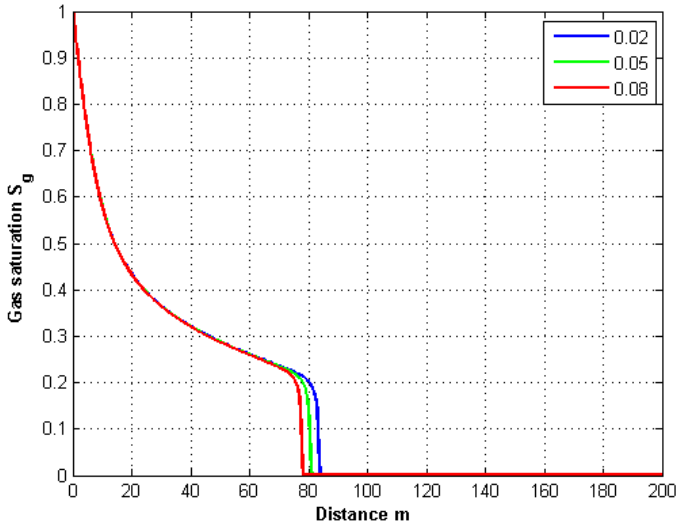

(1) Original movement of gas front

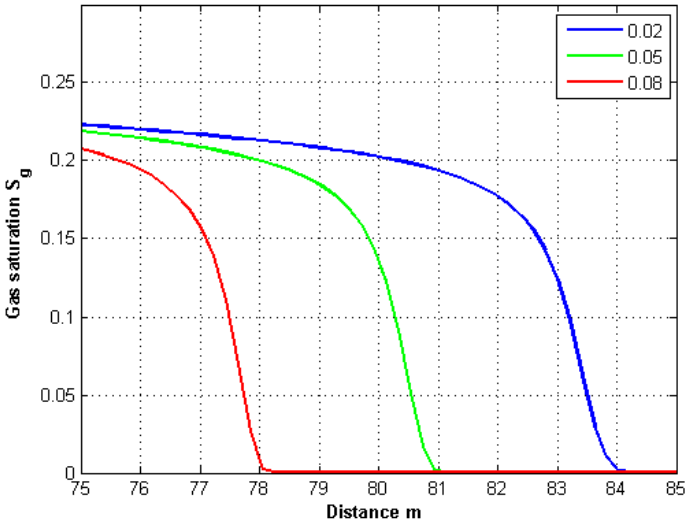

(2) Magnified gas front

Figure 76 Influence of equilibrium phase composition on gas saturation at 200 days

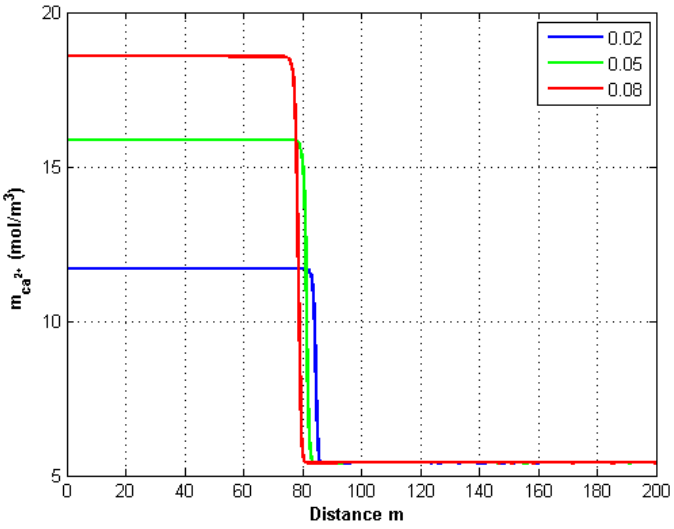

Figure 77 Influence of equilibrium phase composition on molar concentration of calcium at 200 days

Effect of geochemical reaction on flow transport

In our model, the influence of geochemical reaction on the fluid transport can be evaluated, as illustrated in Section 4.3.4.2. In Figure 77, although the injection period of CO_2 EOR process is shorter compared with long-term CO_2 sequestration, the geochemical reaction could also influence the fluid transport as it modifies the porosity and permeability of reservoir formation. The geochemical reaction could also retard the movement of gas front. Further, the influence of equilibrium composition on fluid transport can be explained by increased amount of dissolved gas in water phase and more dissolved CO_2 reacting with rock formation together, as shown in Figure 76.

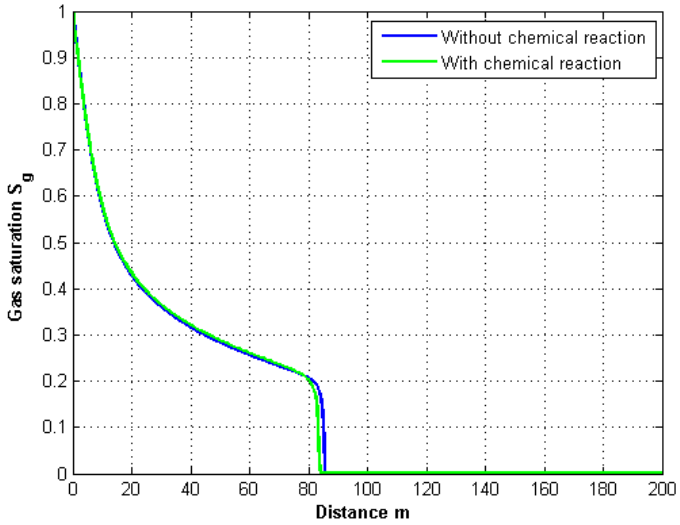

(1) Original movement of gas front

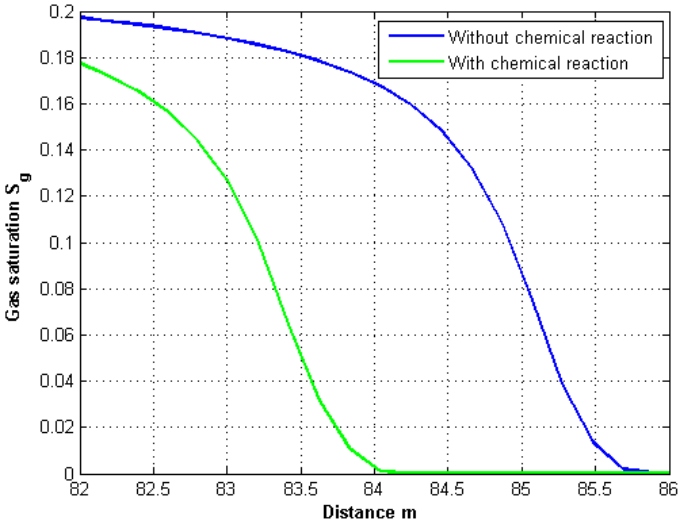

(2) Magnified gas front

Figure 78 The effect of geochemical reaction on flow transport in reservoir scale simulation

4.3.4.5 Simulation of lab core flooding

As comparison, the model was also used to simulate CO_2 flooding in a chalk core in the lab experiment. The core length is 120 mm, and the diameter is 1.5 inch (38.1 mm). The injection rate under experimental condition is 1 cc/min, corresponding to an injection velocity of 1.5E-6 m/s, and the rest parameters used in this simulation are the same as simulation of reservoir scale flooding. Figure 79 shows the influence of kinetic reaction on the increase of the concentration of calcium $m_{Ca^{2+},w}$. $m_{Ca^{2+},w}$ increases with time but its value is far below the equilibrium value, 11.7 mol/m^3, indicating that the dissolution of calcite is limited for short injection time at the Lab experiment.

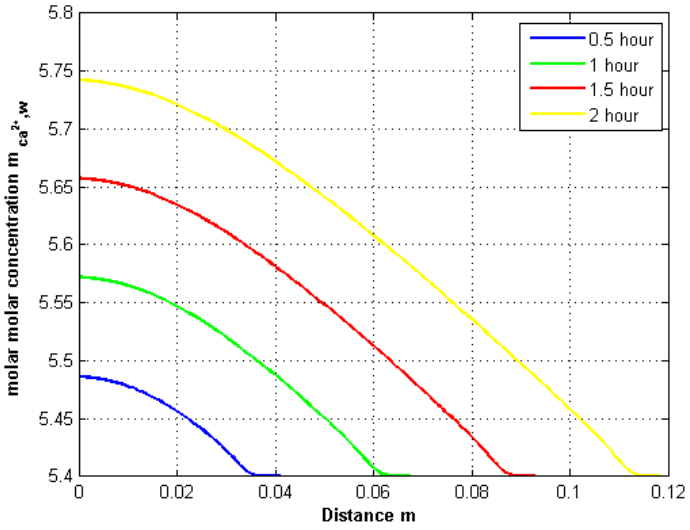

Figure 79 $m_{Ca^{2+},w}$ from 0.5 to 2 hours along the core

Influence of reactive surface area

Since reactive surface area is a complicating factor when introducing kinetic controlled reactions [103]. Figure 80 and Figure 81 illustrate the influence of reactive surface area, A_m. For A_m=1E+6 m^2/m^3, the molar concentration of calcium $m_{Ca^{2+},w}$ almost reaches equilibrium, while for A_m=1E+4 m^2/m^3, the change of $m_{Ca^{2+},w}$ is almost negligible.

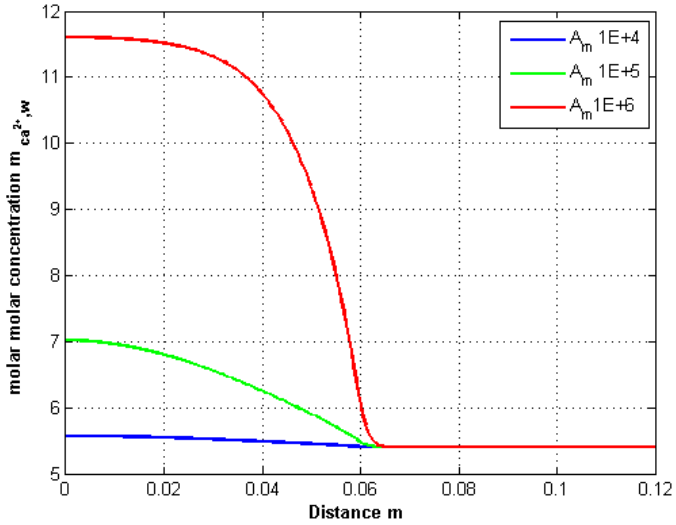

Figure 80 Effect of A_m on $x_{Ca^{2+},w}$ after 1 hour

In Figure 81, the effect of A_m on the porosity is illustrated. Its change is almost negligible even near the equilibrium condition.

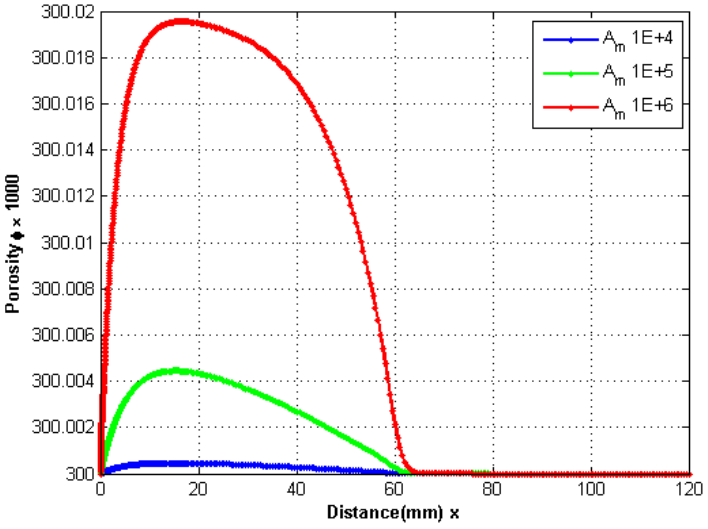

Figure 81 Effect of A_m on ϕ after 1 hour

Influence of equilibrium phase composition

In Figure 82, even on the core scale, the influence of equilibrium phase composition on flow transport is still clear, with retarding the movement of gas front.

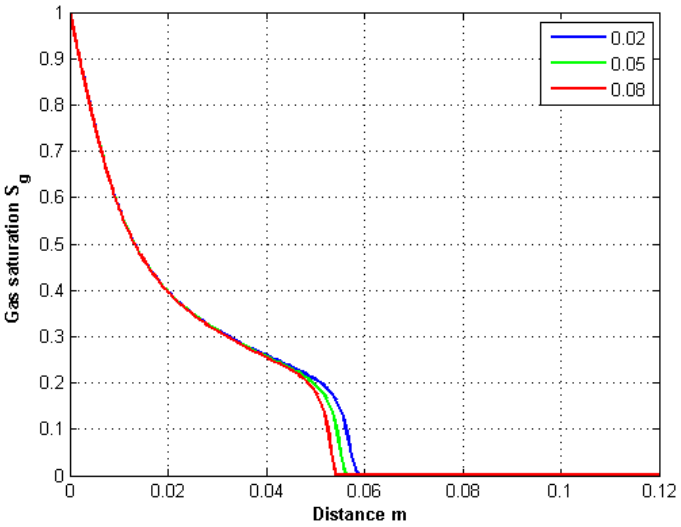

Figure 82 Influence of equilibrium phase composition on gas saturation

Effect of geochemical reaction on flow transport

In Figure 83, the movement of gas front is not clearly affected by the geochemical reaction. This observation again confirms that the effect of geochemical reaction in CO_2 at core scale negligible.

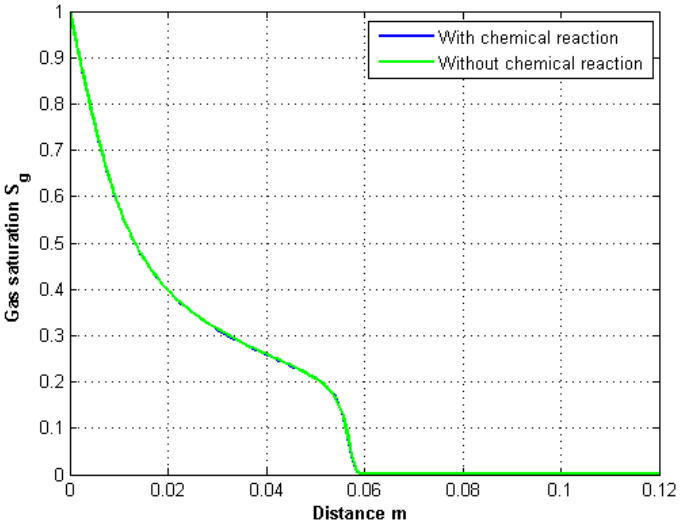

Figure 83 The effect of geochemical reaction on flow transport in core scale simulation

Reference

[1] F. A. Campbell and V. G. Ethier, "Environment of Deposition of the Sullivan Orebody," *Mineralium Deposita*, vol. 18, no. 1, pp. 39–55, April 2004.

[2] E. K. Yanful, R. M. Quigleya, and H. W. Nesbitt, "Heavy Metal Migration at a Landfill Site, Sarnia, Ontario, Canada – 2: Metal Partitioning and Geotechnical Implications," *Applied Geochemistry*, vol. 3, no. 6, pp. 623–629, November-December 1988.

[3] K. Miotlinski, "Coupled Reactive Transport Modelling of Redox Processes in a Nitrate-Polluted Sandy Aquifer," *Aquatic Geochemistry*, vol. 14, no. 2, pp. 117–131, June 2008.

[4] M. Sophocleous, "Interactions between Groundwater and Surface Water: the State of the Science," *Hydrogeology Journal*, vol. 10, no. 1, pp. 52–67, February 2002.

[5] P. McMahon and F. Chapelle, "Redox Processes and Water Quality of Selected Principal Aquifer Systems," *GROUND WATER*, vol. 46, no. 2, pp. 259–271, March -April 2008.

[6] S. L. Bryant and R. S. Schechter and L. W. Lake, "Interactions of Precipitation/Dissolution Waves and Ion Exchange in Flow through Permeable Media," *AIChE Journal*, vol. 32, no. 5, pp. 751 – 764, 1986.

[7] C. Fredd and H. Fogler, "Optimum Conditions for Wormhole Formation in Carbonate Porous Media: Influence of Transport and Reaction," *SPE Journal*, vol. 4, no. 3, pp. 196–204, September 1999.

[8] A. Araque-Martinez and L. W. Lake. (1999, 3-6 October) A Simplified Approach to Geochemical Modelling and Its Effect on Well Impairment. Paper SPE 56678 presented at the SPE Annual Technical Conference and Exhibition, Houston, Texas.

[9] J. Ennis-King and L. Paterson. (2002, 8-10 October) Engineering Aspects of Geological Sequestration of Carbon Dioxide. Paper SPE 77809 presented at the SPE Asia Pacific Oil and Gas Conference and Exhibition, Melbourne, Australia.

[10] K. Caldeira, "Accelerating Carbonate Dissolution to Sequestrate Carbon Dioxide in the Ocean: Geochemical implication," *GEOPHYISICAL RESEARCH LETTERS*, vol. 27, no. 2, pp. 225–228, January 2000.

[11] S. Bachu, J. C. Shaw, and R. M. Pearson. (2004, 17-21 April) Estimation of Oil Recovery and CO_2 Storage Capacity in CO_2 EOR Incorporating the Effect of Underlying Aquifers. Paper SPE 89340 presented at the SPE/DOE Symposium on Improved Oil Recovery, Tulsa, Oklahoma.

[12] L. Marini, *Developments in Geochemistry - Geological Sequestration of Carbon Dioxide: Thermodynamics, Kinetics and Path Modelling*. Elsevier, 2007, vol. 11.

[13] F. M. Orr Jr, "Storage of Carbon Dioxide in Geologic Formations," *Journal of Petroleum Technology*, vol. 56, no. 9, pp. 90–97, September 2004.

[14] A. Espie. (2005, 21-23 November) A New Dawn for CO_2 EOR. Paper SPE 10935 presented at the International Petroleum Technology Conference, Doha, Qatar.

[15] C. I. Steefel, D. J. DePaolo, and P. C. Lichtner, "Reactive Transport Modelling: An Essential Tool and A New Research Approach for the Earth Sciences," *Earth and Planetary Science Letters*, vol. 240, no. 3-4, pp. 539–558, December 2005.

[16] P. C. Lichtner, "Continuum Model for Simultaneous Chemical Reactions and Mass Transport in Hydrothermal Systems," *Geochimica et Cosmochimica Acta*, vol. 49, no. 3, pp. 779–800, March 1985.

[17] G.A. Pope and L.W. Lake and F.G. Helfferich, "Cation Exchange in Chemical Flooding: Part 1: Basic Theory without Dispersion," *SPE Journal*, vol. 18, no. 6, pp. 418–434, December 1978.

[18] L.W. Lake and F.G. Helfferich, "Cation Exchange in Chemical Flooding: Part 2: the Effect of Dispersion, Cation Exchange, and Polymer/Surfactant Adsorption on Chemical Flood Environment," *SPE Journal*, vol. 18, no. 6, pp. 435–444, December 1978.

[19] M.P. Walsh and S.L. Bryant and R.S. Schechter and L.W. Lake, "Precipitation and Dissolution of Solids Attending Flow through Porous Media," *AIChE Journal*, vol. 30, no. 2, pp. 317–328, March 1984.

[20] F. Helfferich, "Theory of Multicomponent, Multiphase Displacement in Porous Media," *SPE Journal*, vol. 21, no. 1, pp. 51–62, February 1981.

[21] F. Helfferich, "The Theory of Precipitation/Dissolution Waves," *AIChE Journal*, vol. 35, no. 1, pp. 75–87, January 1989.

[22] G. T. Yeh and V. S. Tripathi, "A Critical Evaluation of Recent Developments in Hydrogeochemical Transport Models of Reactive Multichemical Components," *WATER RESOURCES RESEARCH*, vol. 25, no. 1, pp. 93–108, 1989.

[23] C. I. STEEFEL and A. C. LASAGA, "A Coupled Model for Transport of Multiple Chemical Species and Kinetic Precipitation/Dissolution Reactions with Application to Reactive Flow in Single Phase Hydrothermal Systems," *American Journal of Science*, vol. 294, no. 5, pp. 529–592, 1994.

[24] L. Nghiem and Y. Li, "Effect of Phase Behavior on CO_2 Displacement Efficiency at Low Temperatures: Model Studies with an Equation of State," *SPE Reservoir Engineering*, vol. 1, no. 4, pp. 414–422, July 1986.

[25] Y. B. Chang, B. K. Coats, and J. Nolen, "A Compositional Model for CO_2 Floods Including CO_2 Solubility in Water," *SPE Reservoir Evaluation & Engineering*, vol. 1, no. 2, pp. 155–160, April 1998.

[26] B. Guler, P. Wang, M. Delshad, G. A. Pope, and K. Sepehrnoori. (2001, 30 September-3 October) Three- and Four-Phase Flow Compositional Simulations of CO_2/NGL EOR. Paper 71485 presented at the SPE Annual Technical Conference and Exhibition, New Orleans, Louisiana.

[27] D. Reichle, B. Kane, J. Houghton, J. Ekmann, S. Benson, J. Ogden, J. Clarke, A. Palmisano, R. Dahlman, R. Socolow, G. Hendrey, J. Stringer, H. Herzog, T. Surles, J. Hunter-Cevera, A. Wolsky, G. Jacobs, N. Woodward, R. Judkins, and M. York, "Carbon Sequestration Research and Development," Office of Science and Office of Fossil Energy, U.S. Department of Energy, Tech. Rep., 1999.

[28] O. Izgec, B. Demiral, H. Bertin, and S. Akin. (2005, 30 March-01 April) CO_2 Injection in Carbonates. Paper SPE 93773 presented at the SPE Western Regional Meeting, Irvine, California.

[29] J. Ennis-king and L. Paterson. (2003, 5-8 October) Role of Convective Mixing in Long-Term Storage of Carbon Dioxide in Deep Saline Formations. Paper SPE 84344 presented at the SPE Annual Technical Conference and Exhibition held in Denver, Colorado, U.S.A.

[30] J. ROOF, "Snap-Off of Oil Droplets in Water-Wet Pores," *SPE Journal*, vol. 10, no. 1, pp. 85–90, March 1970.

[31] R. Juanes, E. J. Spiteri, F. M. O. Jr., and M. J. Blunt, "Impact of Relative Permeability Hysteresis on Geological CO_2 Storage," *WATER RESOURCES RESEARCH*, vol. 42, no. W12418, 2006.

[32] R. Qi, V. Beraldo, T. LaForce and M .J. Blunt. (2007, November) Design of Carbon Dioxide Storage in a North Sea Aquifer using Streamline-Based Simulation. Paper SPE 109905 presented at the SPE Annual Technical Conference and Exhibition, Anaheim, California, U.S.A.

[33] T. Xu, J. A. Apps, and K. Pruess, "Reactive Geochemical Transport Simulation to Study Mineral Trapping for CO_2 Disposal in Deep Saline Arenaceous Aquifers," Earth Sciences Division, Lawrence Berkeley National Laboratory, University of California, Berkeley, CA 94720, USA, Tech. Rep., 2002.

[34] S. Molins and K. U. Mayer. "Coupling between Geochemical Reactions and Multicomponent Gas and Solute Transport in Unsaturated Media: A Reactive Transport Modelling Study," *Water Resource Research*, vol. 43, no. 5, 2007.

[35] J. P. Kaszuba, D. R. Janecky, and M. G. Snow, "Carbon Dioxide Reaction Processes in a Model Brine Aquifer at 200 c and 200 bars: Implications for Geologic Sequestration of Carbon," *Applied Geochemistry*, vol. 18, no. 7, pp. 1065–1080, 2003.

[36] Y. K. Kharaka, J. J. Thordsen, S. D. Hovorka, H. S. Nance, D. R. Cole, T. J. Phelps, and K. G. Knauss, "Potential Environmental Issues of CO_2 Storage in Deep Saline Aquifers: Geochemical Results from the Frio-I Brine Pilot Test, Texas, USA," *Applied Geochemistry*, vol. 24, pp. 1106–1112, 2009.

[37] E. Lindeberg, P. Zweigel, P. Bergmo, A. Ghaderi, and A. Lothe. (2000, 13-16 August) Prediction of CO_2 Dispersal Pattern Improved by Geology and Reservoir Simulation and Verified by Time Lapse Seismic. The proceedings of the 5th International Conference on Greenhouse Gas Control Technologies, Cairns (Australia).

[38] I. Gaus, M. Azaroual, and I. Czernichowski-Lauriol, "Reactive Transport Modelling of the Impact of CO_2 Injection on the Clayey Cap Rock at Sleipner (North Sea)," *Chemical Geology*, vol. 217, pp. 319 – 337, 2005.

[39] B. P. McGrail, P. F. Martin, K. P. Saripalli, S. L. Bryant, and B. M. Sass. (2001, 14-17 May) Use of Forced Mineral Trapping for Sequestration of CO_2. First National Conference on Carbon Sequestration.

[40] Y. Kharaka, D. Cole, S. Hovorka, W. Gunter, K. Knauss, and B. Freifeld, "Gas-Water-Rock Interactions in Frio Formation Following CO_2 Injection: Implications for the Storage of Greenhouse Gases in Sedimentary Basins," *Geology*, vol. 34, no. 7, pp. 577–580, 2006.

[41] M. Wilson and M. Monea. (2004, 5-9 September) IEA GHG Weyburn CO_2 Monitoring & Storage Project Summary Report 2000-2004. The proceedings of the 7th International Conference on Greenhouse Gas Control Technologies, Vancouver, Canada.

[42] B. Cailly, P. L. Thiez, P. Egermann, A. Audibert, S. Vidal-Gilbert, and X. Longaygue, "Geological Storage of CO_2: A State-of-the-Art of Injection Processes and Technologies," *Oil & Gas Science and Technology*, vol. 60, no. 3, pp. 517–525, 2005.

[43] A. S. Shedid and A. Y. Zekri, "Formation Damage Caused by Simultaneous Sulfur and Asphaltene Deposition," *SPE Production & Operations*, vol. 21, no. 1, pp. 58–64, February 2006.

[44] P. Egermann, B. Bazin, and O. Vizika. (2005, 12 - 15 March) An Epxerimental Investigation of Reaction-Transport Phenomena during CO_2 Injection. Paper SPE 93674 presented at the SPE Middle East Oil and Gas Show and Conference, Kingdom of Bahrain.

[45] J. D. Rogers and R. B. Grig, "A Literature Analysis of the WAG Injectivity Abnormalities in the CO_2 Process," *SPE Reservoir Evaluation & Engineering*, vol. 4, no. 5, pp. 375–386, October 2001.

[46] I. Gaus, P. Audigane, L. Andre, J. Lions, N. Jacquemet, P. Durst, I. Czernichowski-Lauriol, and M. Azaroual, "Geochemical and Solute Transport Modelling for CO_2 Storage, What to Expect From It?" *INTERNATIONAL JOURNAL OF GREENHOUSE GAS CONTROL*, vol. 2, pp. 605–625, 2008.

[47] K. Pruess, T. Xu, J. Apps, and J. Garcia. (2001, 26-28 February) Numerical Modelling of Aquifer Disposal of CO_2. Paper SPE 66537 presented at the SPE/EPA/DOE Exploration and Production Environmental Conference, San Antonio, Texas.

[48] X. Tianfu, A. J. A, and P. Karsten, "Numerical Simulation of CO_2 Disposal by Mineral Trapping in Deep Aquifers," *Applied Geochemistry*, vol. 19, no. 6, pp. 917–936, 2004.

[49] B. Ülker and H. Alkan and G. Pusch. (2007, 11-14 June) Implications of the Phase-Solubility Behaviour on the Performance Predictions of the CO_2 Trapping in Depleted Gas Reservoirs and Aquifers. Paper SPE 107189 presented at the EUROPEC/EAGE Conference and Exhibition, London, U.K.

[50] K. Jessen, L. C. Sam-Olibale, A. R. Kovscek, and F. M. O. Jr. Increasing CO_2 Storage in Oil Recovery.

[51] E. J. Spiteri, R. Juanes, M. J. Blunt, and F. M. O. Jr. (2005, 9-12 October) Relative Permeability Hysteresis: Trapping Models and Application to Geological CO_2 Sequestration. Paper SPE 96448 presented at the SPE Annual Technical Conference and Exhibition, Dallas, Texas.

[52] C. M. Oldenburg and S. M. Benson. (2002, 10-12 February) CO_2 Injection for Enhanced Gas Production and Carbon Sequestration. Paper SPE 74367 presented at the SPE International Petroleum Conference and Exhibition in Mexico, Villahermosa, Mexico.

[53] T. Xu, E. Sonnenthal, N. Spycher, and K. Pruess, "TOUGHREACT - A Simulation Program for Non-Isothermal Multiphase Reactive Geochemical Transport in Variably Saturated Geologic Media: Applications to Geothermal Injectivity and CO_2 Geological Sequestration," *Computers & Geosciences*, vol. 32, no. 2, pp. 145–165, 2006.

[54] L. Nghiem, P. Sammon, J. Grabenstetter, and H. Ohkuma. (2004, 17-21 April) Modelling CO_2 Storage in Aquifers with a Fully-Coupled Geochemical EOS Compositional Simulator. Paper SPE 89474 presented at the SPE/DOE Symposium on Improved Oil Recovery, Tulsa, Oklahoma.

[55] T. Xu, E. Sonnenthal, N. Spycher, and K. Pruess. (2003, 12-15 October) Using TOUGHREACT to Model Reactive Fluid Flow and Geochemical Transport in Hydrothermal Systems. GRC 2003 Annual Meeting, Morelia, Mexico.

[56] P. Audigane, I. Gaus, I. Czernichowski-Lauriol, K. Pruess, and T. Xu, "Two-Dimensional Reactive Transport Modelling of CO_2 Injection in a Saline Aquifer at the Sleipner Site," *American Journal of Science*, vol. 307, no. 7, pp. 974–1008, 2007.

[57] M. Calabrese, F. Masserano, and M. Blunt. (2005, 9-12 October) Simulation of Physical-Chemical Processing during Carbon Dioxide Sequestration in Geological Structures. Paper SPE 95820 presented at the SPE Annual Technical Conference and Exhibition, Dallas, Texas.

[58] S. Thibeau, L. Nghiem, and H. Ohkuma. (2007, 11-14 November) A Modelling Study of the Role of Selected Minerals in Enhancing CO_2 Mineralization during CO_2 Aquifer Storage. Paper SPE 109739 presented at the SPE Annual Technical Conference and Exhibition, Anaheim, California, U.S.A.

[59] N. Kumar, "CO_2 Sequestration: Understanding the Plume Dynamics and Estimating Risk," Master's thesis, The Graduate School of the University of Texas at Austin, 2008.

[60] W. D. Gunter, B. Wiwehar, and P. E. H., "Aquifer Disposal of CO_2-Rich Greenhouse Gases: Extension of the Time Scale of Experiment for CO_2-Sequestering Reactions by Geochemical Modelling," *Mineralogy and Petrology*, vol. 59, no. 1-2, pp. 121–140, 1997.

[61] T. P. Wellman, R. B. Grigg, B. J. McPherson, R. K. Svec, and P. C. Lichtner. (2003, 5-7 February) Evaluation of CO_2-Brine-Reservoir Rock Interaction with Laboratory Flow Tests and Reactive Transport Modelling. Paper SPE 80228 presented at the International Symposium on Oilfield Chemistry, Houston, Texas.

[62] C. Michael, J. M. Nordbotten, and S. Gasda. (2004, September) Quantitative Estimation of CO_2 Leakage from Geological Storage: Analytical Models, Numerical Models, and Data Needs. The proceedings of the 7th International Conference on Greenhouse Gas Control Technologies, (GHGT-7).

[63] R.G. Bruant Jr and A. J. Guswa and M. A .Celia and C. A. Peters, "Safe Storage of CO_2 in Deep Saline Aquifers," *Environmental Science and Technology*, vol. 36, no. 11, pp. 240A–245A, June 2002.

[64] G. Benge. (2009, 17-19 March) Improving Wellbore Seal Integrity in CO_2 Injection Wells. Paper SPE 119267 presented at the SPE/IADC Drilling Conference and Exhibition, Amsterdam, The Netherlands.

[65] V. Barlet-Gouedard, G. Rimmele, B. Goffe, and O. Porcherie. (2006, 21-23 February) Mitigation Strategies for the Risk of CO_2 Migration through Wellbores. Paper SPE 98924 presented at the IADC/SPE Drilling Conference, Miami, Florida, USA.

[66] N. acquement, "Well Materials Durability in Case of Carbon Dioxide and Hydrogen Sulphide Geological Sequestration," Ph.D. dissertation, Laboratoire de Géologie et Gestion des Ressources Minérales et Energétiques, Université Henri Poincaré , Nancy, 2006.

[67] M. Azaroual, K. Pruess, and C. Fouillac. (2007, 1-4 April) Feasibility of Using Supercritical CO_2 as Heat Transmission Fluid in the EGS (Enhanced Geothermal System) Integrating the carbon storage

constraints. ENGINE - Enhanced Geothermal Innovative Network for Europe. Workshop: Exploring High Temperature Reservoirs: New Challenges for Geothermal Energy, SIAF Campus, Valera, Italy.

[68] A. L., Audigane, P., M. Azaroual, and M. A., "Numerical Modelling of Fluid-Rock Chemical Interactions at the Supercritical CO_2-Liquid Interface during CO_2 Injection into a Carbonate Reservoir, the Dogger aquifer (Paris Basin, France)," *Energy Conversion and Management*, vol. 48, no. 6, pp. 1782–1797, 2007.

[69] T. Xu and Y. K. Kharaka and C. Doughty and B. M. Freifeld and T. M. Daley, "Reactive Transport Modelling to Study Changes in Water Chemistry Induced by CO_2 Injection at the Frio-I Brine Pilot," *Chemical Geology*, vol. 271, no. 3-4, pp. 153–164, 2010.

[70] D. H. Bacon and B. M. Sass and M. Bhargava and J. Sminchak and N. Gupta, "Reactive Transport Modelling of CO_2 and SO_2 Injection into Deep Saline Formations and Their Effect on the Hydraulic Properties of Host Rocks," *Greenhouse Gas Control Technologies 9*, vol. 1, no. 1, pp. 3283–3290, 2009.

[71] S. P. White and R. G. Allis and J. Moore and T. Chidsey and C. Morgan and W. Gwynn and M. Adams, "Simulation of Reactive Transport of Injected CO_2 on the Colorado Plateau, Utah, USA," *Chemical Geology*, vol. 217, no. 3-4, pp. 387–405, 2005.

[72] F. Johann, L. Nghiem, E. Caroli, and S. Thibeau. (2004, 18-21 April) Sleipner/Utsira CO_2 Geological Storage Full Field Flow and Geochemical Coupling to Assess the Long Term Fate of the CO_2. AAPG Annual Meeting, Dallas, Texas, April 18-21, 2004.

[73] J. W. Johnson, J. J. Nitao, C. I. Steefel, and K. G. Knauss. (14-17 May) Reactive Transport Modelling of Geologic CO_2 Sequestration in Saline Aquifers: the Influence of Intra-Aquifer Shales and the Relative Effectiveness of Structural, Solubility, and Mineral Trapping during Prograde and Retrograde Sequestration. First Annual Conference on Carbon Sequestration.

[74] I. Gaus, M. Azaroual, and I. Czernichowski-Lauriol, "Reactive Transport Modelling of the Impact of CO_2 Injection on the Clayey Cap Rock at Sleipner (North Sea)," *Chemical Geology*, vol. 217, no. 3-4, pp. 319–337, 2005.

[75] R. Metcalfe and L. Yarborough, "The Effect of Phase Equilibrium on the CO_2 Displacement Mechanism," *SPE Journal*, vol. 19, no. 4, pp. 242–252, August 1979.

[76] A. Zick. (1986, 5-8 October) A Combined Condensing/Vaporizing Mechanism in the Displacement of Oil by Enriched Gases. Paper SPE 15493 presented at the SPE Annual Technical Conference and Exhibition, New Orleans, Louisiana.

[77] A. Firoozabadi and R. Nutakki and T. W. Wong and K. Aziz, "EOS Predictions of Compressibility and Phase Behavior in Systems Containing Water, Hydrocarbons, and CO_2," *SPE Reservoir Engineering*, vol. 3, no. 3, pp. 673–684, May 1988.

[78] R. Nutakki, A. Firoozabadi, T. Wong, and K. Aziz. (1988, 16-21 April) Calculation of Multiphase Equilibrium for Water-Hydrocarbon Systems at High Temperature. Paper SPE 17390 presented at the SPE Enhanced Oil Recovery Symposium, Tulsa, Oklahoma.

[79] N. Pollack, R. Enick, D. Mangone, and B. Morsl, "Effect of An Aqueous Phase on CO_2/Tetradecane and CO_2/Maljamar-Crude-Oil System," *SPE Reservoir Engineering*, vol. 3, no. 2, pp. 533–541, May 1988.

[80] J. G. Shyeh-Yung. (1991, 6-9 October) Mechanisms of Miscible Oil Recovery: Effects of Pressure on Miscible and Near-Miscible Displacements of Oil by Carbon Dioxide. Paper SPE 22651 presented at the SPE Annual Technical Conference and Exhibition, Dallas, Texas.

[81] B. F. Kohse, L. X. Nghiem, H. Maeda, and K. Ohno. (2004, 16-18 October) Modelling Asphaltene Precipitation and Deposition in a Compositional Reservoir Simulator. Paper SPE 64465 presented at the SPE Asia Pacific Oil and Gas Conference and Exhibition, Brisbane, Australia.

[82] T. I. Bjørnarå and E. Aker and E. Skurtveit. (2009) Safe Storage Parameters during CO_2 Injection Using Coupled Reservoir-Geomechanical Analysis. The The proceedings of the COMSOL Conference 2009 Milan.

[83] S. L. Bryant and K. E. Thompson, "Theory, Modelling and Experiment in Reactive Transport in Porous Media," *Current Opinion in Colloid & Interface Science 6*, vol. 6, no. 3, pp. 217–222, 2001.

[84] F. Helferich and G. Kevin, *Multicomponent Chromatography*. Marcel Dekker Inc. New York City, 1970.

[85] N. P. Hankins and J. H. Harwell, "Application of Coherence Theory to a Reservoir Enhanced Oil Recovery Simulator," *Journal of Petroleum Science and Engineering*, vol. 42, no. 1, pp. 29–55, 2004.

[86] C. F. Novak, R. S. Schechter, and L. W. Lake, "Rule-Based Mineral Sequences in Geochemical Flow Processes," *AIChE Journal*, vol. 34, pp. 1607–1614, October 1988.

[87] A. N. A. Martinez, "Modelling the Effects of Geochemistry on Well Impairment," Ph.D. dissertation, The University of Texas at Austin, May 2001.

[88] E. Zuluaga and L. W. Lake, "Modelling of Experiments on Water Vaporization for Gas Injection Using Traveling Waves," *SPE Journal*, vol. 13, no. 2, pp. 248–256, June 2008.

[89] T. Xu, K. Pruess, and G. Brimhall, "An Improved Equilibrium-Kinetics Speciation Algorithm for Redox Reactions in Variably Saturated Subsurface Flow Systems," *Computers and Geosciences*, vol. 25, no. 6, pp. 655–666, 1999.

[90] S. D. Sevougian, L. W. Lake, and R. S. Schechter, "KGEOFLOW: A New Reactive Transport Simulator for Sandstone Matrix Acidizing," *SPE Production & Facilities*, vol. 10, no. 1, pp. 13–17, February 1995.

[91] C. I. Steefel and K. T. MacQuarrie, "Approaches to Modelling of Reactive Transport in Porous Media," *Reactive Transport in Porous Media, Reviews in Mineralogy*, vol. 34, pp. 83–130, 1996.

[92] A. L. Walter, E. O. Frind, D. W. Blowes and C. J. Ptacek and J. W. Molson, "Modelling of Multicomponent Reactive Transport in Groundwater 1: Model Development and Evaluation," *Water Resources Research*, vol. 30, no. 11, pp. 3137-3148, 1994.

[93] T. Xu, J. Sampera, C. Ayorab, M. Manzanoc, and E. Custodioc, "Modelling of Non-Isothermal Multi-Component Reactive Transport in Field Scale Porous Media Flow Systems," *Journal of Hydrology*, vol. 214, no. 1-4, pp. 144–164, 1999.

[94] G. Strang, "On the Construction and Comparison of Difference Schemes," *SIAM Journal on Numerical Analysis*, vol. 5, pp. 506–517, 1968.

[95] T. Xu, E. Sonnenthal, N. Spycher, and K. Pruess, *TOUGHREACT User's Guide: A Simulation Program for Non-isothermal Multiphase Reactive Geochemical Transport in Variably Saturated Geologic Media*, Earth Sciences Division, Lawrence Berkeley National Laboratory, University of California, Berkeley, CA 94720., September 2004.

[96] *COMSOL Multiphysics - User Guide Version 3.5a*.

[97] C. Zheng, "COMSOL Multiphysics: A Novel Approach to Ground Water Modelling," *GROUND WATER*, vol. 47, no. 4, pp. 480–487, July-August 2009.

[98] M. Diaz-Viera, D. Lopez-Falcon, A. Moctezuma-Berthier, and A. Ortiz-Tapia. (2008) COMSOL Implementation of a Multiphase Fluid Flow Model in Porous Media. The proceedings of the COMSOL Conference 2008 Boston.

[99] T. I. Bjørnarå and E. Aker and E. Skurtveit. (2008) Comparing Equations for Two-Phase Fluid Flow in Porous Media. The proceedings of the COMSOL Conference 2008 Hannover.

[100] M. Carrizales and L. W. Lake. (2009) Two-Dimensional COMSOL Simulation of Heavy-Oil Recovery by Electromagnetic Heating. The proceedings of the COMSOL Conference 2009 Boston.

[101] F. M. Orr Jr, *Theory of Gas Injection Processes*. Tie-Line Publications, 2007.

[102] H. K. Rhee, R. Aris and N. Amundson, *First-Order Partial Differential Equations volume 2: Theory and Application of Hyperbolic Systems of Quasilinear Equations*. DOVER PUBLICATIONS, INC, 2001.

[103] A. White and M. Peterson, *Chemical Modelling of Aqueous Systems II*, 1990, ch. 35, pp. 461–475.

Chapter 5. Conclusions and Suggestions for Future Work

This thesis includes both an experimental study on CO_2 flooding experiments with X-ray CT scanning, as described in Chapter 2 and Chapter 3, and a simulation study for miscible gas flooding coupled with geochemical reaction, as described in Chapter 4. The major achievements and important conclusions are summarized below, together with a section for possible improvements that can be made in the future.

Conclusions for the experimental study:

- A literature study has been made about that the application of X-ray CT scanning in the petroleum industry. The technique is widely applied to acquire qualitative or quantitative information of core properties or fluid distribution in porous media. One of the important applications is the determination of saturations in core flooding. However, most of saturation determination attempts are for two-phase immiscible flow. Simultaneous saturation determination for three phases is rare in the literature and usually conducted under low pressure and temperature conditions.

- A high pressure high temperature flooding rig has been established for reservoir conditions flooding experiments with X-ray CT scanning. With the rig, it is possible to perform quantitative measurement of in-situ phase saturations and to accurately record the produced fluids and differential pressure across the core dynamically.

- Through a number of trial experiments, several pitfalls in saturation determination with CT-scanning have been identified:

    1. Sodium tungstate dihydrate, recommended as dopant in a previous study using dual energy scanning in high permeable rocks, has been found to adsorb seriously in low permeable chalk, even at low concentrations. Potassium iodide was finally selected to dope the water phase.

    2. In certain situations, a portion of CT numbers on a CT scanning slice can be higher than the upper limit of the CT scanner. This can happen when there is high density area due to heterogeneity and when the scanning energy level is low (e.g., at 80 kV). Image processing

software like FPImage® or ImageJ® will give wrong mean CT numbers. The nonlinear Huber estimation has been used to process the CT data to get the correct mean values.

3. The CT numbers of the iodododecane doped oil phase, the Potassium Iodide doped water phase, and the high density CO_2 phase increase similarly when the energy level changes from 120 to 80 kV. This makes the equations for saturation calculation ill-conditioned and the calculated saturations sensitive to smaller errors in CT numbers. Therefore, the dual energy CT scanning technique can not provide accurate saturation information in our flooding case.

4. Two dopants, lead disodium ethylene-diaminetetraacetate and lead nitrate, were chosen to investigate the possibility of applying K_{edge} of specific dopants. The results indicate that the K_{edge} method does not work in our case because X-ray beams from our CT scanner are polychromatic with moderately broad energy spectrum.

- A new method, 'Pseudo two-phase flooding', for applying CT scanning to tertiary CO_2 flooding experiments, has been proposed. Using this method, the live oil and water were doped to the same CT number so that the CO_2 saturation could be accurately determined by using single energy scanning and the application of low concentration dopant could preserve the original properties of fluids as much as possible. Two successful tertiary CO_2 flooding experiments with CT scanning have been performed using the new method.

- An approach of tuning concentration of dopants in different phases under reservoir condition by using an artificial hollow core plug was proposed. The approach resolves the problem of how to determine the CT numbers of live fluids accurately and quickly. The results of in situ saturation indicate that the proposed way of tuning dopant concentration is one way to guarantee the successful application of our new method in the tertiary CO_2 flooding at reservoir conditions

- CT scanning can provide both quantitative information for the average saturation change through the core (1-D) and qualitative insight into the saturation change in the core (3-D). The saturation results from the CT scanning and the mass balance are in general agreement while the deviations are probably due to the dissolution of CO_2 in water and oil and the incomplete displacement of pure water by doped water before the CO_2 flooding step.

- In Exp. #6 and Exp. #7, core plugs from two different formations are used. Water flooding in Exp. #6 gives very high recovery, while that in Exp. #7 gives just moderate recovery. This indicates that two formations have different responses to water flooding, although their permeability and porosity are similar. CO_2 flooding into the water flooded cores has produced a lot of additional oils in both cases. This shows that the potential of tertiary CO_2 flooding to extract the remaining oils after water flooding, especially for formations where water flooding is not very efficient.

Conclusions for the simulation study:

- A literature study on importance of geochemical reaction in CO_2 injection into aquifers and oil reservoir has been made. It indicates that quite an amount of calcite and dolomite can dissolve in the first thirty years during CO_2 injection into aquifers. Therefore, it is worth studying the geochemical reactions in short-term CO_2 storage, such as CO_2 injection into oil reservoir.

- COMSOL Multiphysics has been used to simulate CO_2 flooding with dissolution reaction in the aqueous phase. The sequential non-iterative approach (SNIA) is used to solve the proposed equations including multiphase transport and kinetically controlled reactions Simulations on two different scales have been tried.

- For the simulation on the reservoir scale, the results suggest that the dissolution of calcite could be treated as equilibrium reactions. The increase of CO_2 solubility in water phase could retard the movement of gas front and increase the concentration of calcium. The geochemical reaction could affect the flow transport by changing porosity and permeability.

- For the simulation on the lab scale, the dissolution of calcite still behaves as kinetically controlled reaction. The increase of CO_2 solubility in water phase could retard the movement of gas front, while geochemical reaction has no visible influence on flow transport. The reactive surface area, which is difficult to estimate and determine by experiments, could influence the concentration of calcite significantly on the lab scale. The porosity change on the lab scale is negligible even with the largest possible reactive surface area.

Suggestions for future work:

- Regarding experimental work, the proposed method, which has been validated and applied in tertiary CO_2 flooding, can be used in the experiments concerning more complex process as WAG

injection or inhomogeneous core with fracture. Flooding with composite cores can be tried in order to minimize the end effects and to reduce the influence from dead volumes.

- The current developed model will be useful to study CO_2 flooding in chalk reservoir and CO_2 sequestration process. The phase equilibrium between CO_2 and oil can be added although it is not included by far. The geochemical model should be extended to include more reactions in order to simulate real CO_2 sequestration scenarios. Other solution method can also be tried in the future. Finally, extension of the current one dimension model into multi-dimension should be considered.

As an effective method to cope with green-house gas emission, and to enhance oil recovery, injection of carbon dioxide (CO_2) into water flooded petroleum reservoirs has obtained increasing attention. This thesis addresses the issues regarding CO_2 injection in chalk reservoirs by performing experimental work and modelling study. The experimental work focuses on improving the current methods for determination of in situ phase saturation during CO_2 flooding in low permeable chalk at reservoir conditions with the application of X-Ray CT. The modelling study focuses on coupling geochemical reactions with multiphase flow in CO_2 enhanced oil recovery (EOR) process.

Center for Energy Resources Engineering
Department of Chemical and
Biochemical Engineering
Technical University of Denmark
Søltofts Plads, Building 229
DK-2800 Kgs. Lyngby
Denmark

Phone: +45 4525 2800
Fax: +45 4525 4588
Web: www.cere.dtu.dk

ISBN: 978-87-92481-28-3